Mon. Not. R. Astron. Soc. **276,** 219–254 (1995)

Mass-losing stars in the South Galactic Cap

Patricia Whitelock,[1]★ John Menzies,[1] Michael Feast,[2] Robin Catchpole,[3] Fred Marang[1] and Brian Carter[1]

[1]*South African Astronomical Observatory, PO Box 9, 7935 Observatory, South Africa*
[2]*Astronomy Department, University of Cape Town, 7700 Rondebosch, South Africa*
[3]*Royal Greenwich Observatory, Madingley Road, Cambridge CB3 0EZ*

Accepted 1995 March 21. Received 1995 February 27; in original form 1994 August 15

ABSTRACT

Observations are presented for 162 late-type stars in the South Galactic Cap ($b < -30°$) which were selected on the basis of their *IRAS* 25/12-μm flux ratios as high-mass-loss candidates. *JHKL* photometry (over 1100 observations) was obtained for all of the stars, $BV(RI)_C$ photometry for 78 of them and optical spectra for 51. 154 of these stars are non-Mira M or S stars, of which many, and possibly all, are semi-regular variables. Of the remaining eight *IRAS* objects, three are T Tauri stars, three are interacting binaries and two are carbon stars.

A few of the M giants and both of the carbon stars have circumstellar envelopes of the type more normally associated with Mira variables. These include two 1612-MHz OH maser sources. It is suggested that such stars may have been Miras in the recent past, but are currently out of the instability strip owing to a recently experienced helium-shell flash. Alternatively, some of them could be binary stars, but there is as yet no evidence for the second star.

The near-infrared colours of the M giants are compared with those of similar stars in the Bulge. They are similar to those of the inner Bulge and unlike those found in either the outer Bulge or the globular clusters. The kinematics and Galactic distribution of the M giants indicate that they are probably from a mixed population and that they could be associated with Miras with a range of periods. A comparison of the observed colours with those derived from models indicates a range of metallicity with the bulk of stars slightly more metal-rich than the Sun. It also reveals significant numbers of stars with colours outside the predicted range, possible due to the effects of circumstellar reddening or to inadequacies in the models. The most metal-rich examples of the M stars have high mass-loss rates for non-Miras ($\sim 10^{-6}$ $M_\odot$ yr^{-1}) and there are far fewer of them outside than inside the solar circle. This may be due to a metallicity gradient. These stars have a scaleheight of more than 500 pc.

The two carbon stars have unusual colours and detached shells. One of them, R Scl, is shown to vary with a period of 379 d superimposed on a possible second period of about 2300 d. The other carbon star, which is more distant and previously unknown, may also have double-period variations.

Key words: stars: carbon – stars: evolution – stars: mass-loss – stars: variables: other – Galaxy: kinematics and dynamics – infrared: stars.

1 INTRODUCTION

Soon after the publication of the *IRAS* Point Source Catalog (*IRAS* Science Team 1986, hereafter PSC), a survey of *IRAS* sources in the South Galactic Cap was initiated at SAAO. The sources were selected on the basis of their 25/12-μm flux ratios as possible asymptotic giant branch (AGB) stars, by criteria which are described in detail in Section 2. A single *JHKL* observation was obtained for each of the *IRAS* sources selected. Optical spectroscopy and photometry and/

★ E-mail address: (I)paw@saao.ac.za

or further *JHKL* photometry were obtained for many of the sources, depending on their near-infrared and *IRAS* colours as well as on their catalogued properties.

It is generally understood that low-mass stars lose most of their hydrogen envelope via a stellar wind towards the end of their AGB evolution. The high-mass-loss phase has been identified with Mira variables. These variables occupy a thin strip at the top of the AGB (Feast & Whitelock 1987). According to theory (e.g. Iben & Renzini 1983) many stars will undergo thermal pulsing (helium-shell flashes) while approaching the top of their AGB. The thermal pulse cycle involves a significant change of luminosity ($\Delta M_{\rm bol} \sim 1$ mag). It seems that during the luminosity minimum of the cycle we should expect AGB stars to leave the Mira instability strip temporarily. For much of the time stars in this luminosity minimum will be only slightly fainter than the Miras; although they will not be large-amplitude pulsators, they will probably be unstable to low-amplitude variations and will be losing mass at a somewhat lower rate than they did as Miras. The sources considered here are almost all late-type stars with dust shells, but *exclude* Mira variables (which were discussed in an associated paper (Whitelock et al. 1994a, hereafter Paper I). It is among the stars considered here that we might expect to find stars about to become Miras as well as some which have recently been Miras.

2 SOURCE SELECTION

Sources at galactic latitudes $b < -30°$ were selected from version 1 of the *IRAS* PSC. All sources with high-quality flux measurements at 12 and 25 μm and flux ratios of $F_{25}/F_{12} > 0.5$ were extracted (where F_λ denotes the flux in Jy at wavelength λ as detected by *IRAS*). This selection largely eliminates 'normal' stars, i.e., those without the infrared excess which is characteristic of high mass-loss rates. It does include some bright galaxies, but these are easily recognized on Schmidt survey plates and were not observed. Several well-known planetary nebulae were rejected in the same way. Objects in the area of the Magellanic clouds were omitted unless they appeared to correspond to bright, probably foreground, stars. A small number of Seyfert galaxies was rejected only after spectra were obtained.

Among the sources selected and studied were a few relatively early-type stars with spectral types ranging from B to K. The observations of these stars have been discussed by Whitelock et al. (1989a,b, 1991b). The present paper contains observations of 162 non-Mira late-type stars, and Paper I deals with the 61 Mira variables. The division betweewn Miras and non-Miras was considered in Paper I (Section 2.1); possibly ambiguous cases are discussed individually in Section 7.9 below. The *IRAS* sources are listed in Table 1, together with their 12-, 25- and 60-μm *IRAS* fluxes and their respective uncertainties (Unc). Also tabulated are the *IRAS* variability index (Var) and the LRS spectral type (LRS); definitions of these parameters as well as the procedure for making the colour corrections can be found in the explanatory supplement to version 2 of the *IRAS* PSC (*IRAS* Science Team 1988, hereafter PSC-ES). For two stars the LRS types from Volk & Cohen (1989) and Volk et al. (1991) are used. In these cases 'C' is equivalent to classes 40–49 and 'F' to classes 10–16. The common name of those stars previously identified is also listed, with preference being given to a variable star (Kholopov et al. 1985, hereafter GCVS) or suspected variable star (Kukarkin et al. 1982, hereafter NSV) designation if available; alternatively, the AFGL number (Price & Murdock 1983), the IRC number (Neugebauer & Leighton 1969), or the SAO, HD or BD number is quoted. Stars named 'Ste-' and 'StHα' were catalogued by Stephenson (1986a and 1986b, respectively).

Note that the initial source selection was made from version 1 of the PSC, while the data used here were taken from version 2. This results in a few faint ($F_{12} < 1$ Jy) sources being included in the study, despite the fact that their colours, as listed in version 2, are outside the selected range (i.e., they have $F_{25}/F_{12} < 0.5$).

A small area of the South Galactic Cap was not surveyed by *IRAS*, as detailed in PSC-ES. A comparison of the Miras within and outside this area (Paper I) suggests that it would contain only about 4 per cent of the stars which are included in the area of the Cap actually covered.

3 OBSERVATIONS

The spectroscopic and photometric observations were made from SAAO Sutherland. It is assumed throughout that the effects of interstellar reddening are negligible on all colours of these high-galactic-latitude sources.

3.1 Near-infrared photometry

The near-infrared photometry is listed in Table 2. This includes measurements made for a number of sources prior

Table 1. *IRAS* sources.

IRAS name	12 μm	25 μm (Jy)	60 μm	Unc	Var	LRS	ident.
00016 − 3056	1.23	0.71	0.78	DCD	2		-
00025 + 0027	7.06	3.72	0.59	CCF	0		-
00045 + 3058	1.16	0.74	0.40	BCL	0		-
00127 − 6030	0.69	0.30	0.40	BDL	5		UY Tuc (SR)
00197 + 0318	3.04	1.65	0.40	BCL	0		-
00204 − 5936	1.61	0.82	0.40	BCL	1		-
00221 − 7614	0.52	0.31	0.40	BCL	0		-
00245 − 0652	116.09	59.01	11.54	BBD	1	14	UY Cet (SRb)
00371 + 1355	14.83	7.60	1.10	BCC	0	15	TW Psc (Lb)
00413 + 2028	0.68	0.45	0.40	CDL	1		-
00477 − 4900	19.23	10.08	1.44	BBC	0	15	-
00542 − 7334	1.18	0.66	1.13	BCL	1		CM Tuc (SRb:)
01083 + 2335	1.42	0.75	0.40	CCL	0		-
01217 + 2341	39.53	20.34	2.92	BBD	0	23	AFGL 5048
01230 − 4611	11.76	6.75	0.74	BBC	1	13	AL Phe (Lb:)
01246 − 3248	162.10	82.07	54.80	BBD	1	C	R Scl (SRb)
01251 + 1626	33.58	18.42	2.71	BBD	0	28	ST Psc (SRb)
01253 + 2816	3.63	2.08	0.49	BCC	0		-
01400 − 6921	7.28	3.68	0.54	ABB	2	14	-
01438 + 1850	76.70	39.87	6.60	BBD	2	23	SV Psc (SRb)
01452 − 8026	37.72	20.78	3.61	CAB	5	15	VZ Hyi (-)
01481 − 1753	15.12	8.99	1.15	BBC	0	16	NSV 634
01483 − 6932	0.47	0.27	0.40	BCL	0		-
01519 + 0427	24.91	12.77	2.10	BCD	0	24	AA Psc (Lb)
01527 + 1656	34.53	20.08	2.67	BBD	0	25	AFGL 4013
01531 − 3602	8.42	4.72	0.88	BCL	0		NSV 665
01597 + 1601	27.18	14.17	2.44	BCD	0	24	RY Ari (Lb)
02095 − 2355	16.82	8.42	1.36	BBC	0		IRC−20°029
02165 + 2750	1.25	0.63	0.40	BCL	1		-
02180 − 7939	0.90	0.49	0.40	BBL	1		SY Hyi (SR)
02404 + 2150	6.19	3.82	0.60	BBB	0		-

Table 1 – *continued*

IRAS name	12 μm	25 μm (Jy)	60 μm	Unc	Var	LRS	ident.
02427 − 5430	181.03	99.85	11.01	ABC	0	22	W Hor (SRb)
02512 − 3758	7.90	5.45	1.45	BBC	0		SY For (SRb)
02537 − 0614	12.44	6.66	1.62	BBC	0	15	IRC−10°042
02538 + 1953	0.69	0.72	0.56	BDC	0		WY Ari (Int)
03033 − 7703	4.06	2.20	0.32	BBC	4		-
03177 − 0017	2.01	1.11	0.40	BCL	0		BD−00°528
03227 − 1231	15.93	8.44	0.62	BBD	0	28	VX Eri (SR:)
03260 − 1534	0.80	0.44	0.40	BCL	0		Ste-23
03287 − 1535	52.55	50.83	12.81	BBC	0	29	Ste-24
03318 − 5334	0.72	0.41	0.40	BFL	0		SAO 233156
03318 − 8244	0.62	0.34	0.40	CCL	6		-
03323 − 2547	6.97	3.94	0.55	BBC	0		-
03324 − 4728	0.98	0.54	0.40	CCL	3		-
03388 − 1054	17.72	10.60	1.36	BBC	0	14	VY Eri (SRb)
03430 + 0325	6.58	8.87	1.27	BBC	0		-
03489 + 1257	0.80	0.46	0.40	CDL	7		-
03499 − 3041	2.77	1.51	0.40	BBL	2		-
04020 − 1551	326.42	183.61	23.63	ABC	0	22	V Eri (SRb)
04026 − 3024	2.76	1.40	0.40	BCL	1		-
04037 − 1846	4.61	2.62	0.40	BBL	1		AT Eri (Lb)
04060 − 0447	3.12	1.56	0.40	BCL	1		Ste-30
04067 − 0922	7.48	4.74	2.84	BBC	2		-
04085 + 0653	1.10	0.63	0.40	BBL	0		-
04120 − 6516	1.02	0.66	0.40	BCL	2		-
04127 + 0110	0.56	0.21	0.40	BDL	9		-
04147 − 1220	1.56	0.85	0.40	CCL	3		Ste-32
04177 − 1850	8.59	4.80	0.68	BBD	1		AV Eri (Lb)
04183 − 4310	2.45	1.39	0.40	BBL	2		-
04191 + 0346	5.15	3.18	0.36	ABC	3		-
04199 − 2248	13.13	7.60	1.29	BBC	0	14	NSV 1578 Ste-34
04238 − 6713	1.09	0.60	0.40	BCL	2		-
04257 − 3220	1.04	0.52	0.40	BEL	0		-
04258 − 0155	0.64	0.27	0.40	BDL	2		-
04375 − 3216	0.32	0.44	0.40	DDL	0		-
04382 − 1417	104.54	53.55	8.55	BAC	6	21	BX Eri (SR)
04451 − 0539	0.27	0.48	0.60	FCC	0		-
04523 − 1359	0.46	0.54	0.40	CDL	5		-
04576 − 2555	6.25	3.52	0.76	BBC	0		-
05074 − 2654	5.40	3.02	0.51	BBC	0		-
05166 − 3109	1.22	0.63	0.40	BCL	3		-
05217 − 3943	31.90	19.49	2.99	BAB	0	26	SW Col (Lb:)
19496 − 6812	4.36	2.49	0.45	BBC	1		-
19521 − 5131	0.77	0.56	0.40	BDL	7		-
19539 − 5915	6.17	3.14	0.57	CBC	2		-
19549 − 4931	8.76	5.37	0.94	BBD	1		HD 188707
19575 − 4317	2.37	1.33	0.40	BCL	0		-
20043 − 4533	1.04	0.55	0.40	BCL	0		-
20116 − 5445	11.38	6.07	1.02	BBD	0	16	NSV 12922
20120 − 4433	38.17	24.95	10.07	BBC	2	16	RZ Sgr (SRb)
20125 − 5153	0.80	0.45	0.40	BCL	1		-
20174 − 7853	2.07	1.15	0.40	BBL	4		-
20176 − 2527	0.83	0.44	0.40	BFL	0		-
20220 − 8027	0.60	0.37	0.40	DCL	8		-
20240 − 2142	2.40	1.32	0.40	BCL	0		-
20250 − 3557	3.21	1.76	0.40	BCL	2		-
20270 − 2858	2.68	1.41	0.40	CCL	0		-
20271 − 2340	1.11	0.54	0.40	CDL	0		-
20277 − 3959	1.02	0.57	0.40	DCL	5		SW Mic (SR:)
20282 − 3310	2.71	1.82	0.40	BCL	0		SAO 212196
20295 − 6546	4.37	2.98	0.69	BBB	0		-
20298 − 3405	7.98	4.39	0.75	BBC	1		-
20333 − 2428	1.26	0.68	0.40	BDL	0		-
20356 − 2815	10.97	5.71	1.01	BBC	0		IRC−30°433
20381 − 2827	1.50	0.76	0.40	BEL	2		-
20412 − 2229	7.26	4.38	0.74	CBC	1		Ste-524
20459 − 4917	1.17	0.62	0.40	CDL	0		-

Table 1 – *continued*

IRAS name	12 μm	25 μm (Jy)	60 μm	Unc	Var	LRS	ident.
20466 − 4105	2.36	1.38	0.50	BCL	0		-
20487 − 1117	18.90	9.48	1.80	BBC	0	15	AFGL 2666 Ste-529
20522 − 5711	3.66	1.83	0.40	ABL	0		-
20545 − 1709	1.05	0.66	0.40	BDL	6		XY Cap (SR)
20559 − 1055	6.21	3.40	0.55	BBC	4		DG Aqr (SR)
20561 − 5253	1.04	0.55	0.40	BDL	0		-
20575 − 5806	0.61	0.40	0.40	DDL	1		-
20577 − 4504	0.84	0.54	0.40	CCL	2		-
20598 − 2358	4.29	2.29	0.40	BCL	1		-
20599 − 3941	5.46	3.00	0.64	BBC	1		-
21015 − 0214	1.00	0.55	0.40	CCL	5		TW Aqr (SR)
21034 − 0823	1.47	0.80	0.40	BCL	0		-
21041 − 5746	2.16	1.16	0.40	BCL	0		-
21060 − 0029	0.44	0.33	0.40	DDL	0		-
21095 − 5222	12.15	6.16	1.00	BBC	0	15	-
21097 − 3627	2.48	1.58	0.40	BCL	3		-
21151 − 2340	1.21	0.76	0.40	CEL	0		-
21159 − 5222	0.77	0.44	0.40	BFL	2		-
21160 − 6728	24.96	14.85	1.58	BBD	0	29	NSV 13648
21208 − 3350	0.89	0.42	0.40	CFL	0		-
21270 + 0702	1.39	0.77	0.40	BCL	8		-
21317 − 5948	1.32	0.72	0.43	BCL	1		-
21318 − 5130	0.91	0.47	0.40	CCL	1		-
21365 + 0526	0.99	0.51	0.40	BDL	0		-
21368 − 3812	55.33	33.36	7.03	BBC	0	21	AFGL 5595
21377 − 0200	60.90	33.56	5.42	BBC	8	14	AFGL 2787 Ste-546
21392 + 0230	1.84	1.65	0.40	BCL	0		StHα 190
21396 − 2256	0.85	0.51	0.40	BDL	2		-
21439 − 0226	637.38	320.66	47.13	BBD	1	23	EP Aqr (SRb)
21447 − 7245	0.74	0.42	0.40	BCL	2		-
21505 − 4320	1.33	0.79	0.40	CDL	1		-
21511 − 6439	0.86	0.45	0.40	BCL	1		-
21543 − 1421	75.07	47.38	8.50	BBC	0	21	NSV 13969
21562 − 2547	1.11	0.53	0.40	BFL	5		-
22003 − 0010	22.98	11.77	1.93	BBC	0	24	AFGL 2835 Ste-549
22066 − 2500	1.63	0.86	0.40	BCL	0		-
22073 − 3632	2.41	1.28	0.40	CCL	2		-
22103 − 2731	1.68	0.99	0.40	CCL	0		RX PsA (SRa)
22142 − 8454	142.63	71.94	10.93	AAB	4	23	BW Oct (Lb:)
22169 − 0955	1.68	0.85	0.40	BCL	1		ZZ Aqr (-)
22190 − 0751	81.27	44.34	6.71	BBC	0	25	DZ Aqr (SR:)
22197 − 3348	1.44	0.72	0.40	BCL	0		HD 212115
22209 − 3508	12.27	6.97	1.08	BBC	0	24	-
22229 − 6855	1.53	2.51	0.32	BBF	2		-
22296 + 2004	1.81	1.00	0.40	BCL	0		-
22359 − 1417	39.24	20.32	3.38	DBD	0	15	AB Aqr (Lb)
22380 + 2306	0.61	0.34	0.40	CCL	1		-
22458 + 1401	1.23	0.63	0.40	EDL	0		-
22494 − 2534	23.94	17.56	3.42	FBD	0	23	TU PsA (Lb:)
22497 + 1733	4.84	2.52	0.55	BCE	0		-
22553 + 1744	23.78	12.91	1.52	CBC	0	26	BI Peg (SRa)
23082 + 1903	6.45	3.39	0.38	BBC	0		BD+18°5117
23115 + 0953	1.88	1.35	0.40	BEL	0		BD+09°5182
23196 + 1615	3.78	2.15	0.40	BCL	0		-
23198 − 0230	2.63	7.10	3.81	BCD	0		StHα 202
23218 − 7719	0.47	0.18	0.40	BEL	2		TV Oct (I)
23236 − 6917	29.79	16.12	2.18	BBC	1	25	-
23261 − 6502	26.66	13.33	1.48	BBB	1	26	CE Tuc (SR)
23261 − 8230	1.98	1.05	0.40	BBL	0		-
23270 − 6837	1.38	0.73	0.40	BCL	2		-
23312 − 3927	11.78	6.27	0.96	BCC	1		-
23370 − 5606	0.50	0.28	0.40	BEL	0		-
23404 + 1713	2.10	1.09	0.40	CCL	0		-
23492 + 0846	27.38	14.16	2.46	BCD	0	F	AFGL 3163
23496 − 1607	7.07	3.74	0.39	BCE	1		Z Aqr (SRa)

Table 2. Near-infrared photometry. An asterisk denotes an observation made on the 1.9-m telescope.

JD −2440000	J	H	K	L
		(mag)		
00025+0027				
6642.56	4.52	3.49	3.19	2.98
00045+3058				
6311.49	6.00	4.98	4.67	4.43
00127−6030 UY Tuc				
6641.66	6.75	5.88	5.64	5.30
6703.86	6.59	5.75	5.52	5.11
6796.30	6.49	5.71	5.52	5.17
6842.25*	6.76	5.89	5.64	5.30
6967.65	7.00	6.14	5.85	5.45
6989.66	6.76	6.00	5.79	5.48
7020.61	6.55	5.74	5.55	5.23
7056.55	6.76	5.88	5.63	5.34
7073.49	6.90	6.10	5.86	5.42
7113.45	6.52	5.74	5.55	5.32
7128.35	6.58	5.76	5.56	(5.2)
7143.31	6.59	5.75	5.52	5.16
7182.28	6.75	5.88	5.63	5.26
7343.63	6.53	5.68	5.46	5.15
7358.57	6.62	5.74	5.50	5.23
7359.53	6.61	5.75	5.51	5.23
7373.61	6.67	5.81	5.57	5.25
7378.58	6.71	5.84	5.59	5.25
7422.54	6.41	5.66	5.44	5.14
7429.41	6.41	5.61	5.40	5.10
7440.42	6.49	5.64	5.41	5.08
7460.42	6.61	5.73	5.48	5.09
7501.31	6.83	5.96	5.68	5.28
7510.28	6.66	5.87	5.63	5.12
7524.33	6.52	5.71	5.51	5.12
7531.30	6.51	5.69	5.49	5.12
7727.66	6.70	5.88	5.64	5.35
7731.61	6.68	5.85	5.61	5.30
7741.66	6.51	5.71	5.50	5.20
7760.58	6.54	5.70	5.49	5.22
7764.58	6.55	5.70	5.49	5.21
7777.55	6.59	5.73	5.49	5.18
7786.53	6.55	5.70	5.46	5.11
7792.49	6.57	5.69	5.45	5.19
7806.49	6.62	5.70	5.45	5.19

JD −2440000	J	H	K	L
		(mag)		
00127−6030 UY Tuc continued				
7810.45	6.65	5.75	5.48	5.16
7823.41	6.71	5.87	5.59	5.28
7834.44	6.59	5.81	5.57	5.22
7838.33	6.57	5.79	5.57	5.27
7861.34	6.50	5.69	5.46	5.11
7868.35	6.55	5.71	5.49	5.17
8074.66	6.51	5.70	5.48	5.17
8078.69	6.49	5.69	5.47	5.11
8094.65	6.54	5.69	5.45	5.14
8104.49	6.50	5.63	5.39	4.93
8106.64	6.48	5.63	5.39	5.06
8115.63	6.51	5.64	5.39	5.08
8129.52	6.62	5.75	5.47	5.15
8163.43	6.52	5.73	5.51	5.21
8164.48	6.49	5.72	5.49	5.18
8211.31	6.57	5.70	5.44	5.11
8232.32	6.71	5.83	5.55	5.22
8253.28	6.88	6.10	5.83	
8280.28	6.41	5.66	5.48	5.09
8452.68	6.74	5.85	5.58	5.10
8491.59	6.53	5.73	5.51	5.18
8496.59	6.50	5.68	5.45	5.16
8521.49	6.53	5.69	5.43	5.05
8529.52	6.61	5.74	5.47	5.14
8554.39	6.71	5.80	5.55	5.21
8793.68	6.74	5.92	5.65	5.25
8840.58	6.59	5.75	5.51	5.14
8851.62	6.63	5.77	5.52	5.13
8868.55	6.71	5.80	5.55	5.25
8897.44	6.74	5.93	5.67	5.27
8932.39	6.43	5.64	5.43	5.03
8990.31	6.58	5.74	5.48	(5.1)
9027.26	6.58	5.76	5.52	5.33
00197+0318				
6264.64*	5.29	4.20	3.92	3.58
00204−5936				
6301.59	6.13	5.14	4.90	4.64
6313.58	6.08	5.10	4.87	4.64

JD −2440000	J	H	K	L
		(mag)		
00221−7614				
6657.61*	7.70	6.70	6.45	6.23
00245−0652 UY Cet				
6642.59	1.64	0.60	0.25	−0.06
00371+1355 TW Psc				
6642.60	3.59	2.55	2.27	2.04
00413+2028				
6309.55*	6.87	5.87	5.53	5.24
00477−4900				
6270.60	3.27	2.26	1.94	1.66
6424.31	3.29	2.27	1.97	1.64
00542−7334 CM Tuc				
4158.47	6.07	5.09	4.79	4.56
4161.40	6.08	5.07	4.80	4.57
4188.32	6.17	5.17	4.87	4.77
5620.49	6.14	5.11	4.81	4.54
5627.39	6.13	5.09	4.79	4.56
5629.45	6.15	5.11	4.79	4.63
5632.40	6.12	5.08	4.80	4.59
5639.37	6.08	5.09	4.81	4.51
5702.31	6.14	5.12	4.81	4.61
5949.59	6.06	5.06	4.77	4.53
6070.33	6.09	5.11	4.82	4.49
6073.33	6.09	5.11	4.82	4.60
6658.54*	6.02	5.02	4.74	4.52
7755.62	6.16	5.15	4.87	4.68
7759.59	6.14	5.15	4.86	4.61
7760.61	6.14	5.14	4.86	4.63
7767.56	6.16	5.21	4.89	4.66
7769.67	6.18	5.19	4.89	4.64
7776.59	6.18	5.20	4.91	4.66
7780.44	6.18	5.18	4.89	4.68
7786.55	6.13	5.15	4.86	4.66
7803.43	6.07	5.09	4.81	4.57
7810.48	6.08	5.10	4.81	4.59
7817.46	6.09	5.09	4.81	4.54
7823.42	6.10	5.11	4.83	4.57

JD −2440000	J	H	K	L
		(mag)		
00542−7334 CM Tuc continued				
7834.46	6.17	5.17	4.88	4.61
7841.37	6.20	5.20	4.90	4.63
7862.35	6.20	5.21	4.91	4.73
7868.37	6.19	5.19	4.91	4.71
8094.67	6.18	5.19	4.90	4.65
8104.60	6.22	5.21	4.93	4.71
8106.65	6.16	5.18	4.89	4.60
8115.64	6.15	5.18	4.89	4.64
8129.53	6.16	5.17	4.87	4.64
8163.47	6.18	5.16	4.86	4.60
8232.33	6.15	5.16	4.86	4.57
8253.30	6.17	5.15	4.86	4.60
8284.27	6.17	5.15	4.87	4.67
8496.60	6.13	5.11	4.82	4.57
8517.52	6.14	5.12	4.83	4.57
8529.54	6.11	5.11	4.81	4.50
01083+2335				
6311.52	5.75	4.75	4.45	4.22
01217+2341 AFGL 5048				
6642.63	2.56	1.54	1.22	0.97
01230−4611 AL Phe				
6643.58	3.76	2.81	2.58	2.36
7856.45	3.79	2.83	2.60	2.39
7889.39	3.78	2.82	2.58	2.39
8875.53	3.83	2.89	2.65	2.43
01246−3248 R Scl				
3123.50	1.75	0.60	−0.03	−0.62
3405.51	2.04	0.76	0.01	−0.54
4187.34	1.87	0.61	−0.04	−0.67
6265.67	2.17	0.74	−0.05	−0.79
6300.58	2.44	0.95	0.09	−0.74
6303.57	2.53	1.03	0.13	−0.61
6334.50	2.55	1.07	0.15	−0.64
6356.45	2.55	1.06	0.13	−0.65
6373.42	2.46	0.98	0.10	−0.70
6391.32	2.43	0.96	0.10	−0.69

Table 2 – *continued*

JD −2440000	J	H	K	L
		(mag)		
01246–3248 R Scl continued				
6640.60	2.02	0.62	−0.14	−0.83
6655.62	2.15	0.71	−0.09	−0.80
6662.62	2.18	0.75	−0.07	−0.84
6690.52	2.40	0.91	0.02	−0.76
6695.52	2.44	0.97	0.08	−0.68
6712.46	2.53	1.02	0.11	−0.67
6741.44	2.54	1.04	0.13	−0.63
6749.39	2.50	1.00	0.11	−0.62
6754.34	2.45	0.98	0.09	−0.67
6775.30	2.31	0.88	0.05	−0.62
6782.30	2.26	0.85	0.03	−0.64
6805.31	2.14	0.77	0.02	−0.56
6984.68	1.61	0.33	−0.28	−0.90
7014.62	1.80	0.44	−0.26	−0.94
7056.59	2.15	0.69	−0.13	−0.88
7073.51	2.28	0.79	−0.09	−0.84
7113.48	2.32	0.86	−0.03	−0.74
7144.29	2.19	0.75	−0.07	−0.79
7176.28	2.07	0.67	−0.07	−0.65
7191.28	2.03	0.67	−0.08	−0.66
7364.65	1.62	0.32	−0.35	−0.98
7379.58	1.70	0.36	−0.31	−1.03
7394.62	1.73	0.41	−0.32	−1.01
7427.52	2.02	0.61	−0.19	−0.94
7447.41	2.16	0.73	−0.12	−0.89
7497.33	2.36	0.92	0.01	−0.69
7512.33	2.30	0.88	0.01	−0.73
7534.28	2.19	0.80	−0.04	−0.72
7732.69	1.56	0.27	−0.35	−0.93
7745.61	1.55	0.25	−0.38	−1.03
7761.58	1.57	0.26	−0.39	−1.01
7779.54	1.74	0.38	−0.31	−1.01
7805.49	2.03	0.61	−0.18	−0.88
7816.43	2.14	0.74	−0.09	−0.88
7821.44	2.21	0.78	−0.06	−0.84
7841.40	2.42	0.96	0.05	−0.77
7873.38	2.54	1.11	0.16	−0.61
8073.65	1.98	0.65	−0.05	−0.68
8077.67	1.96	0.64	−0.05	−0.73
8109.68	1.91	0.55	−0.14	−0.74
8141.64	2.00	0.61	−0.12	−0.77
01246–3248 R Scl continued				
8172.58	2.13	0.70	−0.08	−0.78
8211.35	2.43	0.96	0.08	−0.67
8224.40	2.50	1.03	0.11	−0.69
8252.35	2.53	1.06	0.14	−0.61
8280.32	2.41	0.97	0.10	−0.58
8492.55	1.76	0.46	−0.19	−0.87
8519.55	1.92	0.55	−0.16	−0.85
8873.53	1.82	0.47	−0.22	−0.88
8900.45	2.03	0.62	−0.15	−0.87
8933.47	2.29	0.81	−0.04	−0.82
8960.32	2.41	0.92	0.04	−0.75
8990.34	2.42	0.94	0.04	−0.73
9000.33	2.41	0.94	0.04	−0.70
9022.28	2.26	0.86	0.02	−0.65
01251+1626 ST Psc				
6642.63	3.06	2.03	1.71	1.44
01253+2816				
6276.62	5.05	4.01	3.68	3.45
01400–6921				
6276.60	4.26	3.27	2.99	2.72
01438+1850 SV Psc				
6642.64	2.01	0.98	0.64	0.38
01452–8026 VZ Hyi				
6276.61	2.51	1.47	1.13	0.86
6440.30	2.48	1.45		0.86
01481–1753 NSV 634				
6642.64	3.76	2.77	2.46	2.16
8214.40	3.74	2.75	2.43	2.13
01483–6932				
6308.68*	6.48	5.51	5.25	5.07
6441.29	6.45	5.48	5.23	(5.1)
01519+0427 AA Psc				
6643.60	3.23	2.18	1.82	1.52
01527+1656 AFGL 4013				
6643.63	3.08	2.04	1.78	1.56
01531–3602 NSV 665				
6643.59	3.85	2.84	2.56	2.35
8171.58	3.84	2.85	2.57	2.35
01597+1601 RY Ari				
6643.64	3.07	2.02	1.69	1.42
02095–2355 IRC−20°029				
6643.61	3.49	2.47	2.17	1.92
02165+2750				
6310.56	6.34	5.30	4.97	4.66
02180–7939 SY Hyi				
6489.25	6.47	5.48	5.21	4.99
6746.43	6.44	5.45	5.18	4.98
02404+2150				
6276.65	5.32	4.15	3.69	3.34
6334.55	5.14	4.05	3.58	3.26
6425.30	5.23	4.06	3.61	3.29
6644.67	5.24	4.09	3.65	3.31
6662.63	5.24	4.11	3.66	3.28
6697.57	5.20	4.07	3.63	3.29
6725.46	5.12	4.01	3.59	3.28
6752.42	5.16	4.04	3.62	3.30
6778.36	5.17	4.06	3.62	3.26
6782.32	5.18	4.06	3.62	3.25
6791.31	5.19	4.07	3.64	3.30
6813.29	5.27	4.12	3.69	3.30
7033.66	5.24	4.08	3.63	3.27
7070.54	5.27	4.12	3.66	3.35
7121.38	5.18	4.05	3.63	3.27
7150.32	5.17	4.06	3.60	3.27
7496.37	5.16	4.02	3.58	3.21
7541.29	5.18	4.04	3.59	3.22
02404+2150 continued				
7792.55	5.20	4.05	3.60	3.27
7810.54	5.23	4.07	3.61	3.26
7836.43	5.21	4.08	3.62	3.24
8164.55	5.26	4.11	3.64	3.26
8962.35	5.18	4.04	3.61	3.27
9000.30	5.22	4.06	3.62	3.26
02427–5430 W Hor				
6489.27	1.71	0.69	0.34	0.03
02512–3758 SY For				
2688.50	5.95	5.04	4.84	3.84
2739.50	6.24	5.35	4.85	4.00
2774.50	6.09	5.22	4.79	3.90
3078.50	6.07	5.15	4.75	4.07
3083.50	6.00	5.18	4.70	3.93
3110.50	5.98	5.10	4.70	3.90
3123.50	6.00	5.06	4.69	3.90
3141.50	6.16	5.21	4.81	4.07
3159.29	6.17	5.30	4.85	4.09
3386.59	6.03	5.11	4.66	3.86
3409.46	6.07	5.16	4.70	4.14
3424.51	6.16	5.23	4.78	4.18
3439.46	6.15	5.28	4.84	4.32
3456.40	6.19	5.31	4.88	4.09
3523.31	6.17	5.20	4.75	3.93
3729.65	6.17	5.27	4.81	4.02
3816.43	6.04	5.11	4.66	3.82
3817.42	6.03	5.12	4.66	3.84
3820.36	6.04	5.11	4.67	3.81
3822.37	6.04	5.11	4.67	3.83
3848.35	6.15	5.21	4.77	4.07
3854.35	6.17	5.24	4.79	4.03
3855.33	6.18	5.22	4.77	3.96
3859.36	6.21	5.26	4.82	4.12
3860.32	6.13	5.23	4.78	4.00
3865.35	6.18	5.25	4.84	4.01
3868.32	6.15	5.25	4.82	4.01
3879.32	6.18	5.25	4.83	4.03
3881.32	6.17	5.26	4.84	4.11

Table 2 – *continued*

JD −2440000	J	H	K	L
		(mag)		
02512–3758 SY For continued				
3891.29	6.13	5.23	4.81	4.04
3895.31	6.13	5.21	4.78	4.04
4578.36	6.18	5.26	4.84	4.08
4582.33	6.23	5.35	4.90	4.17
4605.30	6.25	5.32	4.90	4.14
4606.31	6.21	5.33	4.90	4.14
4615.30	6.23	5.32	4.90	4.17
4621.33	6.23	5.32	4.91	4.22
4622.32	6.22	5.32	4.90	4.15
4625.31	6.18	5.31	4.90	4.08
4626.29	6.22	5.32	4.90	4.09
4815.66	6.21	5.22	4.79	4.02
4851.57	6.26	5.35	4.89	4.10
4904.39	6.08	5.15	4.73	3.90
4907.41	6.06	5.16	4.74	3.91
4911.39	6.04	5.13	4.71	3.97
4914.36	5.96	5.10	4.67	3.80
4915.41	5.99	5.08	4.64	3.87
4917.46	6.11	5.23	4.81	4.12
4918.41	6.07	5.18	4.74	3.97
4920.53	6.07	5.18	4.74	3.89
4930.35	6.05	5.15	4.72	4.02
4947.37	5.99	5.10	4.63	3.90
4948.35	6.02	5.13	4.69	4.12
4949.35	6.02	5.12	4.68	4.00
4956.35	6.09	5.18	4.75	3.93
4959.29	6.13	5.21	4.77	3.94
5157.68	6.20	5.27	4.81	3.93
5215.59	6.11	5.20	4.74	3.89
5220.56	6.13	5.20	4.73	3.91
5251.51	6.11	5.16	4.71	3.79
5336.29	6.20	5.30	4.82	3.95
8197.53	6.22	5.27	4.81	4.02
8223.42	6.33	5.38	4.90	4.09
8256.33	6.24	5.31	4.86	4.01
8284.31	6.24	5.30	4.84	4.01
8298.29	6.20	5.26	4.83	3.98
8322.25	6.14	5.21	4.78	3.99
8468.68	6.16	5.24	4.82	3.99
8474.65	6.17	5.24	4.82	3.99
8498.65	6.13	5.23	4.80	3.97
8517.57	6.16	5.24	4.80	4.01
8576.49	6.18	5.27	4.84	4.03
8617.33	6.17	5.26	4.83	4.03
8855.62	6.29	5.34	4.90	4.07
8895.58	6.26	5.32	4.89	4.09
8931.48	6.16	5.25	4.82	3.97
8960.37	6.19	5.27	4.83	3.98
9004.30	6.33	5.41	4.94	4.04
02537–0614 IRC−10°042				
6491.24	3.77	2.64	2.27	1.99
6644.65	3.69	2.60	2.23	1.93
02538+1953 WY Ari				
6643.66	10.19	9.39	8.85	
6704.56	9.94	9.13	8.55	
6721.54*	10.15	9.23	8.57	7.68
6751.42*	10.15	9.31	8.75	7.75
6798.30	10.18	9.24	8.63	
7081.52*	10.16	9.28	8.67	
7099.42*	10.25	9.35	8.76	7.84
7132.31*	10.24	9.35	8.79	
03033–7703				
6308.59	5.29	4.23	3.85	3.59
6441.37	5.21	4.20	3.84	3.58
03177–0017 BD−0°528				
6304.60	5.70	4.71	4.48	4.28
6442.29	5.75	4.76	4.51	4.28
03227–1231 VX Eri				
6488.28	4.11	3.15	2.87	2.65
03260–1534 Ste-23				
6313.59	6.42	5.49	5.14	4.97
6334.56	6.45	5.43	5.14	4.90
6430.40	6.45	5.45	5.19	4.94
6438.37	6.45	5.44	5.16	4.99
03287–1535 Ste-24				
6276.67	4.54	3.56	3.21	2.81
6304.62	4.51	3.55	3.20	2.81
6334.58	4.56	3.58	3.23	2.82
6390.46	4.66	3.69	3.32	2.89
6428.30	4.49	3.51	3.18	2.73
6487.26	4.57	3.57	3.23	2.82
6642.69	4.52	3.53	3.19	2.77
6655.68	4.54	3.55	3.22	2.83
6690.57	4.59	3.61	3.26	2.82
6729.51	4.53	3.55	3.20	2.80
6750.43	4.54	3.53	3.19	2.78
6758.41	4.53	3.52	3.18	2.79
6779.35	4.59	3.56	3.21	2.80
6782.37	4.57	3.56	3.20	2.78
6804.31	4.63	3.61	3.24	2.81
6834.29	4.63	3.63	3.28	2.83
6874.22	4.46	3.48	3.13	2.70
7011.56	4.68	3.62	3.27	2.88
7056.61	4.52	3.54	3.20	2.81
7122.44	4.59	3.62	3.27	2.79
7147.32	4.60	3.59	3.25	2.87
7148.35	4.57	3.58	3.23	2.79
7177.34	4.56	3.55	3.20	2.78
7460.50	4.63	3.60	3.24	2.85
7495.42	4.53	3.54	3.20	2.78
7538.36	4.60	3.57	3.22	2.82
7730.66	4.55	3.54	3.19	2.80
7743.62	4.58	3.57	3.21	2.82
7778.62	4.61	3.60	3.23	2.85
7811.60	4.60	3.59	3.26	2.85
7834.54	4.53	3.53	3.18	2.79
7867.45	4.58	3.57	3.22	2.80
7905.30	4.56	3.57	3.22	2.82
7921.35	4.48	3.49	3.16	2.75
8104.68	4.63	3.62	3.29	2.90
8107.66	4.60	3.61	3.26	2.84
8160.61	4.49	3.51	3.17	2.76
8962.32	4.62	3.61	3.27	2.85
8997.34	4.65	3.64	3.30	2.89
9005.28	4.60	3.61	3.28	2.85
9023.30	4.60	3.60	3.26	2.88
03318–5334 SAO 233156				
6488.31	5.77	4.81	4.61	4.46
6644.59	5.74	4.81	4.60	4.46
03318–8244				
6309.56*	6.68	5.65	5.34	5.08
6442.36	6.74	5.72	5.41	(5.2)
6657.66	6.70	5.69	5.40	5.16
6663.58	6.65	5.64	5.35	5.12
6693.57	6.79	5.76	5.42	5.26
6723.53	6.64	5.62	5.32	5.16
6748.40	6.60	5.59	5.30	5.02
6753.42	6.62	5.61	5.30	5.02
6779.32	6.64	5.62	5.33	5.05
6781.32	6.62	5.61	5.30	5.05
6812.36	6.66	5.64	5.34	5.19
6833.27	6.68	5.63	5.32	5.19
6876.24*	6.67	5.63	5.33	5.09
7013.68	7.06	6.05	5.74	5.44
7056.56	6.68	5.66	5.36	5.09
7073.52	6.76	5.74	5.47	5.25
7125.39	6.91	5.88	5.63	5.46
7143.35	6.67	5.66	5.38	5.16
7173.32	6.67	5.63	5.33	
7410.62	6.71	5.72	5.45	5.21
7416.54	6.70	5.69	5.39	5.12
7438.55	6.75	5.72	5.41	5.18
7461.49	6.73	5.72	5.42	5.14
7492.40	6.75	5.71	5.41	5.17
7508.37	6.76	5.76	5.48	5.22
7509.39	6.70	5.69	5.39	5.05
7524.43	6.75	5.73	5.43	(5.1)
7532.32	6.75	5.74	5.43	5.05
7539.37	6.76	5.76	5.45	5.08
7546.29	6.76	5.74	5.43	5.11
7728.70	6.63	5.61	5.32	5.08
7742.67	6.62	5.61	5.31	5.04
7760.67	6.87	5.83	5.56	5.43
7776.65	6.74	5.74	5.47	5.19
7794.53	6.70	5.67	5.44	5.15
7807.53	6.67	5.65	5.35	5.11

Table 2 – *continued*

JD −2440000	J	H	K	L
		(mag)		
03318–8244 continued				
7815.50	6.65	5.66	5.37	5.07
7817.48	6.93	5.91	5.59	5.36
7823.51	6.68	5.67	5.37	5.17
7836.49	6.64	5.66	5.36	5.11
7843.42	6.70	5.67	5.37	5.18
7862.39	6.66	5.66	5.37	5.12
7875.46	6.68	5.67	5.36	5.16
7890.44	6.65	5.65	5.35	5.11
7897.34	6.65	5.65	5.34	5.04
7903.37	6.65	5.66	5.36	5.10
7917.30	6.66	5.66	5.36	5.21
8110.68	6.70	5.67	5.37	5.16
8116.68	6.70	5.67	5.36	5.18
8163.53	6.69	5.64	5.34	5.11
8172.60	6.66	5.65	5.36	5.10
03323–2547				
6276.70	4.64	3.63	3.30	2.99
6465.28	4.57	3.55	3.24	
03324–4728				
6308.66	7.46	6.49	6.15	
6430.42	7.08	6.14	5.86	5.48
6463.32	7.15	6.19	5.87	
8931.51	7.06	6.18	5.88	(5.5)
8960.40	7.15	6.23	5.92	
8967.41	7.17	6.24	5.94	(5.7)
8986.32	7.14	6.21	5.90	
8997.35	7.13	6.20	5.88	5.52
9004.32	7.12	6.21	5.90	5.52
9024.29	7.22	6.27	5.93	5.66
03388–1054 VY Eri				
6488.30	3.38	2.33	2.05	1.84
03430+0325				
6308.61	4.85	3.71	3.38	3.18
6356.49	4.86	3.74	3.41	3.12
03489+1257				
6313.62	6.24	5.13	4.79	4.57
6356.50	6.23	5.14	4.79	4.56
03499–3041				
6310.54	5.10	4.11	3.82	3.54
6441.37	5.15	4.16	3.85	3.57
04020–1551 V Eri				
6487.27	0.88	−0.19	−0.56	−0.86
04026–3024				
6309.60	5.47	4.48	4.20	3.96
6440.32	5.51	4.53	4.22	3.92
04037–1846 AT Eri				
6487.28	5.32	4.32	4.04	3.81
04060–0447 Ste-30				
6311.54	5.24	4.19	3.82	3.54
6440.38	5.20	4.17	3.80	3.52
04067–0922				
6310.68	5.84	4.47	3.69	3.06
6335.59	5.96	4.62	3.78	3.18
6356.51	5.85	4.56	3.77	3.17
6390.47	5.41	4.25	3.61	3.03
6440.39	5.31	4.13	3.53	3.00
6490.31	5.36	4.07	3.45	2.90
6641.69	5.40	4.22	3.63	3.09
6663.61	5.36	4.16	3.58	3.03
6690.64	5.34	4.11	3.49	2.93
6721.56	5.55	4.23	3.52	2.90
6750.44	5.77	4.37	3.60	2.93
6758.43	5.78	4.39	3.61	2.95
6777.38	5.73	4.35	3.59	2.88
6782.38	5.70	4.34	3.58	2.93
6810.31	5.62	4.29	3.56	3.00
6826.31	5.53	4.26	3.57	2.99
04067–0922 continued				
6865.27	5.39	4.19	3.59	3.08
7007.68	6.01	4.57	3.73	3.02
7054.59	5.77	4.45	3.70	3.10
7120.44	5.35	4.15	3.58	3.03
7138.43	5.32	4.07	3.51	3.00
7150.34	5.32	4.08	3.48	2.86
7173.36	5.55	4.22	3.52	2.92
7366.66	5.14	3.98	3.46	2.97
7422.64	5.64	4.31	3.61	2.91
7462.49	5.95	4.54	3.71	3.03
7498.48	5.83	4.44	3.68	3.06
7536.33	5.61	4.34	3.69	3.15
7744.65	5.80	4.48	3.71	3.15
7778.63	5.53	4.32	3.67	3.19
7812.56	5.28	4.12	3.57	3.03
7843.47	5.38	4.15	3.55	2.94
7866.47	5.58	4.29	3.60	2.96
8107.68	5.78	4.42	3.66	2.97
8160.62	6.38	4.90	3.95	3.14
8256.35	5.50	4.28	3.64	3.08
8298.31	5.38	4.13	3.51	2.90
8500.64	5.12	3.99	3.49	2.97
8588.44	6.05	4.61	3.77	3.01
8619.36	6.25	4.76	3.87	3.15
8634.35	6.12	4.67	3.84	3.16
8875.61	5.52	4.24	3.55	2.98
8899.52	5.55	4.28	3.62	3.05
8932.49	5.23	4.09	3.53	2.99
8961.42	5.13	3.96	3.44	2.92
8968.36	5.12	3.97	3.44	2.83
9001.32	5.45	4.18	3.52	2.85
04085+0653				
6310.66	6.47	5.41	5.07	4.77
6443.29	6.58	5.49	5.13	4.77
6463.29	6.57	5.49	5.11	
04120–6516				
6309.63	7.15	6.13	5.77	5.29
6338.50	7.24	6.22	5.84	5.45
6392.42*	7.22	6.17	5.76	5.32
04120–6516 continued				
6439.35	7.55	6.51	6.10	(5.7)
6493.26	7.38	6.39	6.02	(5.6)
6643.68	7.40	6.35	5.99	5.57
6664.59	7.63	6.64	6.23	5.84
6692.50	7.59	6.62	6.21	5.86
6724.49	7.38	6.40	6.03	(5.7)
6752.46	7.31	6.32	5.98	5.62
6778.37	7.25	6.27	5.94	5.51
6782.41	7.26	6.27	5.93	5.55
6812.34	7.24	6.25	5.91	
6823.32	7.30	6.28	5.93	
6833.30	7.35	6.31	5.94	(5.5)
6844.31	7.36	6.33	5.97	5.69
6847.26	7.34	6.35	5.98	
6868.27	7.49	6.49	6.11	
7007.69	7.24	6.23	5.88	5.51
7054.64	7.31	6.27	5.91	5.45
7122.47	7.60	6.62	6.23	5.87
7143.36	7.44	6.45	6.10	5.61
7179.32	7.21	6.24	5.91	5.45
7409.62	7.17	6.19	5.86	5.52
7417.54	7.19	6.19	5.85	5.58
7438.57	7.27	6.24	5.89	5.50
7460.55	7.28	6.23	5.88	5.54
7492.56	7.28	6.24	5.87	(5.5)
7499.48	7.30	6.27	5.89	(5.6)
7501.48	7.30	6.26	5.89	5.47
7506.41	7.33	6.29	5.92	5.49
7512.45	7.40	6.37	6.00	5.51
7526.30	7.51	6.51	6.11	5.66
7531.32	7.59	6.58	6.19	5.56
7539.39	7.65	6.68	6.27	(5.8)
7543.29	7.69	6.72	6.31	(5.8)
7579.28	7.46	6.53	6.18	(5.8)
7608.25	7.26	6.30	5.98	(5.6)
7644.21	7.30	6.32	5.97	
7713.72	7.30	6.28	5.92	
7719.69	7.34	6.30	5.94	5.62
7730.68	7.39	6.36	5.99	5.67
7743.65	7.47	6.44	6.05	5.76

Table 2 – *continued*

JD −2440000	J	H	K	L
		(mag)		
04120–6516 continued				
7767.62	7.50	6.48	6.11	5.72
7780.63	7.47	6.47	6.09	5.72
7792.59	7.37	6.36	5.99	5.66
7803.58	7.27	6.24	5.89	5.61
7815.53	7.12	6.15	5.82	5.44
7821.53	7.11	6.13	5.78	5.39
7836.52	7.12	6.15	5.80	(5.3)
7842.47	7.16	6.16	5.81	5.44
7847.49	7.18	6.17	5.81	5.41
7853.49	7.22	6.20	5.82	5.45
7862.41	7.23	6.22	5.86	
7865.46	7.26	6.23	5.86	5.44
7872.49	7.32	6.27	5.88	
7873.45	7.27	6.26	5.89	5.42
7889.45	7.30	6.27	5.88	5.47
7896.43	7.32	6.28	5.91	
7902.37	7.33	6.27	5.90	5.45
7905.37	7.31	6.28	5.89	5.55
7917.33	7.35	6.30	5.91	5.54
7961.31	7.42	6.40	6.00	5.65
8116.66	7.27	6.22	5.84	5.50
8129.68	7.19	6.18	5.80	5.39
8161.62	7.39	6.36	5.98	5.52
8172.62	7.45	6.44	6.03	5.62
8196.55	7.55	6.55	6.15	(5.8)
8212.43	7.53	6.54	6.15	
8227.44	7.49	6.50	6.13	(5.6)
8254.36	7.27	6.29	5.96	(5.5)
8284.33	7.18	6.19	5.82	(5.4)
8295.31	7.22	6.21	5.83	5.45
8317.39	7.25	6.20	5.82	
8326.29	7.19	6.17	5.79	5.50
8491.63	7.16	6.16	5.84	5.36
8502.55	7.16	6.16	5.79	5.33
8517.61	7.26	6.22	5.85	5.52
8529.57	7.26	6.24	5.87	5.45
8576.50	7.23	6.19	5.81	5.42
8620.45	7.50	6.47	6.06	(5.7)
8630.31	7.51	6.49	6.08	5.62
8672.27	7.34	6.36	5.99	5.51
8851.66	7.56	6.55	6.15	5.75
8872.66	7.54	6.51	6.12	5.73
8877.58	7.47	6.48	6.09	5.61
8899.56	7.30	6.30	5.96	5.44
8931.53	7.16	6.16	5.80	5.31
8936.44	7.17	6.17	5.81	5.43
8960.42	7.16	6.14	5.77	(5.4)
8966.40	7.17	6.14	5.77	5.38
8988.34	7.26	6.20	5.81	5.45
9002.31	7.31	6.26	5.85	5.30
9022.33	7.45	6.41	5.98	5.55
04127+0110				
6313.66	6.94	5.88	5.55	5.25
6335.61	7.00	5.95	5.59	5.30
7502.43	7.01	5.93	5.60	(5.3)
7531.37	6.98	5.92	5.59	
7542.31	7.03	5.94	5.61	5.36
7620.23	6.99	5.93	5.59	5.38
7746.65	7.05	5.93	5.60	
7793.61	7.04	5.96	5.63	5.39
7816.53	7.01	5.95	5.62	5.33
7842.50	6.98	5.92	5.60	5.34
7865.49	6.97	5.92	5.59	5.32
7900.44	7.05	5.98	5.64	(5.4)
7918.29	7.03	5.95	5.62	5.37
7962.25	7.05	5.98	5.64	5.42
8163.61	7.01	5.93	5.61	5.41
8211.46	7.04	5.95	5.63	
8232.47	7.03	5.97	5.62	(5.3)
8255.43	6.97	5.89	5.56	(5.4)
8283.32	7.00	5.92	5.59	5.47
8326.27	7.02	5.95	5.61	(5.4)
8520.64	7.07	5.98	5.65	5.36
8589.49	7.07	5.98	5.65	5.33
8617.42	7.01	5.93	5.58	5.36
8897.64	7.12	6.03	5.70	(5.4)
8935.44	7.03	5.96	5.63	5.38
8967.37	7.07	5.97	5.65	5.35
04147–1220 Ste-32				
6314.58	6.06	5.09	4.76	4.46
6440.37	6.04	5.06	4.74	4.50
7417.60	5.94	4.95	4.62	4.31
7551.32	5.99	4.99	4.64	4.31
04177–1850 AV Eri				
6488.33	4.26	3.23	2.89	2.63
04183–4310				
6314.60	5.57	4.57	4.25	3.99
6430.45	5.49	4.47	4.16	3.88
6438.37	5.48	4.49	4.18	3.96
04191+0346				
5958.63	5.17	4.07	3.74	
6317.59	5.20	4.06	3.75	3.50
6356.52	5.19	4.06	3.73	3.50
04199–2248 NSV 1578 Ste-34				
6489.30	3.73	2.71	2.40	2.17
7412.66	3.66	2.67	2.37	2.12
04238–6713				
6309.65	7.04	6.06	5.72	(5.3)
6338.52	7.02	6.06	5.70	5.32
6392.43*	6.97	5.99	5.61	5.20
6438.38	6.93	5.96	5.61	
6493.27	6.98	6.01	5.64	(5.2)
6643.69	6.99	6.01	5.67	5.21
6664.62	7.04	6.07	5.70	5.30
6694.61	6.92	5.98	5.65	(5.1)
6724.52	6.91	5.94	5.60	5.17
6751.51	6.97	5.97	5.64	5.27
6779.36	6.98	6.00	5.65	5.30
6783.39	6.94	5.97	5.63	5.28
6788.33	6.90	5.94	5.61	(5.4)
6828.32	6.98	6.01	5.64	5.31
6847.28	6.99	6.03	5.67	5.04
6868.28	6.94	6.01	5.66	
7025.62	6.91	5.93	5.58	5.24
7070.57	6.93	5.98	5.61	5.17
7128.39	6.93	5.98	5.60	
7149.33	6.99	6.01	5.64	(5.0)
7185.36	7.06	6.10	5.72	5.27
04257–3220				
6317.63	6.26	5.26	5.03	4.81
6439.39	6.28	5.27	5.02	
04258–0155				
6490.28	8.91	7.89	7.61	
04375–3216				
6308.56*	7.22	6.26	6.04	5.86
6439.38	7.20	6.22	5.98	
04382–1417 BX Eri				
6488.34	1.99	0.87	0.45	0.14
04451–0539S				
6308.58*	11.05	9.81	8.99	7.97
6392.38*	11.08	9.84	8.95	7.93
6489.26*	10.69	9.45	8.61	7.70
7099.46*	11.06	9.82	8.92	7.78
8942.43*	11.19	9.87	9.06	7.98
04451–0539N				
6392.36*	11.19	10.37	10.18	9.89
6489.28*	11.27	10.44	10.21	9.99
7099.47*	11.23	10.43	10.23	10.00
8942.44*	11.20	10.34	10.14	
04523–1359				
6308.61*	6.82	5.83	5.58	5.41
6430.48	6.78	5.78	5.54	
04576–2555				
6309.67	4.42	3.41	3.10	2.84
6439.37	4.50	3.45	3.11	2.88

Table 2 – *continued*

JD −2440000	J	H	K	L
		(mag)		
05074–2654				
6317.64	4.70	3.67	3.36	3.10
6439.41	4.74	3.72	3.38	3.12
05166–3109				
6314.65	6.76	5.73	5.48	5.30
6430.49	6.73	5.72	5.48	
05217–3943 SW Col				
6488.35	2.30	1.36	1.16	1.00
19496–6812				
6334.39	4.92	3.87	3.53	3.26
19521–5131				
6310.48*	9.18	8.31	8.00	7.45
6338.36	9.06	8.16	7.89	
6348.32	9.04	8.13	7.83	
6561.62	9.11	8.12	7.82	
6595.59	8.99	8.02	7.71	
6627.50	8.99	8.01	7.70	
6639.47	9.04	8.05	7.71	
6691.30	9.16	8.18	7.85	
6726.33	9.02	8.07	7.80	
6910.60	9.12	8.10	7.81	
6915.66	9.15	8.15	7.84	
6923.64	9.22	8.19	7.86	
6959.57	9.29	8.31	7.93	
6967.60	9.27	8.32	7.97	
6990.52	9.10	8.17	7.89	
7021.41	9.10	8.14	7.83	
7034.39	9.14	8.16	7.86	
7055.39	9.14	8.12	7.81	
7071.39	9.13	8.12	7.81	
7082.38	9.12	8.10	7.79	
7322.60	9.04	8.06	7.76	
7337.49	9.13	8.11	7.82	
7343.51	9.11	8.10	7.80	
7358.46	9.11	8.14	7.81	
7369.47	9.12	8.12	7.83	
7379.49	9.11	8.11	7.77	
7385.39	9.09	8.10	7.81	
19521–5131 continued				
7429.30	9.06	8.09	7.80	
7666.66	9.14	8.15	7.84	
7684.65	9.14	8.19	7.89	
7698.55	9.04	8.10	7.85	
7702.52	9.01	8.06	7.77	
7709.53	8.99	8.02	7.75	
7723.45	8.98	8.00	7.74	
7732.49	9.02	8.03	7.74	
7741.46	9.05	8.07	7.77	
7764.51	9.13	8.14	7.84	
7776.35	9.11	8.12	7.82	
7789.33	9.10	8.10	7.81	
7807.28	9.10	8.10	7.80	
7815.30	9.08	8.11	7.80	
7821.31	9.07	8.09	7.79	
7836.33	8.99	8.01	7.71	
8054.64	9.25	8.24	7.94	
8060.58	9.24	8.25	7.95	
8074.58	9.33	8.28	7.97	
8079.48	9.25	8.26	7.94	
8089.59	9.22	8.27	7.95	
8104.45	9.12	8.15	8.00	
8115.48	9.09	8.14	7.85	
8124.36	9.04	8.10	7.83	
8129.39	9.02	8.07	7.80	
8135.36	9.03	8.07	7.79	
8144.38	9.10	8.12	7.84	
8162.38	9.18	8.19	7.86	
8173.34	9.18	8.19	7.88	
8177.26	9.13	8.18	7.87	
8195.28	9.19	8.21	7.90	
8210.29	9.18	8.17	7.89	
8211.26	9.18	8.20	7.88	
8212.25	9.19	8.19	7.89	
8214.25	9.17	8.20	7.87	
8389.66	9.04	8.05	7.77	
8437.49	9.09	8.08	7.82	
8450.49	9.13	8.14	7.80	
8456.48	9.12	8.13	7.83	
8462.44	9.08	8.06	7.81	
19521–5131 continued				
8465.45	9.12	8.13	7.80	
8491.44	9.16	8.17	7.87	
8492.37	9.09	8.08	7.78	7.20
8499.40	9.06	8.10	7.80	
8521.42	9.07	8.06	7.78	
8528.38	9.03	8.07	7.78	
8758.65	9.20	8.27	7.95	
8760.60	9.16	8.23	7.91	
8768.59	9.17	8.21	7.93	
8793.59	9.06	8.11	7.81	
8785.57	9.05	8.10	7.81	
8787.58	9.05	8.11	7.83	
8790.56	9.07	8.13	7.85	
8815.56	9.14	8.15	7.86	
8817.52	9.13	8.14	7.87	
8840.41	9.09	8.13	7.87	
8853.39	9.09	8.13	7.83	
8869.35	9.09	8.12	7.81	
8874.37	9.11	8.11	7.81	
8899.37	9.10	8.13	7.80	
8932.28	9.00	8.04	7.75	
19539–5915				
6301.36	4.48	3.44	3.12	2.86
19549–4931 HD 188707				
6301.37	4.20	3.18	2.84	2.51
19575–4317				
6276.36	6.78	5.82	5.53	5.32
6304.40	6.69	5.76	5.46	5.25
6338.37	6.70	5.74	5.45	5.30
6568.62	6.57	5.65	5.36	5.03
6643.43	6.76	5.83	5.53	
6693.37	6.59	5.66	5.38	(5.1)
6726.30	6.54	5.62	5.41	(5.1)
20043–4533				
6305.39	6.27	5.28	5.02	4.84
20116–5445 NSV 12922				
6623.51	3.32	2.33	2.04	1.82
20120–4433 RZ Sgr				
2587.50	3.12	1.90	1.41	1.06
2620.50	3.18	2.02	1.59	1.32
2912.50	2.38	1.38	1.07	0.65
2940.50	2.33	1.31	0.97	0.58
2971.50	2.67	1.53	1.13	0.76
3012.50	3.27	2.01	1.50	1.16
3059.50	2.66	1.78	1.47	1.11
3083.50	2.75	1.73	1.44	1.11
3287.59	2.76	1.81	1.50	1.13
3311.62	2.61	1.64	1.33	0.96
3346.48	2.40	1.36	1.02	0.68
3379.39	2.58	1.47	1.08	0.71
3386.40	2.63	1.51	1.10	0.72
3412.33	2.90	1.72	1.29	0.91
3428.37	3.01	1.84	1.43	1.06
3439.34	3.08	1.92	1.48	1.16
3453.30	3.00	1.88	1.47	1.15
3644.65	3.14	1.98	1.52	1.17
3698.57	2.80	1.80	1.46	1.11
3818.25	2.91	1.70	1.22	0.89
4079.54	2.97	1.89	1.51	1.18
4109.44	2.84	1.81	1.47	1.11
4185.26	2.51	1.40	1.03	0.73
4441.46	2.97	1.74	1.28	0.92
4449.51	3.09	1.82	1.35	1.00
5261.38	2.80	1.65	1.17	0.83
5632.29	2.38	1.32	1.00	0.67
5924.43	3.34	2.06	1.55	1.22
8779.68	2.38	1.30	0.94	0.55
20125–5153				
6310.48*	7.09	6.14	5.87	5.63
20174–7853				
6276.41	7.67	6.66	6.39	
7399.36*	7.67	6.63	6.34	6.05

Table 2 – *continued*

JD −2440000	J	H	K	L
		(mag)		
20176–2527				
6309.48*	6.45	5.41	5.07	4.81
20220–8027				
6310.49*	6.75	5.73	5.39	5.13
6338.39	6.79	5.74	5.41	
6581.68	6.77	5.70	5.39	
6597.61	6.81	5.72	5.39	5.22
6644.52	6.77	5.71	5.38	
6697.35	6.81	5.74	5.41	5.22
6725.34	6.71	5.67	5.37	5.10
20240–2142				
6276.44	6.46	5.49	5.20	4.93
6339.43	6.51	5.55	5.26	5.04
6394.27	6.69	5.75	5.46	(5.2)
6597.60	6.48	5.51	5.21	4.87
6640.46	6.52	5.54	5.25	4.92
6644.50	6.49	5.54	5.24	4.88
6696.34	6.46	5.51	5.22	4.97
6729.40	6.55	5.58	5.27	
6749.27	6.61	5.62	5.32	5.16
6954.52	6.54	5.61	5.30	5.03
6965.61	6.56	5.62	5.31	5.01
7007.56	6.56	5.62	5.34	5.08
7025.41	6.58	5.62	5.32	5.00
7054.39	6.49	5.55	5.27	
7073.38	6.51	5.54	5.25	5.02
7330.59	6.60	5.63	5.32	
7355.52	6.51	5.59	5.29	4.96
7379.54	6.44	5.52	5.22	4.86
7410.38	6.43	5.49	5.21	4.94
7431.30	6.49	5.55	5.27	4.96
7460.27	6.52	5.56	5.28	4.98
7668.66	6.51	5.56	5.25	4.97
7685.66	6.55	5.56	5.26	5.00
7705.53	6.56	5.59	5.30	5.04
7736.45	6.50	5.54	5.23	4.90
7742.54	6.50	5.53	5.23	4.93
7780.34	6.50	5.53	5.23	5.00
7812.39	6.51	5.53	5.23	4.96
7821.34	6.50	5.53	5.24	4.97
20240–2142 continued				
7834.32	6.48	5.51	5.22	4.98
7842.29	6.49	5.51	5.23	4.94
8048.66	6.53	5.57	5.29	5.00
8074.60	6.55	5.61	5.32	5.03
8087.54	6.54	5.59	5.31	5.00
8116.53	6.52	5.57	5.28	5.01
8125.45	6.59	5.62	5.32	5.09
8141.41	6.56	5.63	5.32	5.02
8161.36	6.58	5.62	5.33	5.07
8173.38	6.55	5.59	5.30	5.05
8179.25	6.55	5.58	5.29	5.07
8198.28	6.53	5.59	5.30	4.95
8211.27	6.55	5.57	5.27	
8212.26	6.58	5.59	5.31	5.08
8213.27	6.57	5.60	5.30	
8454.50	6.59	5.63	5.34	5.08
8465.49	6.61	5.65	5.35	5.09
8499.44	6.64	5.68	5.40	5.16
8574.26	6.59	5.60	5.30	5.12
8760.65	6.41	5.46	5.16	4.82
8768.62	6.49	5.53	5.23	4.92
8783.61	6.56	5.61	5.31	5.04
8812.52	6.51	5.57	5.29	5.02
8852.56	6.64	5.68	5.38	5.11
8874.41	6.61	5.66	5.37	5.09
8875.42	6.62	5.67	5.37	5.15
8876.43	6.61	5.66	5.37	5.16
8895.29	6.63	5.67	5.37	5.11
8897.33	6.60	5.66	5.35	4.98
8932.32	6.61	5.63	5.32	(5.1)
20250–3557				
6620.60	5.93	4.84	4.43	4.09
6645.53	5.94	4.84	4.43	4.08
20270–2858				
6328.42*	6.76	5.79	5.42	4.95
6339.36	6.81		5.42	
6357.30	6.89	5.84	5.44	4.97
6394.26*	7.05	6.02	5.59	4.98
20270–2858 continued				
6568.66	7.00	5.99	5.56	4.98
6597.63				5.07
6642.51	6.88	5.95	5.56	5.01
6691.35	6.80	5.77	5.36	4.97
6721.34	6.99	5.94	5.48	5.01
6748.30	7.05	5.97	5.53	4.98
6949.63	6.94	5.87	5.47	4.93
6983.65	6.95	5.89	5.47	4.99
6990.53	6.91	5.86	5.46	5.02
7009.55	6.78	5.75	5.39	
7055.22	6.94	5.87	5.47	4.99
7073.40	7.02	5.97	5.55	5.00
7121.26	6.90	5.83	5.43	4.84
7366.48	6.80	5.76	5.37	4.88
7378.50	6.77	5.72	5.33	4.87
7410.40	6.86	5.78	5.36	4.91
7428.33	6.94	5.83	5.41	4.93
7438.29	6.92	5.84	5.43	4.93
7460.25	7.03	5.91	5.49	5.03
7666.67	6.92	5.84	5.41	4.89
7685.68	6.89	5.83	5.40	4.91
7702.54	6.84	5.79	5.39	4.91
7709.57	6.80	5.76	5.36	4.90
7723.52	6.77	5.72	5.32	4.86
7730.57	6.76	5.70	5.31	4.80
7742.55	6.79	5.70	5.31	4.79
7759.43	6.86	5.74	5.33	4.85
7767.42	6.87	5.79	5.37	4.90
7780.36	6.94	5.83	5.41	4.91
7792.38	6.97	5.87	5.44	5.01
7807.31	6.97	5.88	5.45	5.02
7815.36	6.95	5.85	5.43	4.95
7834.33	6.86	5.77	5.36	4.87
8068.66	6.75	5.69	5.26	4.76
8087.58	6.81	5.72	5.29	4.79
8110.55	6.85	5.78	5.34	4.83
8129.42	6.78	5.71	5.29	4.77
8134.39	6.77	5.70	5.28	4.75
8141.42	6.72	5.67	5.25	4.70
8162.40	6.78	5.67	5.24	
8164.35	6.77	5.68	5.26	4.81
20270–2858 continued				
8172.36	6.76	5.68	5.26	4.75
8179.30	6.70	5.64	5.23	4.67
8198.31	6.70	5.64	5.22	4.67
8211.26	6.72	5.64	5.22	4.71
8390.67	6.81	5.72	5.27	4.75
8427.57	6.89	5.81	5.38	4.81
8453.52	6.80	5.72	5.30	4.81
8465.50	6.78	5.72	5.31	4.82
8499.46	6.76	5.70	5.30	4.80
8519.32	6.63	5.59	5.21	4.72
8575.26	6.79	5.75	5.32	4.77
8760.66	6.84	5.78	5.35	4.86
8783.62	6.99	5.93	5.50	5.03
8790.58	7.00	5.98	5.53	5.01
8812.54	6.87	5.84	5.44	4.95
8840.44	6.63	5.59	5.23	4.72
8851.56	6.66	5.61	5.23	4.69
8869.36	6.70	5.65	5.24	4.71
8874.42	6.72	5.66	5.25	4.73
8897.34	6.66	5.60	5.20	4.60
8933.30	6.82	5.78	5.34	4.81
8964.25	7.10	6.07	5.62	5.10
20271–2340				
6309.43	6.72	5.82	5.52	
6339.35	6.53	5.59	5.32	5.04
6357.31	6.49	5.54	5.26	5.02
6392.27*	6.47	5.49	5.19	4.87
6568.68	6.48	5.53	5.25	4.91
6644.49	6.86	5.91	5.57	
6664.48	6.88	5.94	5.63	5.36
6696.38	6.66	5.74	5.47	5.22
6729.36	6.48	5.56	5.28	5.18
6750.26	6.45	5.50	5.23	5.00
6949.64	6.43	5.47	5.19	(4.8)
6983.64	6.55	5.55	5.23	
6990.55	6.59	5.60	5.27	4.94
7009.54	6.73	5.78	5.45	5.06
7055.43	6.87	5.97	5.64	5.24
7074.36	6.80	5.88	5.61	5.16

Table 2 – *continued*

JD −2440000	J	H	K	L
		(mag)		
20271–2340 continued				
7081.40	6.72	5.81	5.51	5.18
7120.25	6.46	5.55	5.26	5.04
7366.49	6.53	5.55	5.24	4.91
7378.52	6.54	5.57	5.24	4.93
7410.42	6.63	5.65	5.29	4.97
7689.62	6.49	5.59	5.32	5.02
7723.50	6.48	5.53	5.24	4.95
7745.47	6.51	5.55	5.26	4.95
7792.39	6.71	5.72	5.39	5.02
7815.34	6.72	5.76	5.43	5.22
8048.69	6.51	5.59	5.29	4.93
8087.56	6.49	5.55	5.26	4.94
8113.52	6.45	5.51	5.22	(4.8)
8129.43	6.50	5.53	5.21	4.95
8164.36	6.76	5.79	5.44	5.10
8198.30	6.84	5.95	5.60	5.20
8210.31	6.74	5.83	5.49	
8213.28	6.72	5.81	5.49	
8427.59	6.57	5.63	5.24	5.02
8453.53	6.50	5.56	5.27	4.94
8465.52	6.50	5.56	5.27	4.96
8499.47	6.43	5.47	5.18	4.82
8520.40	6.49	5.50	5.18	4.91
8575.28	6.81	5.90	5.56	5.30
8760.67	6.72	5.75	5.41	5.05
8787.63	6.78	5.83	5.50	(5.2)
8812.56	6.64	5.72	5.40	5.11
8840.45	6.41	5.47	5.18	4.85
8850.55	6.36	5.45	5.15	
8869.37	6.40	5.47	5.16	4.79
8874.44	6.43	5.47	5.15	4.79
8897.37	6.47	5.50	5.18	4.80
8933.31	6.61	5.63	5.29	4.98
20277–3959 SW Mic				
6623.53	6.78	5.84	5.56	5.25
20282–3310 SAO 212196				
6623.55	6.05	5.05	4.80	4.54
20295–6546				
6276.48	5.09	4.03	3.66	3.37
20298–3405				
6309.44	3.92	2.89	2.59	2.35
20333–2428				
6311.40	6.17	5.15	4.83	4.48
20356–2815 IRC−30°433				
6624.51	4.12	3.07	2.68	2.37
20381–2827				
6313.41	5.72	4.72	4.45	4.18
20412–2229 Ste-524				
6313.44	4.62	3.56	3.23	2.92
20459–4917				
6313.47	6.76	5.78	5.56	5.32
20466–4105				
6276.49	5.45	4.47	4.14	3.81
20487–1117 AFGL 2666 Ste-529				
6624.53	3.30	2.27	1.94	1.68
7385.50	3.26	2.24	1.91	1.62
20522–5711				
6276.51	5.16	4.18	3.89	3.66
20545–1709 XY Cap				
6624.54	6.33	5.30	5.00	(4.9)
20559–1055 DG Aqr				
6642.47	4.71	3.67	3.33	3.06
20561–5253				
6305.41	6.13	5.13	4.83	4.59
20575–5806				
6311.48*	6.86	5.88	5.62	5.41
20577–4504				
6310.50*	6.55	5.57	5.26	5.00
20598–2358				
6276.46	4.80	3.81	3.52	3.27
20599–3941				
6305.42	4.61	3.60	3.23	2.93
21015–0214 TW Aqr				
6642.48	6.26	5.28	5.00	4.75
21034–0823				
6642.49	5.78	4.81	4.54	4.34
21041–5746				
6276.58	5.40	4.40	4.09	3.86
21060–0029				
6309.53*	8.77	7.81	7.56	7.25
21095–5222				
6305.44	3.78	2.76	2.44	2.14
21097–3627				
6276.56	5.40	4.48	4.22	3.99
21151–2340				
6314.43	6.64	5.60	5.31	5.06
21159–5222				
6311.49*	6.57	5.58	5.29	5.02
21160–6728 NSV 13648				
6643.47	3.54	2.52	2.25	2.04
21208–3350				
6311.50*	5.58	4.63	4.39	4.20
21270+0702				
6314.45	6.26	5.25	4.94	4.67
6347.37	6.26	5.26	4.95	
7466.26	6.27	5.24	4.93	4.69
7688.63	6.30	5.28	4.95	4.69
7794.37	6.28	5.26	4.95	4.68
7835.29	6.30	5.29	4.96	4.72
8050.63	6.31	5.28	4.98	4.71
8094.59	6.39	5.37	5.03	4.76
8164.40	6.34	5.29	4.96	4.66
8211.29	6.27	5.22	4.90	4.61
8501.47	6.16	5.13	4.81	4.51
8577.26	6.25	5.19	4.86	4.57
8760.68	6.18	5.13	4.80	4.51
8785.61	6.22	5.16	4.83	4.56
8843.47	6.18	5.15	4.82	4.50
8869.40	6.30	5.26	4.94	4.61
8936.32	6.13	5.12	4.80	4.53
21317–5948				
6314.50	5.83	4.82	4.52	4.33
21318–5130				
6314.49	6.65	5.64	5.36	5.14
21365+0526				
6334.38	6.56	5.56	5.21	
21368–3812 AFGL 5595				
6270.50	2.34	1.30	0.95	0.64
21377–0200 AFGL 2787 Ste-546				
6641.55	2.17	1.13	0.77	0.45
7426.36	2.06	1.04	0.71	0.43
7447.31	2.11	1.07	0.75	0.48
7688.66	2.16	1.13	0.80	0.52
7735.52	2.02	1.04	0.75	0.41
7746.55	2.08	1.08	0.76	0.45
7761.44	2.11	1.08	0.76	0.48
7817.32	2.18	1.15	0.81	0.54
7843.28	2.21	1.15	0.84	0.53

Table 2 – *continued*

JD −2440000	J	H	K	L
		(mag)		
21377–0200 AFGL 2787 continued				
8050.61	2.14	1.12	0.80	0.52
8073.58	2.14	1.11	0.77	0.51
8109.53	2.18	1.13	0.79	0.52
8164.41	2.19	1.13	0.78	0.49
8210.32	2.13	1.10	0.75	0.46
8500.47	2.14	1.12	0.77	0.47
8577.28	2.19	1.17	0.82	0.53
8760.69	2.08	1.07	0.73	0.41
8785.62	2.11	1.09	0.75	0.44
8843.48	2.24	1.21	0.85	0.55
8869.42	2.30	1.26	0.87	0.61
8936.34	2.12	1.09	0.75	0.46
21392+0230 StHα 190				
5633.32	8.77	8.18	7.87	
5650.28	8.76	8.17	7.87	
5849.65	8.76	8.16	7.79	
5874.60	8.73	8.16	7.78	
5893.53	8.75	8.17	7.79	
5897.58	8.72	8.17	7.76	
5920.52	8.67	8.16	7.77	
5939.45	8.73	8.16	7.75	
5957.39	8.75	8.20	7.77	
6028.29	8.73	8.14	7.75	
6219.63	8.74	8.16	7.80	
6302.45	8.77	8.19	7.87	
6334.39	8.77	8.19	7.89	
6356.39	8.78	8.20	7.89	
7078.38*	8.73	8.16	7.80	6.75
7368.59*	8.73	8.17	7.88	6.96
21396–2256				
6313.50	6.24	5.25	4.99	4.78
21439–0226 EP Aqr				
6641.56	−0.19	−1.20	−1.50	−1.77
21447–7245				
6311.50*	6.47	5.47	5.24	5.08
21505–4320				
6311.45	6.07	5.09	4.79	4.50
21511–6439				
6308.45*	6.27,	5.29	5.01	4.80
6704.41	6.24	5.26	4.99	4.75
21543–1421 NSV 13969				
6641.56	2.08	1.05	0.71	0.41
21562–2547				
6314.53	6.36	5.33	4.90	4.73
6338.39	6.37	5.36	5.04	4.80
22003–0010 AFGL 2835 Ste-549				
6641.57	3.02	2.01	1.72	1.47
7385.51	3.10	2.11	1.81	1.57
22066–2500				
6305.47	5.41	4.43	4.16	3.92
22073–3632				
6274.55	5.24	4.25	3.98	3.72
22103–2731 RX PsA				
3379.52	6.36	5.41	5.17	
3386.48	6.41	5.48	5.19	5.00
22142–8454 BW Oct				
6643.49	1.14	0.06	−0.29	−0.54
6703.36	1.16	0.08	−0.26	−0.52
8905.21	1.18	0.08	−0.28	−0.53
8963.26	1.11	0.04	−0.31	−0.58
22169–0955 ZZ Aqr				
6624.55	6.75	5.84	5.53	
6644.50	6.66	5.76	5.47	5.02
6703.38	7.01	6.07	5.70	5.25
7056.45	7.04	6.11	5.72	
7387.51	6.84	5.90	5.56	
22169–0955 ZZ Aqr continued				
8214.29	6.72	5.82	5.50	
8224.29	6.76	5.84	5.50	5.10
8499.51	7.08	6.17	5.83	5.36
8529.45	6.74	5.86	5.57	5.19
8577.29	6.77	5.84	5.51	5.05
8792.65	6.99	6.02	5.67	5.18
8843.51	7.07	6.18	5.83	5.35
8853.53	6.96	6.07	5.74	5.27
8873.44	6.80	5.91	5.60	5.21
8934.38	6.88	5.93	5.58	(5.2)
22190–0751 DZ Aqr				
6624.56	1.84	0.79	0.45	0.22
22197–3348 HD 212115				
6643.52	5.64	4.69	4.49	4.36
8434.68	5.64	4.68	4.49	4.34
8452.48	5.64	4.68	4.47	4.34
22209–3508				
6272.55	4.22	3.12	2.72	2.41
6334.44	4.22	3.14	2.75	2.43
6381.28	4.26	3.15	2.76	2.47
6392.29	4.23	3.14	2.75	2.46
6596.63	4.17	3.10	2.71	2.37
6638.52	4.17	3.09	2.71	2.39
6655.47	4.19	3.10	2.72	2.42
6691.43	4.24	3.15	2.76	2.44
6713.31	4.21	3.12	2.74	2.42
6741.38	4.11	3.05	2.66	2.28
6753.29	4.12	3.04	2.66	2.34
6794.27	4.21	3.10	2.70	2.43
6959.62	4.14	3.07	2.68	2.33
6986.58	4.18	3.12	2.74	2.41
7009.58	4.22	3.16	2.75	2.42
7033.50	4.23	3.14	2.73	2.40
7071.47	4.18	3.09	2.69	2.35
7114.36	4.27	3.19	2.72	2.39
7142.29	4.28	3.15	2.74	2.41
7335.64	4.32	3.19	2.77	2.45
7358.52	4.24	3.13	2.74	2.42
22209–3508 continued				
7373.54	4.23	3.12	2.72	2.40
7377.59	4.24	3.13	2.72	2.39
7393.46	4.28	3.14	2.73	2.40
7427.34	4.34	3.20	2.78	2.47
7438.34	4.25	3.14	2.73	2.39
8930.34	4.27	3.16	2.77	2.45
8963.29	4.24	3.15	2.75	2.39
8987.27	4.29	3.16	2.75	2.45
22229–6855				
6309.48	6.43	5.45	5.18	5.04
22296+2004				
6334.36	7.46	6.55	6.28	
6710.38	7.42	6.51	6.23	
22359–1417 AB Aqr				
6624.58	2.38	1.36	1.02	0.75
22380+2306				
6334.37	6.64	5.63	5.37	
22458+1401				
6313.52	6.34	5.33	5.05	4.86
22494–2534 TU PsA				
6624.58	2.70	1.67	1.32	1.03
22497+1733				
6655.54*	4.77	3.71	3.36	3.07
22553+1744 BI Peg				
6624.60	3.66	2.51	2.12	1.88
23082+1903 BD+18°5117				
6264.61*	5.10	4.10	3.86	3.53
23115+0953 BD+09°5182				
6624.60	5.07	4.07	3.84	3.66

Table 2 – *continued*

JD −2440000	J	H	K	L
		(mag)		
23196+1615				
6642.53	5.15	4.14	3.84	3.64
23198–0230 StHα 202				
6655.60*	9.47	8.43	7.59	6.32
6703.43	9.57	8.47	7.57	
6719.36*	9.57	8.45	7.53	6.23
6959.68	9.63	8.49	7.55	6.27
6986.60	9.54	8.44	7.56	
7011.55	9.57	8.44	7.60	
7023.54	9.40	8.32	7.50	
7054.50	9.52	8.38	7.47	
7082.50	9.43	8.31	7.45	
7113.38	9.44	8.34	7.46	
7330.67	9.78	8.45	7.38	
7364.59	9.65	8.39	7.33	
7376.57	9.51	8.34	7.33	
7426.42	9.60	8.39	7.44	
7446.36	9.46	8.36	7.44	
7709.64	9.48	8.28	7.34	
7735.58	9.38	8.25	7.36	
7760.52	9.50	8.35	7.39	6.24
7793.47	9.84	8.59	7.56	
7815.43	9.67	8.48	7.49	
7835.34	9.61	8.43	7.48	
8067.69	9.59	8.43	7.49	
8093.66	9.43	8.33	7.44	
8109.58	9.32	8.26	7.43	
8160.48	9.04	8.05	7.27	
8173.46	9.07	8.09	7.30	
8212.30	9.31	8.19	7.32	
8491.50	9.41	8.28	7.37	6.03
8529.48	9.57	8.38	7.38	(6.1)
8582.29	9.33	8.18	7.23	6.00
8785.69	9.18	8.16	7.38	(6.4)
8846.66	9.20	8.15	7.33	
8874.49	9.40	8.25	7.35	
8899.45	9.27	8.21	7.34	
8936.39	9.35	8.21	7.31	(6.0)
8961.33	9.33	8.24	7.33	
8966.31	9.31	8.23	7.30	

JD −2440000	J	H	K	L
		(mag)		
23218–7719 TV Oct				
6641.63	6.98	5.98	5.67	5.45
23236–6917				
6272.59	3.39	2.32	1.95	1.64
23261–6502 CE Tuc				
6270.55	3.53	2.52	2.22	1.95
23261–8230				
6309.53	5.86	4.74	4.38	4.15
6353.37	5.87	4.75	4.38	4.16
23270–6837				
6303.60	6.73	5.72	5.47	5.31
6308.58	6.78	5.78	5.53	(5.4)
23312–3927				
6270.56	3.84	2.87	2.54	2.29
23370–5606				
6309.55*	8.00	7.01	6.73	6.41
23404+1713				
6270.57	6.35	5.34	4.99	4.72
6314.56	6.45	5.41	5.04	4.78
6338.46	6.33	5.34	4.99	4.68
6379.32	6.34	5.33	4.97	4.68
6639.60	6.33	5.31	4.96	4.67
6662.52	6.31	5.30	4.95	4.65
6694.45	6.43	5.37	5.01	(4.8)
6729.35	6.34	5.32	4.96	4.71
6756.28	6.31	5.29	4.94	4.66
7005.58	6.35	5.33	4.99	4.70
7022.52	6.29	5.30	4.96	4.63
7034.53	6.34	5.32	4.96	4.70
7054.48	6.34	5.33	4.99	4.64
7072.41	6.37	5.36	5.02	4.75
7121.29	6.38	5.36	5.01	4.64
7334.69	6.35	5.34	5.00	4.67
7365.58	6.36	5.36	5.00	4.70

JD −2440000	J	H	K	L
		(mag)		
23404+1713 continued				
7372.58	6.38	5.36	5.00	4.69
7382.55	6.38	5.36	5.01	4.74
23492+0846 AFGL 3163				
6642.55	2.76	1.71	1.38	1.12
23496–1607 Z Aqr				
2630.50	4.95	4.02	3.84	3.43
2647.50	4.74	3.91	3.70	3.43
2706.50	4.66	3.71	3.50	3.30
2737.50	4.86	3.91	3.66	3.38
2971.50	4.67	3.71	3.51	3.30
3014.50	4.86	3.89	3.66	3.45
3059.50	4.77	3.87	3.67	3.48
3079.50	4.72	3.83	3.60	3.39
3112.50	4.65	3.74	3.49	3.36
3387.55	4.73	3.81	3.58	3.41
4819.64	4.81	3.90	3.64	3.37
5251.39	4.72	3.84	3.64	3.38
5682.30	4.73	3.80	3.57	3.38
7863.30	4.75	3.88	3.67	3.43

to the publication of the *IRAS* Catalog as parts of other programmes. It does not include data for 00016−3056 which appeared in Whitelock et al. (1994b). The times of the observations are given as Julian dates from which 244 0000 d have been subtracted. Most of the *JHKL* measurements were made with the MkII photometer on the 0.75-m telescope, and are on the Carter (1990) system. A few measurements, particularly for fainter sources, were made with the 1.9-m telescope; these are marked by an asterisk against the Julian date. They have been transformed to the same system as the 0.75-m observations, following the procedure given by Carter. The 1.9-m measurements and the *JHK* measures with the 0.75-m telescope are accurate to better than ±0.03 mag, and the *L* observations from the 0.75-m telescope are better than ±0.06 mag. Photometry listed in brackets is accurate to about ±0.1 mag. A smaller number of the older observations of certain variable stars were published by Catchpole et al. (1979) and discussed by Feast et al. (1982). The values listed here for such stars differ slightly from those given by Catchpole et al., as they have been corrected to Carter's improved values for the standards.

Table 3 lists the intensity-mean *J*, *H*, *K* and *L* magnitudes for each star. In the case of stars with an observation on only one date, these are obviously the same as listed in Table 2. Where observations with *JHK* and *L* were available, those with only *JHK* were omitted from the means.

3.2 Optical photometry

The $BV(RI)_C$ measurements are listed in Table 4, together with V_{GSC} estimates derived from the *Space Telescope* Guide Star Catalog (GSC, see Section 7.3). The observations were made with an RCA C31034 photomultiplier on the 0.5-m telescope at Sutherland. The standard stars were taken from the E-regions (Menzies et al. 1989). Unfortunately, the majority of the stars have colours outside the range of the standards and therefore outside the range of the non-linear terms in the transformation equations. This means that stars with $B-V>2.0$, $V-R>2.0$ or $V-I>3.7$ cannot be accurately transformed to the Cousins system, and the relevant colour will therefore be uncertain by up to 0.1 mag.

The three observations listed in Table 4 without a date were taken from Sharples, Whitelock & Feast (1995, hereafter SWF). These were observed with the same photometric set-up as the rest of the data. SWF also tabulate a measurement of 20412−2229 (Ste-524) which is different ($\Delta V \sim 0.4$ mag) from the one listed here, consistent with our expectation that most of these stars are variable. *V* magnitudes listed without a date and without any colours are the means of the maximum and minimum from the GCVS, assuming that $V \sim m_p - 1.5$. These were used for only two stars where no satisfactory GSC magnitude was available.

3.3 Spectroscopy

After the first series of infrared measurements had been made, it was clear that there were some unusual objects in the sample. Optical spectra were obtained of many of these, as well as of several stars that were obviously of M type, in order to gain more insight into their nature. As for the observations of the Miras described in Paper I, the intensified Reticon detector attached to the grating spectrograph on the 1.9-m telescope at Sutherland was used. The spectra were obtained with a 600 line mm^{-1} grating set for the first order; they have a resolution of 3.5 Å (FWHM), and cover the range from 3500 to 5500 Å or from 5400 to 7400 Å.

The red spectra of the M stars were used as described in Paper I to derive radial velocities and spectral types. It is assumed that the velocity scale and zero-point are the same as for the Miras in Paper I, and thus the estimated accuracy of an individual measurement (18 km s^{-1}) is also the same. Spectral types from our spectra and from the literature are listed in Table 3. The heliocentric radial velocities are listed in Table 6.

4 NATURE OF THE SOURCES

The stars under discussion can be divided into four distinct groups on the basis of their spectra and colours, namely oxygen-rich giants, T Tauri stars, binary systems and carbon stars. Almost all (154) fall in the first group; those which do not are given the appropriate classification in the final column of Table 3 (the meaning of the class assigned to the M stars is discussed in Section 7.8). These four groups of stars are considered separately below, following a general discussion of their colours and variability. Individual stars are discussed at the end of each section when there is sufficient information to do so usefully.

5 INFRARED COLOURS

Figs 1 and 2 show the mean near-infrared colours derived from the magnitudes in Table 3. Two-colour diagrams involving *IRAS* and near-infrared magnitudes are shown in Figs 3 and 4. The *IRAS* colours are calculated from colour-corrected fluxes using the calibration given in the PSC-ES. The Mira colours from Paper I are shown for comparison in each of the figures. Figs 3 and 4 are directly comparable with the plots shown by Hacking et al. (1985) in their discussion of the brightest high-latitude *IRAS* sources. The $K-[12]$ colour is closely correlated with mass-loss rate, at least for Mira variables (Paper I).

6 VARIABILITY

It was shown in Paper I that selecting *IRAS* sources with Var = 9 was an effective way of selecting Mira variables, although the reverse is not true. 54 per cent of the Miras in Paper I had Var = 9 and 67 per cent had Var ≥ 5. This is in marked contrast to the present sample where only one star has Var = 9 and 9 per cent have Var ≥ 5. It is clear that these stars taken as a group have a much lower level of variability at *IRAS* wavelengths than do the Miras. Nevertheless, 26 per cent of the *IRAS* sources under discussion are classified as variables or suspected variables (GCVS; NSV), and this fraction rises to 64 per cent for those with 12-μm fluxes in excess of 10 Jy. A breakdown of the classification follows: 10 SR or SR:, 3 SRa, 11 SRb or SRb:, 10 Lb or Lb: and one each of I, Int and unclassified. The variability type quoted here differs from that in the GCVS for three stars. The GCVS gives an M classification for 22103−2731 (RX PsA), which had been classified as SRa in previous versions of the catalogue. No information was given to justify the change, and

Table 3. Mean near-infrared and spectral data.

IRAS name	J	H	K (mag)	L	m_{bol}	D (kpc)	Sp	ref	name	class	IRAS name	J	H	K (mag)	L	m_{bol}	D (kpc)	Sp	ref	name	class
00016 − 3056	9.32	7.88	7.35	6.81			M1e	1		Binary	03318 − 5334	5.76	4.81	4.61	4.46	7.59	1.3	M4	1	SAO 233156	1
00025 + 0027	4.52	3.49	3.19	2.98	6.39	1.1				2	03318 − 8244	6.70	5.69	5.39	5.15	8.57	2.9				2
00045 + 3058	6.00	4.98	4.67	4.43	7.87	2.1				2	03323 − 2547	4.64	3.63	3.30	2.99	6.45	1.1				2
00127 − 6030	6.60	5.77	5.53	5.19	8.23	1.6	M3e	1	UY Tuc	3	03324 − 4728	7.17	6.24	5.93	5.57	8.95	3.1				3
00197 + 0318	5.29	4.20	3.92	3.58	7.15	1.6				1	03388 − 1054	3.38	2.33	2.05	1.84	5.26	0.6	M6,	2	VY Eri	1
00204 − 5936	6.11	5.12	4.89	4.64	7.94	1.8	M7	1		1	03430 + 0325	4.85	3.73	3.40	3.15	6.68	1.6	M7	1		1
00221 − 7614	7.70	6.70	6.45	6.23	9.53	4.0				1	03489 + 1257	6.24	5.13	4.79	4.56	8.12	2.9	M6	1		1
00245 − 0652	1.64	0.60	0.25	−0.06	3.49	0.3	M7	2	UY Cet	2	03499 − 3041	5.13	4.14	3.83	3.56	6.98	1.3	M6	1		2
00371 + 1355	3.59	2.55	2.27	2.04	5.46	0.7	M8	2	TW Psc	1	04020 − 1551	0.88	−0.19	−0.55	−0.86	2.71	0.2	M6	2	V Eri	2
00413 + 2028	6.87	5.87	5.53	5.24	8.73	3.3				3	04026 − 3024	5.49	4.51	4.21	3.94	7.33	1.5	M6	1		2
00477 − 4900	3.28	2.27	1.95	1.65	5.13	0.6				2	04037 − 1846	5.32	4.32	4.04	3.81	7.16	1.4	M7:	2	AT Eri	2
00542 − 7334	6.02	5.02	4.74	4.52	8.00	2.1			CM Tuc	2	04060 − 0447	5.22	4.18	3.81	3.53	7.08	1.7	M6	1	Ste-30	2
01083 + 2335	5.75	4.75	4.45	4.22	7.62	1.8				2	04067 − 0922	5.55	4.28	3.61	3.00			C	1		Carbon
01217 + 2341	2.56	1.54	1.22	0.97	4.42	0.4	M3	3	AFGL 5048	2	04085 + 0653	6.54	5.46	5.10	4.77	8.38	3.2				2
01230 − 4611	3.78	2.82	2.59	2.38	5.61	0.6	M3/4	2	AL Phe	2	04120 − 6516	7.32	6.31	5.94	5.54	9.12	4.3				3
01246 − 3248	2.12	0.73	−0.06	−0.77			C	2	R Scl	Carbon	04127 + 0110	7.02	5.95	5.61	5.36	8.89	3.9				1
01251 + 1626	3.06	2.03	1.71	1.44	4.91	0.6	M5	2	ST Psc	2	04147 − 1220	6.01	5.02	4.69	4.39	7.86	2.1	M7	1	Ste-32	3
01253 + 2816	5.05	4.01	3.68	3.45	6.92	1.5				2	04177 − 1850	4.26	3.23	2.89	2.63	6.13	1.0	M2	2	AV Eri	2
01400 − 6921	4.26	3.27	2.99	2.73	6.11	0.9				2	04183 − 4310	5.51	4.51	4.20	3.94	7.37	1.7	M8	1		2
01438 + 1850	2.01	0.98	0.64	0.38	3.87	0.4	M5	2	SV Psc	2	04191 + 0346	5.19	4.06	3.74	3.50	7.03	1.8	M6	1		1
01452 − 8026	2.49	1.46	1.13	0.86	4.36	0.4	M	2	VZ Hyi	2	04199 − 2248	3.70	2.69	2.38	2.14	5.56	0.7	M7	1	NSV 1578 Ste-34	2
01481 − 1753	3.75	2.76	2.45	2.14	5.59	0.7	M5	5	NSV 634	2	04238 − 6713	6.97	6.00	5.64	5.22	8.77	3.3	M7	1		3
01483 − 6932	6.48	5.51	5.25	5.07	8.35	2.2				2	04257 − 3220	6.26	5.26	5.03	4.81	8.11	2.0	M5	1		1
01519 + 0427	3.23	2.18	1.82	1.52	5.08	0.7	M6ep-M7	2	AA Psc	2	04258 − 0155	8.91	7.89	7.61		10.54	7.7				1
01527 + 1656	3.08	2.04	1.78	1.56	4.93	0.5	M6	3	AFGL 4013	1	04375 − 3216	7.22	6.26	6.04	5.86	9.05	2.8	M6	1		1
01531 − 3602	3.84	2.84	2.57	2.35	5.71	0.7	M0	3	NSV 665	2	04382 − 1417	1.99	0.87	0.45	0.14	3.81	0.5	M8,M2-7	1,2	BX Eri	2
01597 + 1601	3.07	2.02	1.69	1.42	4.93	0.6	M6,5	2	RY Ari	2	04451 − 0539S	10.99	9.73	8.89	7.89				1		Young
02095 − 2355	3.49	2.47	2.17	1.92	5.35	0.7	M6	1	IRC−20°029	2	04451 − 0539N	11.20	10.41	10.20	9.94				1		Young
02165 + 2750	6.34	5.30	4.97	4.66	8.20	2.7				2	04523 − 1359	6.82	5.83	5.58	5.41	8.67	2.6	M5	1		2
02180 − 7939	6.46	5.46	5.19	4.99	8.32	2.3	M6	1	SY Hyi	2	04576 − 2555	4.46	3.43	3.11	2.86	6.33	1.1	M6	1		2
02404 + 2150	5.21	4.07	3.63	3.28	7.00	2.1	M8	1	OH maser	2	05074 − 2654	4.72	3.70	3.37	3.11	6.58	1.2	M6	1		2
02427 − 5430	1.71	0.69	0.34	0.03	3.53	0.3	M7	1	W Hor	2	05166 − 3109	6.74	5.72	5.48	5.30	8.60	2.7	M4	1		1
02512 − 3758	6.14	5.23	4.79	4.00					SY For	Binary	05217 − 3943	2.30	1.36	1.16	1.00	4.10	0.3	M1	2	SW Col	2
02537 − 0614	3.73	2.62	2.25	1.96	5.58	1.0	M7	1	IRC−10°042	2	19496 − 6812	4.92	3.87	3.53	3.26	6.78	1.4				2
02538 + 1953	10.15	9.28	8.69	7.76					WY Ari	Young	19521 − 5131	9.11	8.13	7.83	7.32	10.68	8.1	M5	1		2
03033 − 7703	5.25	4.22	3.84	3.59	7.10	1.7	M8	1		3	19539 − 5915	4.48	3.44	3.12	2.86	6.35	1.1				2
03177 − 0017	5.72	4.74	4.50	4.28	7.57	1.6	M0	7	BD−0°528	1	19549 − 4931	4.20	3.18	2.84	2.51	6.05	1.0	M	6	HD 188707	2
03227 − 1231	4.11	3.15	2.87	2.65	5.93	0.8	M3/4	2	VX Eri	2	19575 − 4317	6.66	5.72	5.45	5.17	8.42	2.3				3
03260 − 1534	6.44	5.45	5.16	4.95	8.31	2.4	M7	1	Ste-23	2	20043 − 4533	6.27	5.28	5.02	4.84	8.13	2.1				2
03287 − 1535	4.57	3.57	3.22	2.81	6.13	1.1	M7	1	Ste-24 OH maser	3	20116 − 5445	3.32	2.33	2.04	1.82	5.19	0.6	M5/6	6	NSV 12922	2

Table 3 – *continued*

IRAS name	J	H	K	L	m_{bol}	D	Sp	ref	name	class
			(mag)			(kpc)				
20120 – 4433	2.77	1.67	1.28	0.93	4.60	0.6	S4ep	2	RZ Sgr	2
20125 – 5153	7.09	6.14	5.87	5.63	8.91	2.9				3
20174 – 7853	7.67	6.63	6.34	6.05	9.37	4.6				1
20176 – 2527	6.45	5.41	5.07	4.81	8.32	2.8				2
20220 – 8027	6.77	5.72	5.39	5.17	8.65	3.3				2
20240 – 2142	6.54	5.58	5.29	5.01	8.33	2.4				3
20250 – 3557	5.94	4.84	4.43	4.09	7.75	2.7	M8-9	1		2
20270 – 2858	6.84	5.78	5.37	4.86	8.58	4.0	M7e	1		3
20271 – 2340	6.58	5.63	5.33	5.00	8.40	2.4	M8	1		3
20277 – 3959	6.78	5.84	5.56	5.25	8.58	2.5			SW Mic	3
20282 – 3310	6.05	5.05	4.80	4.54	7.86	1.9			SAO 212196	1
20295 – 6546	5.09	4.03	3.66	3.37	6.94	1.7	M7	1		2
20298 – 3405	3.92	2.89	2.59	2.35	5.79	0.8	M	4		2
20333 – 2428	6.17	5.15	4.83	4.48	8.01	2.3				2
20356 – 2815	4.12	3.07	2.68	2.37	5.97	1.1	M9	1	IRC−30°433	3
20381 – 2827	5.72	4.72	4.45	4.18	7.58	1.7				2
20412 – 2229	4.62	3.56	3.23	2.92	6.47	1.3			Ste-524	2
20459 – 4917	6.76	5.78	5.56	5.32	8.57	2.4				1
20466 – 4105	5.45	4.47	4.14	3.81	7.29	1.6				3
20487 – 1117	3.28	2.25	1.92	1.65	5.14	0.6	M7	5	A FGL 2666 Ste-529	2
20522 – 5711	5.16	4.18	3.89	3.66	7.02	1.3				2
20545 – 1709	6.33	5.30	5.00	4.90	8.22	2.5			XY Cap	2
20559 – 1055	4.71	3.68	3.33	3.06	6.57	1.3			DG Aqr	2
20561 – 5253	6.13	5.13	4.83	4.59	8.00	2.2				2
20575 – 5806	6.86	5.88	5.62	5.41	8.71	2.7				2
20577 – 4504	6.55	5.57	5.26	5.00	8.39	2.5	M7	1		3
20598 – 2358	4.80	3.81	3.52	3.27	6.66	1.1				2
20599 – 3941	4.61	3.60	3.23	2.93	6.47	1.2	M8	1		3
21015 – 0214	6.26	5.28	5.00	4.75	8.11	2.1	M5	2	TW Aqr	2
21034 – 0823	5.78	4.81	4.54	4.34	7.63	1.6				2
21041 – 5746	5.40	4.40	4.09	3.86	7.27	1.6				2
21060 – 0029	8.77	7.81	7.56	7.25	10.49	6.0				2
21095 – 5222	3.78	2.76	2.44	2.14	5.64	0.8				2
21097 – 3627	5.40	4.48	4.22	3.99	7.19	1.2				3
21151 – 2340	6.64	5.60	5.31	5.06	8.49	2.9				2
21159 – 5222	6.57	5.58	5.29	5.02	8.43	2.5				2
21160 – 6728	3.54	2.52	2.25	2.04	5.39	0.6	M5	6	NSV 13648	1
21208 – 3350	5.58	4.63	4.39	4.20	7.43	1.4				2
21270 + 0702	6.25	5.23	4.90	4.62	8.11	2.5				2
21317 – 5948	5.83	4.83	4.52	4.33	7.71	1.9				2
21318 – 5130	6.65	5.65	5.36	5.14	8.51	2.7				2
21365 + 0526	6.56	5.56	5.21		8.40	2.8				3
21368 – 3812	2.34	1.31	0.95	0.64	4.19	0.4	M6	1	AFGL 5595	2
21377 – 0200	2.14	1.12	0.78	0.49	4.00	0.4	M5	5	AFGL 2787 Ste-546	2
21392 + 0230	8.74	8.17	7.81	6.86			pec	1	StHα 190	Binary
21396 – 2256	6.24	5.25	4.99	4.78	8.10	2.0				2
21439 – 0226	−0.19	−1.19	−1.50	−1.77	1.65	0.1	M8	2	EP Aqr	2
21447 – 7245	6.47	5.47	5.24	5.08	8.34	2.2				1
21505 – 4320	6.08	5.09	4.79	4.50	7.92	2.0				2
21511 – 6439	6.25	5.28	5.00	4.78	8.11	2.1	M6	1		2
21543 – 1421	2.08	1.05	0.71	0.41	3.93	0.4	M7	3	NSV 13969	2
21562 – 2547	6.36	5.35	4.97	4.76	8.23	2.8				3
22003 – 0010	3.06	2.06	1.76	1.52	4.92	0.5	M8	3	AFGL 2835 Ste-549	2
22066 – 2500	5.41	4.43	4.16	3.92	7.26	1.4				2
22073 – 3632	5.24	4.25	3.98	3.73	7.09	1.3				2
22103 – 2731	6.41	5.48	5.19	5.00	8.21	2.1	Me	2	RX PsA	3
22142 – 8454	1.15	0.07	−0.28	−0.54	3.01	0.3	M7,7	1,2	BW Oct	2
22169 – 0955	6.86	5.95	5.62	5.19	8.62	2.7	M5-6	1	ZZ Aqr	3
22190 – 0751	1.84	0.79	0.45	0.22	3.71	0.4	M7	2	DZ Aqr	2
22197 – 3348	5.64	4.68	4.48	4.35	7.47	1.3	M2/3	3	HD 212115	1
22209 – 3508	4.23	3.13	2.73	2.41	6.06	1.2	M8	1		2
22229 – 6855	6.43	5.45	5.18	5.04	8.25	2.2				2
22296 + 2004	7.44	6.53	6.25		9.05	3.1				3
22359 – 1417	2.39	1.36	1.02	0.75	4.25	0.4	M7	2	AB Aqr	2
22380 + 2306	6.64	5.63	5.37		8.50	2.6				2
22458 + 1401	6.34	5.33	5.05	4.86	8.20	2.3				2
22494 – 2534	2.70	1.67	1.32	1.03	4.57	0.5	M7,M8	1,2	TU PsA	2
22497 + 1733	4.77	3.71	3.36	3.07	6.63	1.4				2
22553 + 1744	3.66	2.51	2.12	1.88	5.49	1.0	M6e	2	BI Peg	1
23082 + 1903	5.10	4.10	3.86	3.53	6.92	1.2	M2	7	BD+18°5117	1
23115 + 0953	5.07	4.07	3.84	3.66	6.94	1.2	M6	1	BD+09°5182	1
23196 + 1615	5.15	4.14	3.84	3.64	7.02	1.4				2
23198 – 0230	9.44	8.32	7.41	6.16					StHα 202	Young
23218 – 7719	6.98	5.98	5.67	5.45	8.85	3.3			TV Oct	2
23236 – 6917	3.39	2.32	1.95	1.64	5.22	0.8	M6	1		2
23261 – 6502	3.53	2.52	2.22	1.95	5.36	0.7	M6	1	CE Tuc	2
23261 – 8230	5.86	4.75	4.38	4.15	7.72	2.6	M7,M6	1,2		1
23270 – 6837	6.75	5.75	5.50	5.35	8.59	2.6				1
23312 – 3927	3.84	2.87	2.54	2.29	5.69	0.8				2
23370 – 5606	8.00	7.01	6.73	6.41	9.81	4.8				3
23404 + 1713	6.35	5.34	4.99	4.69	8.19	2.7	M8	1		3
23492 + 0846	2.76	1.71	1.38	1.12	4.63	0.5	M5.5	7	AFGL 3163	2
23496 – 1607	4.76	3.84	3.62	3.39	6.51	0.8	M1-7e	2	Z Aqr	2

References: (1) this paper; (2) GCVS or reference therein; (3) SAO Catalogue; (4) Cohen et al. (1989); (5) Bidelman (1980) or reference therein; (6) Michigan Catalogue; (7) SIMBAD dataase, reference unspecified.

Table 4. Optical photometry.

IRAS name	JD– 2446700	V	B–V	$(V-R)_C$ (mag)	$(V-I)_C$	V_{GSC}
00025 + 0027						10.77
00045 + 3058	29.37	11.96	1.61	1.75	3.76	11.94
00127 – 6030						10.02
00197 + 0318	23.41	11.92	1.70	2.05	4.23	12.36
00204 – 5936	21.39	10.70	1.65	1.31	2.98	10.75
00221 – 7614						11.91
00245 – 0652						9.32
00371 + 1355						9.30
00413 + 2028	29.38	14.24	1.59	2.24	4.47	13.64
00477 – 4900	19.38	10.25	1.59	2.04	4.28	10.43
00542 – 7334						11.83:
01083 + 2335	23.43	11.34	1.53	1.68	3.59	11.84
01217 + 2341						8.75
01230 – 4611						7.87
01251 + 1626						9.37
01253 + 2816	29.99	11.87	1.69	2.05	4.21	12.05
01400 – 6921	19.39	10.74	1.56	1.90	4.06	10.25
01438 + 1850						8.65
01452 – 8026						9.25
01481 – 1753						9.97
01483 – 6932	23.43	11.07	1.56	1.32	2.96	11.11
01519 + 0427						11.06
01527 + 1656						8.09
01531 – 3602						9.99
01597 + 1601		9.50				14.76::
02095 – 2355						10.09
02165 + 2750	29.45	13.24	1.69	2.09	4.27	13.34:
02180 – 7939						11.87
02404 + 2150						13.34
02427 – 5430						9.61
02537 – 0614						11.79
03033 – 7703	21.50	12.80	1.46	2.21	4.50	12.44
03177 – 0017	23.50	9.57	1.74	1.15	2.50	10.44
03227 – 1231						9.14
03260 – 1534	23.52	11.59	1.71	1.52	3.30	11.88
03287 – 1535						12.16
03318 – 5334						9.38
03318 – 8244						12.90:
03323 – 2547	23.54	10.89	1.62	1.95	4.06	11.00
03324 – 4728						13.62
03388 – 1054						9.00
03430 + 0325	25.56	10.90	2.07	1.92	3.96	10.95
03489 + 1257	25.46	13.14	1.77	2.08	4.27	12.95
03499 – 3041	23.55	11.36	1.57	1.83	3.90	11.28
04020 – 1551						8.67
04026 – 3024	23.58	11.56	1.57	1.91	4.03	12.45
04037 – 1846						10.54
04060 – 0447	24.57	12.49	1.79	2.20	4.45	12.38
04085 + 0653	29.48	13.68	1.73	2.16	4.37	13.48
04120 – 6516						12.23
04127 + 0110	25.57	13.67	1.48	2.10	4.26	13.46
04147 – 1220	24.58	12.78	1.63	2.05	4.22	12.10
04177 – 1850						11.27
04183 – 4310	23.59	12.26	1.57	1.99	4.14	11.87
04191 + 0346	25.58	10.94	2.09	1.79	3.74	10.99
04199 – 2248						9.99
04238 – 6713						13.06
04257 – 3220	24.58	10.85	1.57	1.32	2.95	10.58
04258 – 0155						13.08
04375 – 3216	25.59	11.39	1.55	1.17	2.69	11.30
04382 – 1417						10.66
04523 – 1359	24.60	11.29	1.50	1.24	2.82	11.13
04576 – 2555	23.60	11.61	1.59	2.01	4.21	11.66
05074 – 2654	24.61	12.20	1.58	1.96	4.11	11.79
05166 – 3109	25.61	11.57	1.89	1.38	3.09	10.92
05217 – 3943						5.33
19496 – 6812	23.26	12.02	1.62	2.13	4.35	12.94::
19521 – 5131						12.94
19539 – 5915	21.28	11.44	1.60	2.03	4.26	11.55
19549 – 4931	19.27	10.69	1.77	1.94	4.10	10.82
19575 – 4317						11.73
20043 – 4533	23.27	11.49	1.63	1.58	3.43	11.92
20116 – 5445						11.08
20120 – 4433		10.20				6.11?
20125 – 5153	29.27	12.06	1.63	1.45	3.19	11.06?
20174 – 7853	29.28	12.25	1.86	1.32	2.90	11.74
20176 – 2527	25.28	13.34	1.58	2.04	4.22	13.51
20220 – 8027						13.33
20240 – 2142						11.67
20250 – 3557						
20270 – 2858						13.93
20271 – 2340						12.85
20277 – 3959						11.09
20282 – 3310						10.18
20295 – 6546	21.29	12.43	1.74	2.15	4.42	12.53
20298 – 3405	19.27	10.00	1.62	1.79	3.89	9.94
20333 – 2428	25.29	10.97	0.72	0.80	2.34	9.82?
20356 – 2815						12.80
20381 – 2827	21.31	11.79	1.50	1.80	3.90	11.70
20412 – 2229	23.31	11.88	1.76	2.23	4.46	11.83
20459 – 4917	27.28	10.87	1.53	1.17	2.63	
20466 – 4105	21.32	12.50	1.56	2.10	4.35	12.36
20487 – 1117		10.04	1.63	2.10	4.24	10.08
20522 – 5711	19.29	10.21	1.66	1.49	3.28	10.25
20545 – 1709						12.36
20559 – 1055						11.88
20561 – 5253	27.28	12.44	1.54	1.82	3.89	12.79
20575 – 5806	28.36	11.46	1.52	1.31	2.98	11.11
20577 – 4504	27.33	12.60	1.57	1.72	3.76	12.89
20598 – 2358	21.33	10.93	1.59	1.75	3.79	10.80
20599 – 3941	23.34	12.55	1.89	2.35	4.66	12.58
21015 – 0214						12.04
21034 – 0823						10.87
21041 – 5746	28.36	12.47	1.62	2.13	4.33	12.40
21060 – 0029	30.27	13.30	1.57	1.28	2.82	13.68
21095 – 5222	19.30	11.61	1.65	2.29	4.64	11.07
21097 – 3627	23.35	10.50	1.54	1.43	3.18	10.48
21151 – 2340	29.29	13.12	1.78	1.97	4.12	12.88
21159 – 5222	28.37	11.58	1.63	1.49	3.25	11.50
21160 – 6728						8.86

Table 4 – *continued*

IRAS name	JD–2446700	V	B–V	$(V-R)_C$ (mag)	$(V-I)_C$	V_{GSC}
21208 – 3350	21.34	9.59	1.58	1.11	2.52	9.70
21270 + 0702	30.28	13.53	1.49	2.14	4.36	13.14
21317 – 5948	23.36	12.46	1.61	1.99	4.13	12.40
21318 – 5130	27.38	12.29	1.56	1.71	3.61	12.78
21365 + 0526	30.29	13.84	1.47	2.01	4.19	13.54
21368 – 3812	19.31	9.93	1.41	1.99	4.26	10.00
21377 – 0200		9.65	1.69	2.34		9.66
21396 – 2256	25.36	12.40	1.60	1.81	3.86	12.50
21439 – 0226						6.53
21447 – 7245						11.40
21505 – 4320	23.37	12.62	1.59	1.93	4.02	12.40
21511 – 6439	25.37	12.03	1.59	1.70	3.61	11.75
21543 – 1421						9.54
21562 – 2547	27.39	12.60	1.28			12.76
22003 – 0010		9.68	1.52	1.95	4.05	9.06:
22066 – 2500	23.38	10.88	1.63	1.64	3.51	10.98
22073 – 3632	19.32	10.86	1.58	1.61	3.53	10.90
22103 – 2731						10.31
22142 – 8454	29.30	8.24	1.71	2.08	4.29	9.24
22169 – 0955						10.97
22190 – 0751						8.52
22197 – 3348						9.33
22209 – 3508						12.58
22229 – 6855	28.38	12.23	1.50	1.70	3.62	12.36
22296 + 2004						11.63
22359 – 1417						8.69
22380 + 2306						12.31
22458 + 1401	23.39	11.99	1.72	1.77	3.76	12.42
22494 – 2534						10.02
22497 + 1733						11.60
22553 + 1744						10.53
23082 + 1903	23.40	8.74	1.82	1.14	2.38	8.73
23115 + 0953						9.40
23196 + 1615						11.39
23218 – 7719						12.02
23236 – 6917	19.34	10.69	1.65	2.20	4.52	11.22
23261 – 6502	29.31	8.87	1.63	1.67	3.55	9.43
23261 – 8230	28.39	12.91	1.91	2.21	4.43	13.45
23270 – 6837	28.40	11.25	1.68	1.32	2.94	11.50
23312 – 3927	19.36	11.19	1.64	2.12	4.37	11.00
23370 – 5606	29.36	12.27	1.81	1.30	2.73	11.86
23404 + 1713						13.52
23492 + 0846						10.08
23496 – 1607						8.32

it is therefore treated here as an SRa. 02180 – 7939 (SY Hyi) is listed as an RCB: in the GCVS, but this was shown to be incorrect by Feast (1979) and it is consequently referred to as an SR here. 04020 – 1551 (V Eri) is classified as SRc in the GCVS where a spectral type of M6II is quoted. The Michigan catalogue (Houk & Smith-Moore 1988) gives a spectral type of M5/6 III/V. In view of this and the lack of evidence that V Eri is a supergiant, we use the variability classification of SRb as given by Houk (1963). The variability of the *JHKL* magnitudes of individual stars is discussed below. It seems reasonable to conclude that most of these stars are probably small-to-moderate-amplitude variables at visual and near-infrared wavelengths.

6.1 Periods

Where observations from 14 or more nights were available for a given star an attempt was made to determine its period, if any, from the Fourier transform of the *K* light curve. The data was checked for periods in the range 40 to 1000 d, although for some stars – those with observations on a small number of nights – the data are not adequate for searching for all periods in this range. The results, including the peak-to-peak amplitudes (ΔJ, ΔK) of the best-fitting sine curves, and the number of observations used in the analysis (no. obs), are given in Table 5. Periods from the GCVS are also listed in the table where available. The accuracy of the new periods varies from one star to the next, depending on the number of observations and the repeatability of the light curves. This can be judged from the illustration in Fig. 5, which show the *K* light curve as a function of phase. Those periods marked with a colon in Table 5 must be regarded as very uncertain. In Paper I, we found no gross discrepancies between the periods we determined and those from elsewhere. The situation here is less clear. It has been possible to redetermine the periods of only very few stars with values listed in the GCVS, and some of those are in agreement while others are not (see Table 5). The disagreements are all amongst SRb variables and are consistent with the GCVS classification for this type of variable, i.e., '... poorly expressed periodicity ... alternating intervals of periodic and slow irregular changes ...'.

The *K* amplitudes of these stars are generally much less than those of the Miras in paper I, which have $0.4 \lesssim \Delta K \gtrsim 2.0$. Only the S star 20120 – 4433 (RZ Sgr) has a *K* amplitude comparable to those of the Miras.

7 OXYGEN-RICH STARS

This group of 154 stars constitutes the bulk of the *IRAS* sources examined in this survey. Not all of these stars have been studied in detail; for many of them we have only the *IRAS* data and a single *JHKL* observation. Most of the stars for which we have spectra are M-type, although there is at least one S star (20120 – 4433 RZ Sgr) in the group and we cannot rule out the possibility that there are others. Group members are defined for the purpose of this discussion by their *JHK* colours which fall in a small area on the left of Fig. 1, which is shown in more detail in Fig. 6(a). In the following, we assume that they are all non-Mira, O-rich giants (referred to hereafter as M stars), while bearing in mind that this assumption has not been confirmed spectroscopically in all cases.

Figs 7(a) and (b) are histograms comparing the numbers of O-rich Miras with the numbers of M stars over the observed range of *K* and [12] magnitude. The most important point illustrated here is the incompleteness of the M-star sample. The *IRAS* survey was incomplete below about [12] = 3.7. The distribution in Fig. 7(a) shows the number of Miras to be decreasing, while the number of M stars is still increasing rapidly at [12] = 3.7 mag. In contrast, the *K*-magnitude

Table 5. Variability data.

IRAS name	P_1 (day)	P_2	ΔJ (mag)	ΔK	no. obs	GCVS (day)	GCVS name	comment
00016 − 3056	508	long	0.9	0.6	91	-		eclipsing
00127 − 6030	107	-	0.25	0.19	68	105	UY Tuc	
00245 − 0652	-	-	-	-	1	440	UY Cet	
00542 − 7334	64:	-	< 0.1	< 0.1	41	-	CM Tuc	
01246 − 3248	379	2315	0.68	0.31	65	370	R Scl	C star
01251 + 1626	-	-	-	-	1	540	ST Psc	
01438 + 1850	-	-	-	-	1	102	SV Psc	
02404 + 2150	-	-	< 0.1	< 0.1	24	-		
02427 − 5430	-	-	-	-	1	137	W Hor	
02512 − 3758	not 55	-	-	-	78	55	SY For	binary
03287 − 1535	109	-	0.10	< 0.1	41	-		
03318 − 8244	-	-	< 0.1	< 0.1	51	-		
03388 − 1054	-	-	-	-	1	102	VY Eri	
04020 − 1551	-	-	-	-	1	97	V Eri	
04067 − 0922	228	-	0.79	0.26	47	-		C star
04120 − 6516	217	-	0.32	0.30	94	-		
	434	-	0.32	0.30	94	-		RV Tau-like
04127 + 0110	-	long	< 0.1	< 0.1	26	-		IRAS Var=9
04238 − 6713	309:	-	0.09	0.10	21	-		
04382 − 1417	-	-	-	-	1	165	BX Eri	
19521 − 5131	590	140	0.13	0.12	88	-		
20120 − 4433	208	-	0.77	0.57	29	223	RZ Sgr	S star
20240 − 2142	415:	-	0.10	0.10	59	-		
20270 − 2858	-	long	-	-	66	-		
20271 − 2340	191	-	0.36	0.34	49	-		
21270 + 0702	-	-	< 0.1	< 0.1	17	-		IRAS Var=8
21377 − 0200	150:	-	0.14	< 0.1	21	-		
21392 + 0230	900:	-	-	0.16	16	-		binary
21439 − 0226	-	-	-	-	1	55	EP Aqr	
22103 − 2731	-	-	-	-	2	366	RX Psa	
22169 − 0955	174	-	0.43	0.35	15	-	ZZ Aqr	
22209 − 3508	154:	-	0.12	< 0.1	29	-		
22553 + 1744	-	-	-	-	1	500	BI Peg	
23198 − 0230	-	long	-	-	37			young
23261 − 6502	-	-	-	-	1	60	CE Tuc	
23404 + 1713	132:	-	< 0.1	< 0.1	19	-		
23496 − 1607	137	-	0.20	0.21	14	136	Z Aqr	

Table 6. Heliocentric radial velocities of M stars.

Name	V_{opt} kms^{-1}	V_{other} kms^{-1}	Notes[a]
00016−3056	−115.4		
00127−6030	−29.2		
00204−5936	67.0		
00245−0652		−3.0	opt:1
		4.1	CO:4
01438+1850		16.0	opt:1
02095−2355	65.8		
02180−7939	33.5		
02404+2150	−19.5	−44.8	OH:9
02427−5430	39.2	6.0	H_2O:2
02537−0614	9.3		
03033−7703	−8.9		
03260−1534	9.3	26.0	opt:8
03287−1535	6.1	18.0	opt:8
		1.2	CO:4
03318−5334	49.9		
03388−1054		32.0	opt:1
03430+0325	41.7		
03489+1257	16.6		
03499−3041	8.2		
04020−1551		−25.5	CO:3
		−20.0	opt:1
04026−3024	27.4		
04060−0447	69.4	76.0	opt:8
04147−1220	53.9	72.0	opt:8
04183−4310	22.4		
04191+0346	43.7		
04199−2248	−0.7	−22.0	opt:8
04257−3220	−18.9		
04375−3216	36.8		
04523−1359	−15.2		
04576−2555	14.2		
05074−2654	−0.8		
05166−3109	107.3		
05217−3943		63.5	opt:5
19521−5131	−206.9		
20120−4433		−24.9	CO:4
20250−3557	−29.3		
20270−2858	−126.9		
20271−2340	41.1		
20295−6546	26.5		
20356−2815	14.4		
20412−2229		11.0	opt:8
20487−1117		−79.0	opt:8
20577−4504	−18.1		
20599−3941	−25.7		
21368−3812	−4.9		
21377−0200		−16.0	opt:8
21439−0226		−41.0	opt:6
		−27.9	CO:3
		−27.7	CO:4
21511−6439	49.8		
22003−0010		−51.0	opt:8
22103−2731		−34.0	opt:1
22142−8454	19.9		
22169−0955	36.1		
22190−0751		21.3	CO:4
22209−3508	−21.4		
22494−2534	4.8		
22553+1744		−20.0	opt:1
23115+0953	−71.9		
23236−6917	19.9		
23261−6502	28.1		
23404+1713	18.1		
23496−1607		69.4	opt:7

[a]Type of measurement - optical (opt) or radio (OH, CO or SiO) - and references for the velocities: (1) Feast et al. (1972); (2) Deguchi et al. (1989); (3) Zuckerman & Dyck (1986); (4) Nyman et al. (1992); (5) Jones & Fisher (1984); (6) Wallerstein & Dominy (1988); (7) Jones (1972); (8) SWF; (9) Eder et al. (1988).

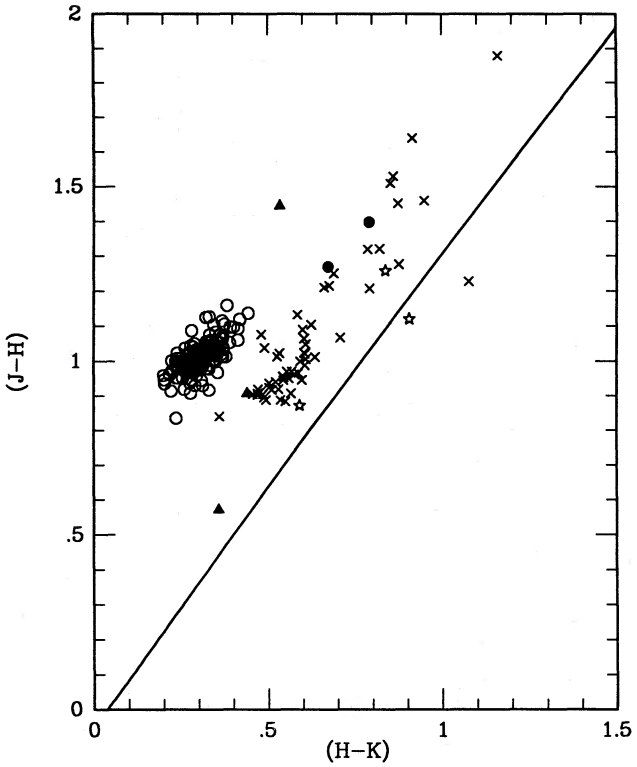

Figure 1. Near-infrared, two-colour diagram. The line going diagonally across the diagram represents the locus of blackbodies of different temperatures. Symbols: crosses: Miras (see Paper I); open circles: M giants; closed circles: C giants; closed triangles: binaries; open asterisks: young stars.

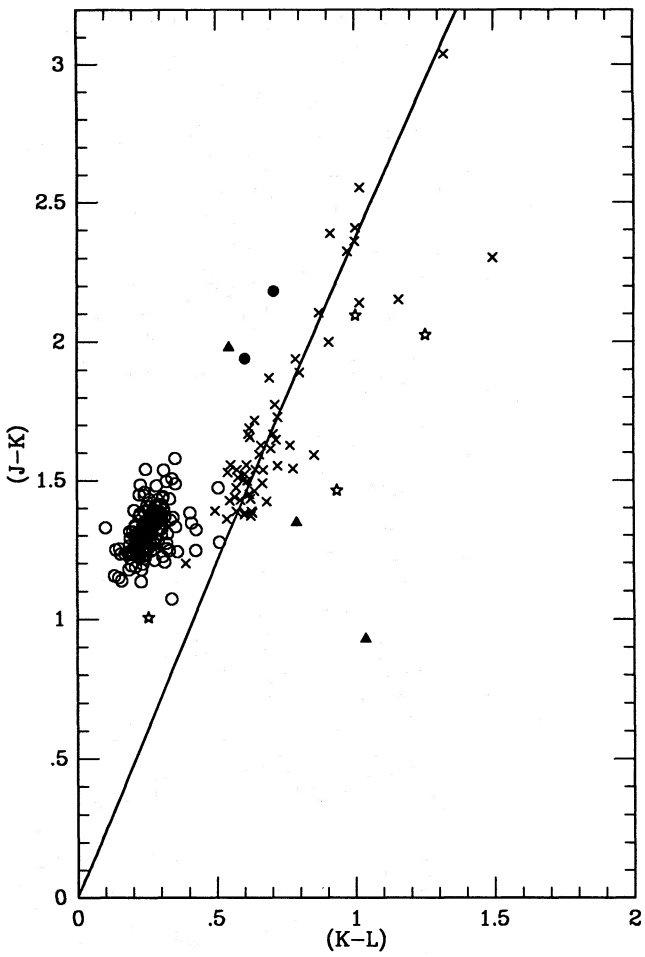

Figure 2. Near-infrared, two-colour diagram. Symbols are as for Fig. 1.

ranges of the two groups are very similar. This is another illustration of the point made in connection with Fig. 3 (see Section 7.1) – that the Miras have thicker dust shells than do other late-type stars.

It should be borne in mind that we are not looking at all the M stars in the South Galactic Cap, but only at those with *IRAS* colours which obey our selection criterion, i.e., those with relatively cool dust shells. This criterion was originally intended to isolate stars with high mass-loss rates, but it is clear from our earlier work (Whitelock et al. 1991a; Paper I) that there is not a particularly good correlation of mass-loss rate with *IRAS* colour. The evidence discussed below suggests that the stars under discussion have later spectral types and higher mass-loss rates on average than do a random sample of M stars from the same volume. Nevertheless, we are unable to define precisely what the difference is between an M star with a cool shell and one with a warmer shell, although we can speculate that it is probably connected with mass and evolutionary status.

7.1 Colours

The tight grouping of these stars in Fig. 1 have already been noted; it is also notable that there is no overlap between their colours and those of the other groups in Fig. 1. Fig. 6(a) is an expansion of the relevant part of Fig. 1 and allows a comparison of the observed colours with those of bright K and M giants in the solar neighbourhood and M giants in the Bulge (Section 7.1.1). The stars under consideration have an almost identical distribution of *JHK* colours to the Stephenson polar-cap M giants which were discussed by Feast et al. (1990) and by SWF. The overlap with the Stephenson (1986a) survey is limited by the fact that Stephenson examined the south polar Cap only north of declination $-25°$ and excluded known variable stars. According to the models by Bessell et al. (1989), the position of M stars in a plot of $J-H$ against $H-K$ is sensitive to surface gravity, atmospheric extension and chemical abundance. Note that the locus of the M stars illustrated in Fig. 6(a), and the almost identical one shown by the Stephenson stars in fig. 4 of Feast et al. (1990), are quite different in shape from any of the evolutionary tracks described by Bessell et al. This may be due at least partly to the influence of circumstellar reddening (see Section 7.8).

In Fig. 2 the M stars also form a tight group, although a few of them have distinctly larger values of $K-L$ than the average and thus have colours similar to those of the bluer Miras. Some of these are discussed further in Section 7.7, where a correlation between $K-L$ and $K-[12]$ is also considered.

The vertical separation in Fig. 3 is largely a function of the thickness of the circumstellar shell and hence of the mass-

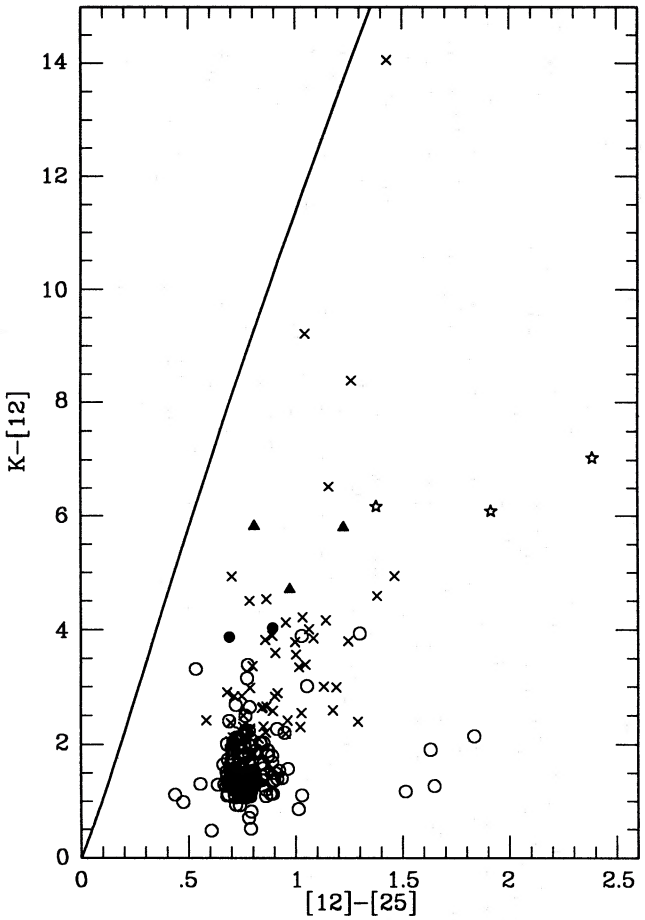

Figure 3. Combined *IRAS* and near-infrared two-colour diagram. Symbols are as for Fig. 1.

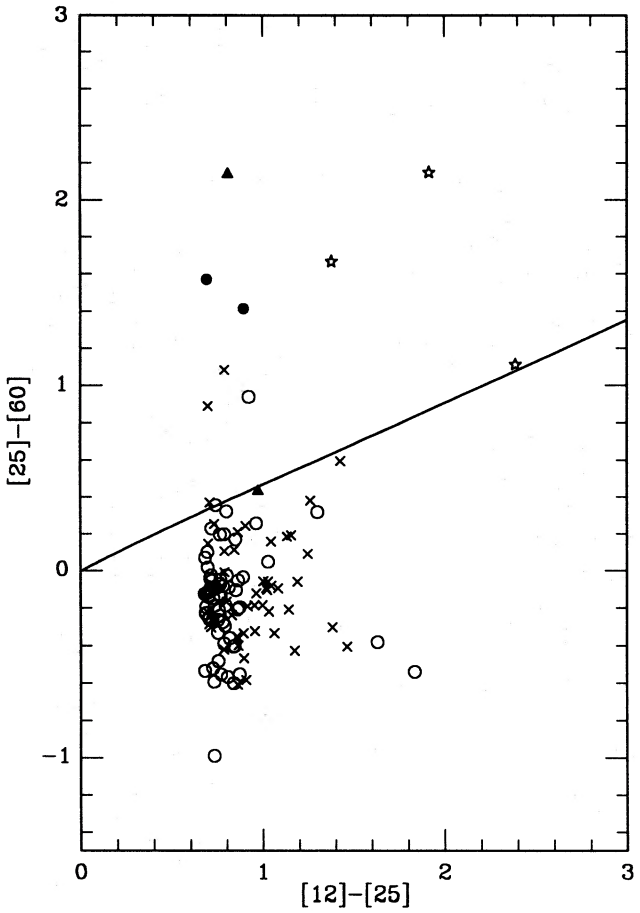

Figure 4. *IRAS* two-colour diagram. Symbols are as for Fig. 1.

loss rate. As discussed in detail in Paper I, the K and [12] fluxes originate from the star and from the shell, respectively, so the larger is $K-[12]$ the thicker is the shell. Most (>90 per cent) of the M stars have thin shells with $K-[12]<2.2$, whereas all of the other stars discussed here and 80 per cent of the Miras have $K-[12]>2.2$. The M stars with shells of similar thickness to those of the Miras are of particular interest and are discussed in more detail below (Section 7.7).

Figs 8–10 compare various colours of the M stars as a function of their spectral type with those of bright M giants discussed by Feast et al. (1990). These can be compared to similar diagrams for the Stephenson stars and symbiotic stars discussed by Whitelock & Munari (1992). The Stephenson stars and the M stars under discussion have similar characteristics, which are quite distinct from those of the bright M giants, except for stars of spectral types M7 or later. The difference between the 25/12-μm flux ratios of the M stars and of the bright M giants is to some extent to be anticipated, as our sample was selected on the basis of this flux ratio. It is therefore not immediately clear if there are two discrete groups or if the stars under discussion are merely the extreme tail of a broad distribution. The Stephenson stars (see Whitelock & Munari 1992), however, show a similar, though less extreme, difference. This, together with the fact that the bright M giants form a distinct group with the kinematics of relatively young, massive objects (cf. SWF), suggests that the M stars of spectral type M6 and earlier are distinctly different from bright local M giants of the same spectral type. The most obvious difference is in the thickness of the circumstellar shell, although this itself must be a consequence of differences in mass and/or composition. For later spectral types the distinction, if any, is less clear, and it may be that all non-Mira M giants later than M6 have similar characteristics, i.e., the local late-type stars may be part of the same population as the stars under discussion.

7.1.1 A comparison with the Bulge M stars

The M stars in the NGC 6522 field of the Bulge (Frogel & Whitford 1987), which is at galactic latitude $b\sim-4°$, have *JHK* colours which lie in the region between the two solid lines in Fig. 6(a) (see Feast et al. 1990). Frogel et al. (1990) examined the colours of M stars from six Bulge fields over a range of galactic latitude and found what they described as 'a steady progression with latitude in the mean $(J-H, H-K)$ relation ...'. Frogel et al. attribute this 'steady progression' to the effects of a metallicity gradient in the Bulge, and comment on the similarity of the stars in the outer Bulge to the ones found in globular clusters. An alternative interpretation (Feast, Whitelock & Sharples 1992) is that there are two dominant populations in the Bulge. At high latitude there are the metal-deficient stars from the inner halo. At low latitudes stars with a range of metallicities are found, but the M stars

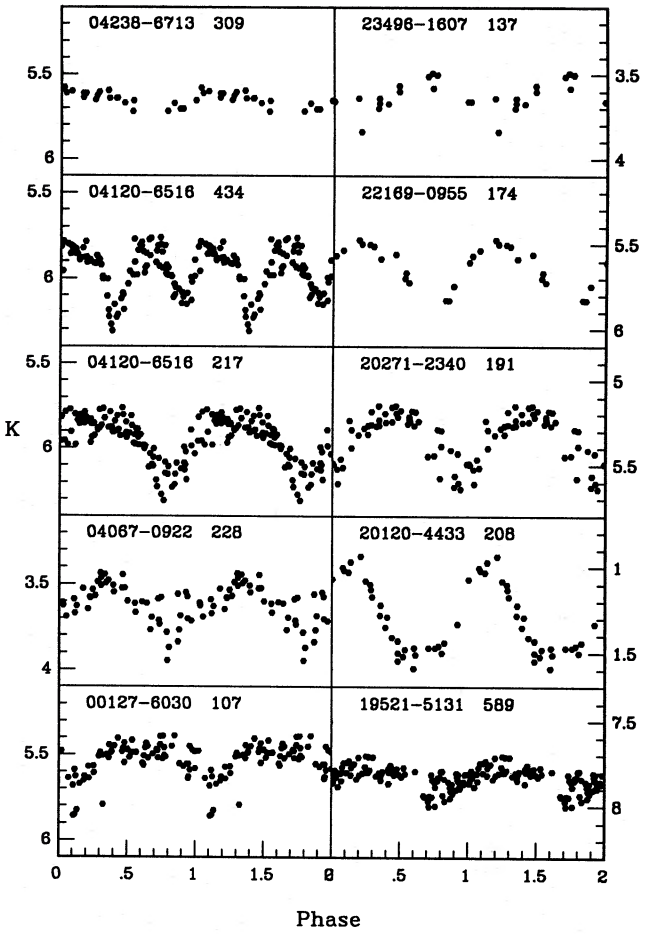

Figure 5. *K* light curves for the variables. Note that each point is plotted twice, and the choice of zero phase is arbitrary. The *IRAS* name and the period are given for each object. 04120−6516 is illustrated twice, once for each of its possible periods.

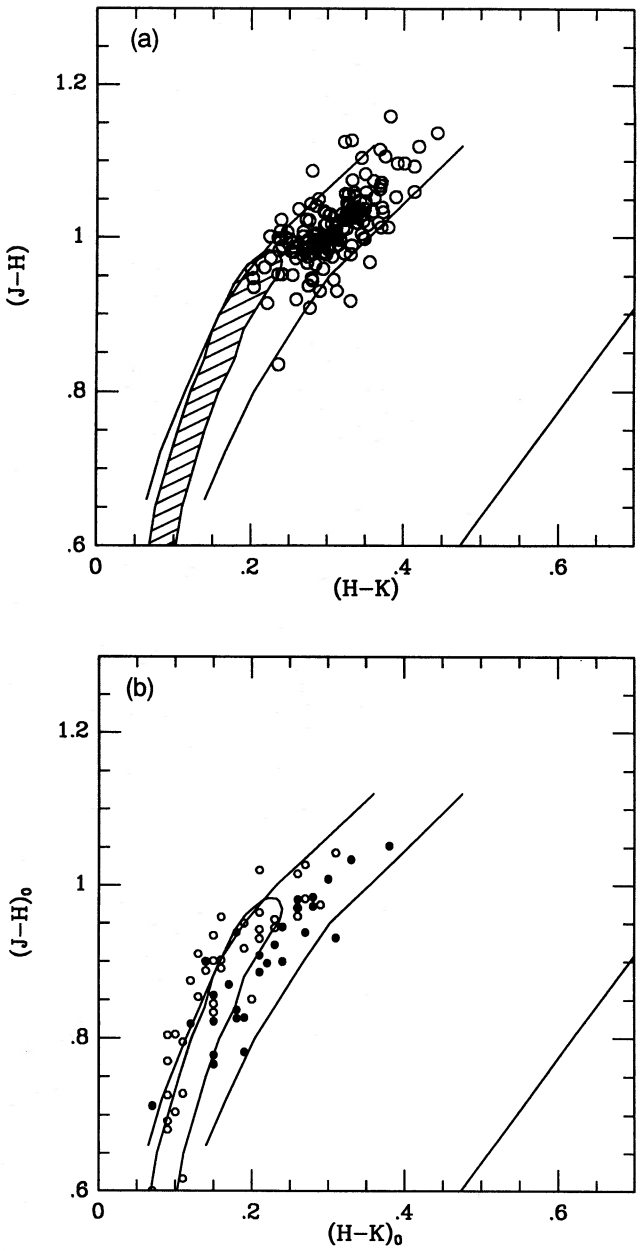

Figure 6. (a) A section of Fig. 1 comparing the M stars with the bright local M giants (hatched region) and M giants from the Bulge field at $b \sim -4°$ (roughly parallel lines) (see Feast, Whitelock & Carter 1990). (b) M giants from the inner Bulge ($b \sim -3°$ closed circles) and outer Bulge ($b \sim -12°$ open circles). The data are from Frogel et al. (1990), tables 2 and 6, converted on to our photometric system.

are dominated by a moderately metal-rich population similar to that of the disc. Intermediate regions contain different proportions of the two groups. The two extremes are illustrated in Fig. 6(b), which shows the colours of the M stars (excluding large-amplitude variables) from the lowest, $b \sim -3°$, and highest, $b \sim -12°$, latitude fields examined by Frogel et al. [after correcting for reddening and transforming to the SAAO (Carter) system].

Following Rich's (1988) conclusion that although there was a large spread of abundances amongst Bulge K stars the mean abundance was about twice the solar value, it has generally been assumed (e.g. Frogel & Whitford 1987; Frogel et al. 1990) that the peculiar colours of M stars in the Bulge were a consequence of supermetallicity. Recent work by McWilliam & Rich (1994) indicates that the mean Fe/H for K stars in the NGC 6522 window of the Bulge is only [Fe/H] ~ −0.25, considerably less than previous work suggested. They did, however, find that abundances of certain α-elements, e.g., Ti and Mg, were considerably enhanced over their solar values. McWilliam & Rich argue convincingly that the excess Ti might reasonably account for many of the peculiarities of the M stars in the Bulge. It is clear that the majority of the M stars in the South Galactic Cap have colours (Fig. 6a) that are similar to those of the reddest stars in the inner Bulge and distinctly different from those in the outer Bulge and in globular clusters. The bulk of these stars are therefore not from the halo but are probably part of a disc population (of thickness to be determined) which is similar and perhaps related to the Galactic Bulge. Possible metallicity effects in the Cap stars are discussed in more detail in Section 7.8, as is the influence of circumstellar reddening.

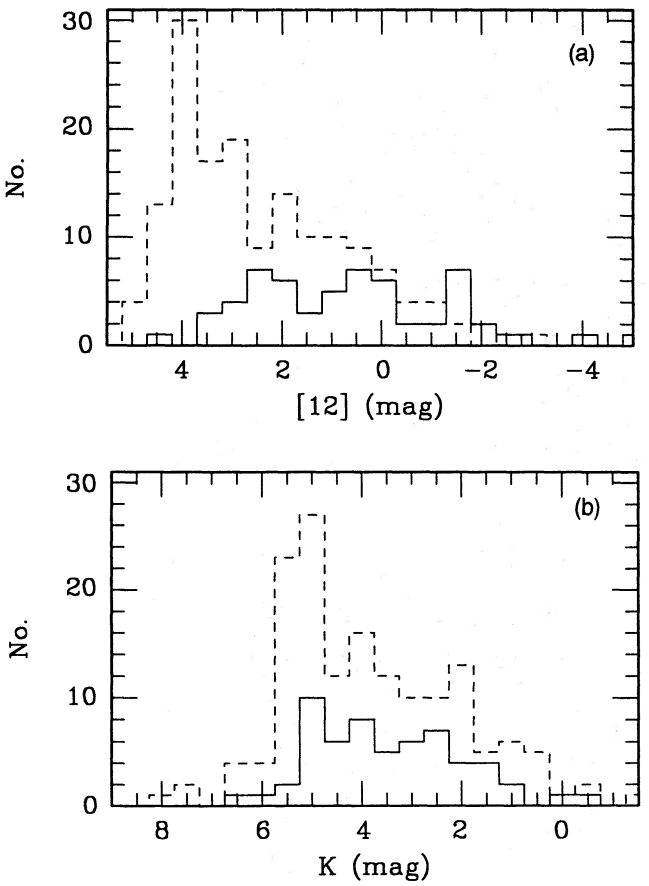

Figure 7. Histograms comparing the (a) [12] and (b) K magnitude distributions of the M stars (broken line) and of the Miras (solid line) from Paper I. The *IRAS* survey is complete to about [12] = 3.7 mag. At this limit the number of M stars is still sharply increasing, while the number of Miras has declined from its broad peak. Thus, while our survey of the South Polar Cap for Miras with dust shells is probably reasonably complete, the survey for M stars with shells is far from complete.

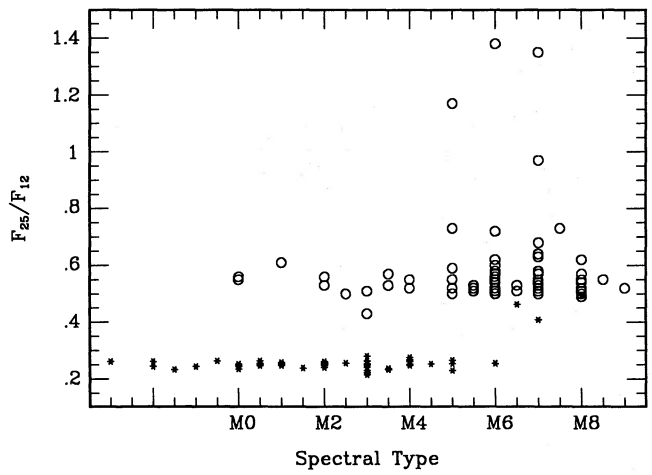

Figure 8. *IRAS* 25- to 12-μm flux ratio (*not* colour-corrected) versus spectral type for the M stars (open circles) and local bright giants (asterisks) from Feast et al. (1990).

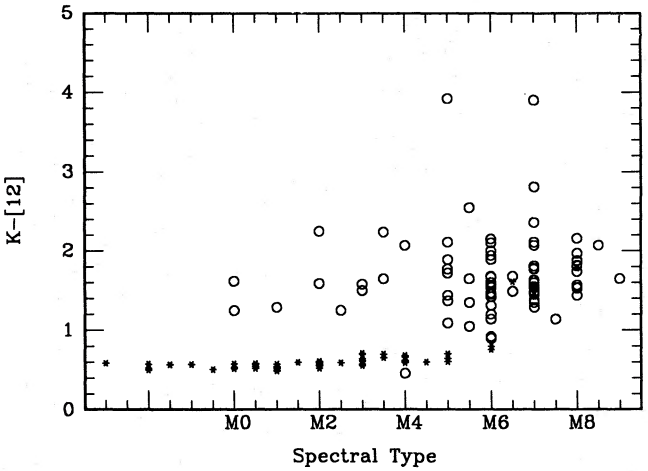

Figure 9. Dust shell thickness as measured by $K-[12]$ as a function of spectral type. Symbols as in Fig. 8.

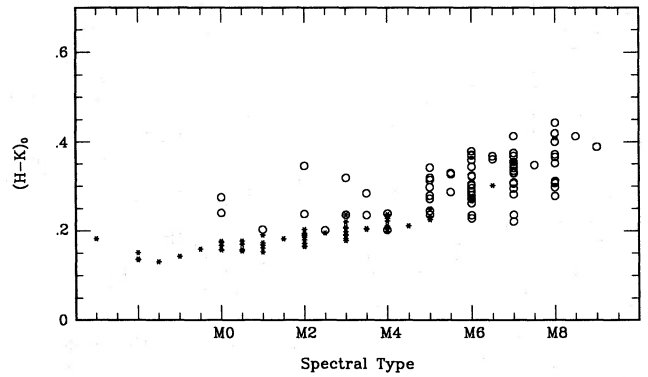

Figure 10. $H-K$ as a function of spectral type. Symbols as in Fig. 8.

7.2 Spectral types

The stars are predominantly late M, with 13 having types between M0 and M4, and 68 between M5 and M9. There are six stars with emission lines, classed as Me, a well-known feature of semiregular variables with extended atmospheres. These types are not necessarily strictly representative of the whole group, because spectral types have been published for the brightest stars only, and the SAAO spectra were preferentially obtained for stars whose colours differed from the mean. The list of spectral types given in Table 3 is not exhaustive, and the literature contains numerous estimates (not referenced here) for some of the bright stars. As might be anticipated, at least some of the stars have variable spectral types.

7.2.1 IRAS spectra

41 of the brightest M stars had low-resolution (LRS) spectra obtained by *IRAS* and illustrated in Olnon et al. (1986) or Volk et al. (1991). Their spectral types from the *IRAS* PSC or Volk et al. are listed in Table 1. 17 of them have blue featureless spectra of type 1*n*, with *n* between 3 and 6.

According to the *IRAS* ES this would imply a spectral type somewhat earlier (<M5) than is found for the sample observed optically. The other 24 have blue spectra with silicate emission: types $2n$ and n ranging from 1 (weak emission) to 9 (strong emission). Similar spectral types were found for the Miras (Paper I) although a few of those had more extreme types (e.g. 69) not represented among these M stars.

7.3 *HST* Guide Star Catalog magnitudes

The GSC contains a magnitude measurement for all but two of the M stars. The magnitudes come from three types of plate, bandpass codes 0, 1 and 6, as described by Russell et al. (1990). It is generally assumed that code 0 magnitudes approximate Johnson B, while code 1 and 6 magnitudes approximate Johnson V. Using Cap stars for which we have both photoelectric and GSC magnitudes (Table 4) the following relations were derived:

$$V = v + 0.34 \quad (\sigma = 0.37, 16 \text{ stars}), \tag{1}$$

$$B = b + 0.45 \quad (\sigma = 0.37, 63 \text{ stars}), \tag{2}$$

$$V = b - 1.17 \quad (\sigma = 0.35, 63 \text{ stars}), \tag{3}$$

where b and v correspond to the values tabulated in the GSC from code 0 and 1 plates, respectively, and B and V are the measured photoelectric values on the standard Johnson system. Equation (3) is valid only because of the narrow range of $B-V$ shown by the stars under discussion. Plots illustrating these fits are shown in Figs 11(a) and (b). The scatter will originate from a combination of real variability of the source and uncertainty in the GSC measurement. The GCVS lists amplitudes, mostly photographic, for known variables in the range $\Delta m_p \sim 0.6$ to 3.0 mag with a mean value of $\Delta m_p = 1.4$ mag. There are only two stars with observations from GSC code 6 plates and no corresponding photoelectric photometry. It is therefore assumed that code 6 values are identical to code 1 values. The last column of Table 4 contains the values of V_{GSC} derived using equations (1) or (3). For the three stars where GSC magnitudes from both code 0 and 1 plates were available a mean of the two derived Vs was used. Magnitudes marked with one or two colons were flagged in the GSC as extended sources; some of these magnitudes seem to be reasonable and others not. Those marked with one colon were used in the analysis below, while those marked with two were not. The three magnitudes flagged with a question mark were also not used in the analysis, because they differed from the photoelectric measurements of the same star by more than 1 mag. One of these stars, 20120−4433 (RZ Sgr), is obviously a large-amplitude variable (see Section 6.1), and the other two might reasonably be expected to show similar variability.

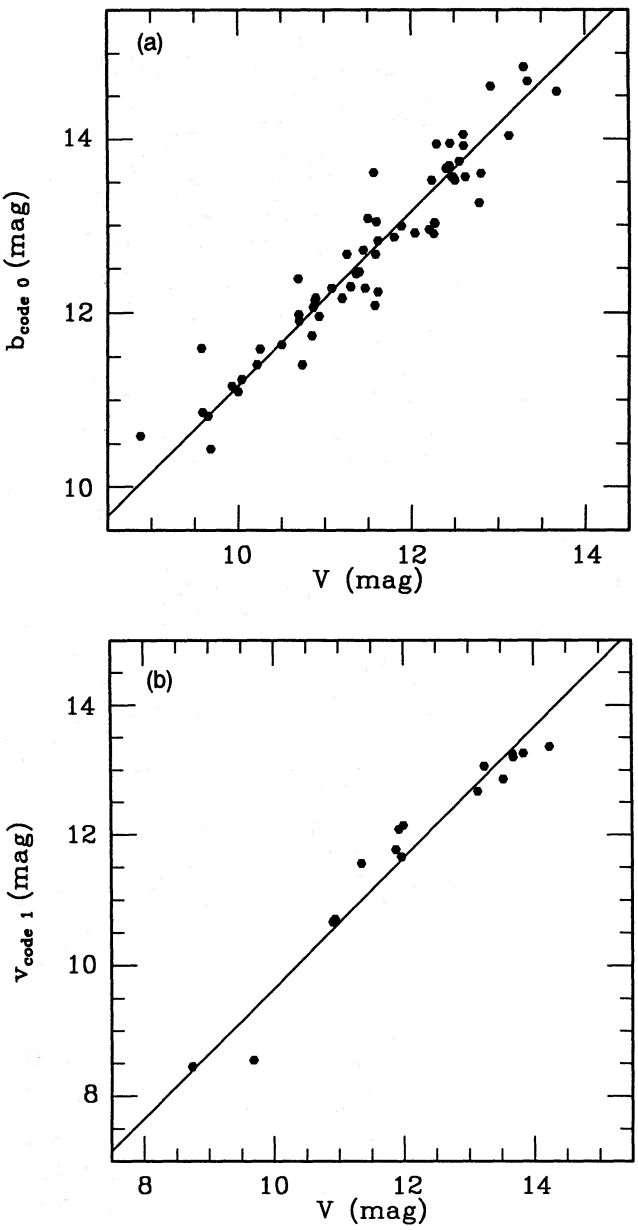

Figure 11. Magnitudes from the *Space Telescope* GSC are plotted against photoelectric values for (a) stars measured on code 0 plates and (b) stars measured on code 1 plates. The straight lines are least-squares fits to the data as specified by equations (1) and (3).

7.4 Distances and bolometric magnitudes

The apparent bolometric magnitudes (m_{bol}), which are listed in Table 3, were calculated by integrating under the *JHKL*, 12- and 25-μm flux curves as described in Section 6 of Paper I.

A major problem arises in the analysis of non-Mira late-type variables, in that we have as yet no way of reliably determining their distances. The literature contains a number of possible approaches to the problem, all of which are open to criticism: Whitelock (1986) determined an approximate period–luminosity (PL) relation for red variables in globular clusters, but these have somewhat different colours from the stars under discussion; Young, Phillips & Knapp (1993) (quoting Kleinmann 1989) assume $M_K = -8.1$; Kerschbaum & Hron (1992) assume $M_{bol} = -4.4$ for O-rich non-Miras; Jura & Kleinmann (1992b) assume either a constant luminosity (e.g. $M_{bol} = -4.5$ for SRs with $300 \leq P \leq 400$ d, or $M_K = -7.57$ for $100 \leq P \leq 150$ d) or a modified version of the Mira PL relation for some other subsets. Stephenson (1986a) assumes $M_V = -0.9$ or $M_V = 0$, and the latter assumption was also used by SWF.

We tested the assumption $M_V = 0$ using the visual magnitudes derived from the GSC and listed in column 7 of Table 4 (except for those marked with two colons or a question mark for which the V given in column 3 of the table was used). This assumption results in absolute bolometric magnitudes of $M_{bol} < -6$ mag, for the reddest stars in the sample, implying initial masses of a few solar masses for these stars. It also puts several of these luminous, and hence moderately massive, stars at heights above the Galactic plane in excess of 2 kpc. We would anticipate that such luminous AGB stars would evolve into Miras with periods of more than 850 d. Miras with such long periods are unknown in this volume, and Miras with periods over 500 d are not found at heights above the plane in excess of 1.5 kpc (fig. 16 in Paper I). These inconsistencies clearly indicate that the assumption $M_V = 0$ results in an overestimate of the luminosity, at least for the reddest stars. This might be anticipated from the statistical parallax results of Mikami & Heck (1982) who determine, for M stars with spectral types of M7/8, a much fainter absolute magnitude than for stars of earlier type.

In view of the similarity of the stars in our sample to those in the Bulge (Section 7.1.1), it was decided to use the Bulge stars in the NGC 6522 field (Frogel & Whitford 1987) to calibrate the distance scale. A second-order polynomial was fitted to the K magnitudes of the Bulge stars as a function of $(J-K)$ to give

$$K = 18.82 - 13.3(J-K)_{CIT} + 3.3(J-K)^2_{CIT}. \quad (4)$$

This can be converted to a relation for M_K by using the mean distance modulus of Miras in the same field (data from Glass & Feast 1982 and Wood & Bessell 1983) and assuming the PL relation given in Paper I (equation 1). Note that this mean modulus is not the best estimate of the modulus of the Galactic Centre. Assuming, in addition, $(J-K) = 1.12(J-K)_{CIT}$, we have

$$M_K = 4.1 - 11.88(J-K) + 2.63(J-K)^2, \quad (5)$$

which is valid for $0.8 < J-K < 1.6$. Thus typical stars under discussion with $1.1 < J-K < 1.6$ will have $-5.8 > M_K > -8.2$.

Distances calculated from this equation and the apparent K magnitude are listed in Table 3. This calibration results in the distribution of absolute V magnitudes shown in Fig. 12 and bolometric magnitudes in the range $-2.8 > M_{bol} > -4.6$. Given the Miras which are found in the same spatial volume (Paper I), we might have anticipated finding M stars with bolometric magnitudes as bright as $M_{bol} \sim -5.4$, although it is difficult to predict this with certainty. It is therefore possible that at least some of the distances are being underestimated by this approach.

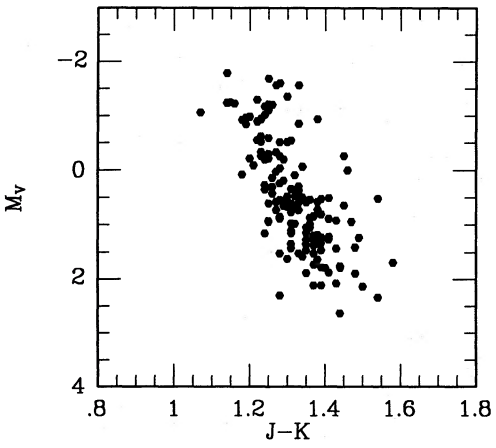

Figure 12. Absolute visual magnitude as a function of colour.

7.5 Scaleheight and galactic distribution

The Galactic distribution of the M stars is shown in Fig. 13. There are more in the hemisphere towards the Galactic Centre (99) than away from it (55), as was also found for the Miras. There is, however, no asymmetry between the first (49) and fourth (50) galactic quadrants of the type found for the Miras. Note that the section of sky not surveyed by *IRAS* falls entirely in the hemisphere towards the Galactic Centre, in the first quadrant at $b > -52°$ and in both quadrants at $b < -52°$. The isolated outlying stars in the figure all have thick shells (large $K-[12]$) and were therefore detected by *IRAS* to greater distances than the other stars.

A rough estimate may be made of the scaleheight of the M stars, following the procedure used by Stephenson (1986a) and by SWF. The observed numbers were extrapolated to

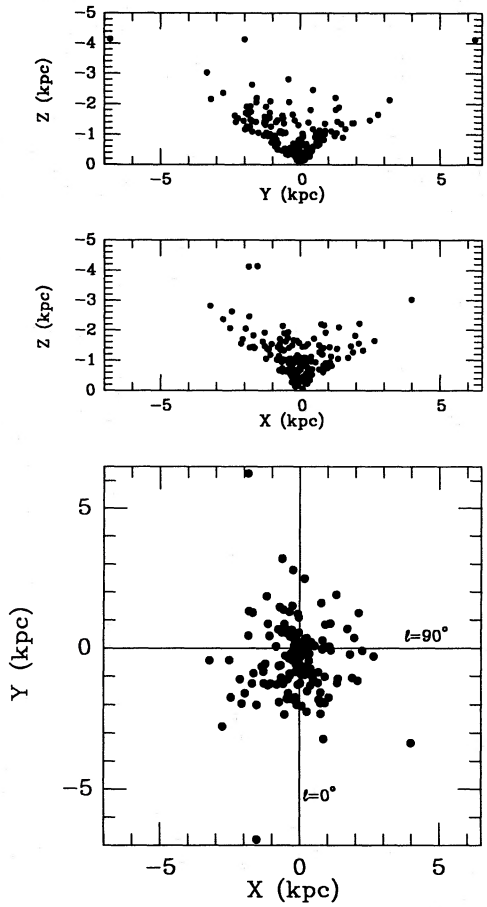

Figure 13. The Galactic distribution of the M stars under discussion. The Sun has (X, Y, Z) coordinates of (0, 0, 0); X and Y increase in the direction of Galactic rotation and the direction of the anticentre, respectively.

calculate the number of stars within a cylinder of radius 1.3 kpc extending 1.2 kpc above the Galactic plane, with the Sun at the centre of its base. No allowance was made for the area not scanned by *IRAS*. Stars with $K-[12]<1.1$ were omitted as they would not have been detected to distances of 1.8 kpc, the distance to which we estimate the survey should otherwise be complete. The resulting distribution of stars, as a function of height above the plane, is shown in Fig. 14. This can be fitted by an exponential with a scaleheight of 400 pc as illustrated, although there is a slight excess of stars below 300 pc. This scaleheight is smaller than the 600 to 700 pc found by SWF for the Stephenson (1986a) star sample. Two factors contribute to the difference: first, SWF assume $M_V=0$, which is, for most stars, more luminous than our estimate; secondly, Stephenson omitted known variables, which are mainly bright nearby objects from his sample, thereby biasing it towards larger distances (see Section 6). Compensating slightly for this, SWF used GSC magnitudes from code 0 plates without correction, so their estimates of apparent luminosity were typically 0.34 mag too bright.

The scaleheights of red variables were discussed by Jura & Kleinmann (1992b) and by Kerschbaum & Hron (1992). They divided their samples up according to period, which we are unable to do, and found scaleheights for most groups that are smaller than the 400 pc quoted above, with the exception of semiregulars with $200 \gtrsim P < 300$ d for which Jura & Kleinmann found a scale of ~500 pc. Both of these surveys suffer from incompleteness, as does ours.

Fig. 15 shows the height above the plane as a function of colour. Between $(J-K)\sim 1.2$ and $(J-K)\sim 1.4$ there is a trend towards lower heights with increasing $J-K$. This may be real or an artefact of the distance scale calibration. If real, the trend may be a consequence of metallicity, in that the reddest and most metal-rich stars are found closer to the plane than the bluer metal-deficient ones.

If we are to understand these M stars as being related to the Miras discussed in Paper I, then we might reasonably anticipate that they originate from groups with a range of scaleheights, in which case the derivation of a single scaleheight is not very meaningful. It is clearly important that the distance scale for these stars is put on a firm footing before the matter is further investigated.

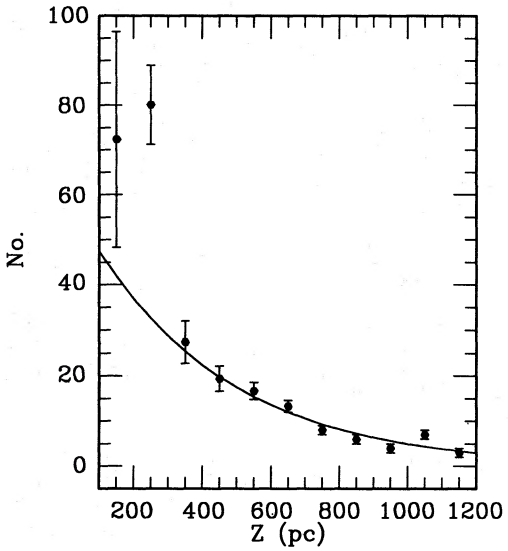

Figure 14. The extrapolated numbers of M stars in a cylinder of radius 1.3 kpc and height 1.2 kpc, with the Sun in the centre of the base. The error bars show the effect of changing the number of stars in a given bin by one star. The curve is an exponential with a scaleheight of 400 pc.

7.6 Kinematics

Table 6 contains the heliocentric velocities for the M stars as measured from our spectra or taken from the literature cited. The velocities measured from radio lines were originally listed relative to the local standard of rest. These have been corrected to heliocentric values, assuming $(U, V, W)=(7, 13, 7\ \mathrm{km\ s^{-1}})$ (Balona & Feast 1974), for use in the analysis described below. In order to work with as uniform a sample as possible, we used our own velocities in preference to others whenever possible. We also used other optical velocities in preference to radio values when there was a choice, and assumed an overall observational uncertainty of 18 km $\mathrm{s^{-1}}$. 19521 − 5131 was omitted from the analysis because of its extreme velocity, leaving a total of 58 stars. Ideally an analysis of the group motion would be made by fitting the observations with the equation

$$\rho = u\cos(l)\cos(b) + v\sin(l)\cos(b) + w\sin(b), \qquad (6)$$

where ρ is the observed radial velocity, and u, v and w are the components of a star's heliocentric space velocity in the direction of the Galactic Centre, in the direction of Galactic rotation, and towards the North Galactic Pole, respectively. Such an analysis was done with the following results: $u=-12\pm7$, $v=-33\pm11$ and $w=-11\pm7$ km $\mathrm{s^{-1}}$; the errors are large due to the small sample of stars. An alternative approach is to assume standard values of $u=-10.1$ and $w=-6.25$ km $\mathrm{s^{-1}}$ (Feast, Woolley & Yilmaz 1972) and to solve for the asymmetrical drift, v, which results in $v=-35\pm10$ km $\mathrm{s^{-1}}$. All of these are in good agreement with the values found by SWF for the Stephenson stars ($u=-5\pm4$, $v=-28\pm5$, $w=-7\pm4$ km $\mathrm{s^{-1}}$; or $v=-27$ km $\mathrm{s^{-1}}$ for assumed u and w). The velocity dispersions in the three coordinates, σ_u, σ_v and σ_w were then determined from a least-squares solution of the equation

$$\varepsilon^2 = \sigma_u^2[\cos(l)\cos(b)]^2 + \sigma_v^2[\sin(l)\cos(b)]^2 + \sigma_w^2[\sin(b)]^2, \qquad (7)$$

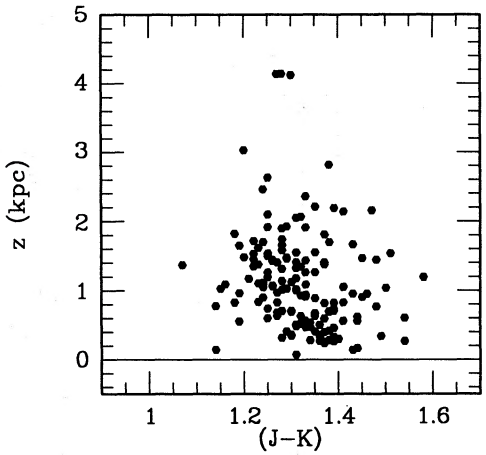

Figure 15. The height above the Galactic plane (Z) as a function of colour ($J-K$).

where ε is the residual radial velocity of a star from equation (6), with the standard values of u and w. The total velocity dispersion can then be written as

$$\sigma_T^2 = \sigma_u^2 + \sigma_v^2 + \sigma_w^2. \quad (8)$$

We find $\sigma_u = 28 \pm 26$, $\sigma_v = 35 \pm 37$ and $\sigma_u = 33 \pm 34$ km s^{-1}, from which $\sigma_T = 56 \pm 33$ km s^{-1}. Correcting the last value for the observational uncertainty of 18 km s^{-1}, we obtain $\sigma_T = 47 \pm 33$ km s^{-1}, in agreement with SWF ($\sigma_T = 63 \pm 4$ km s^{-1}) for the Stephenson stars, but again the uncertainty is large.

The value of the asymmetrical drift derived above, $v = -35 \pm 10$ km s^{-1}, can be compared with the values given in Paper I for Miras in the South Galactic Cap *IRAS* sample. Miras in the period range $250 \leq P < 350$ d have $v = -99 \pm 17$ km s^{-1}. Those with $P \geq 450$ d have no significant asymmetrical drift, while those of intermediate periods have a small drift (-19 ± 14 km s^{-1}). The result found here could indicate that the M stars are drawn from a mixed population which contains Miras with a range of periods, or that they are related to the intermediate-period group ($350 \leq P < 450$ d). Majewski (1992) (see also Norris 1993) has shown that for stars in the thick disc the asymmetrical drift is a function of the height above the plane. If this is true for the stars under consideration, then we would anticipate that the M stars would show a smaller asymmetrical drift than would the Miras from the same population, because the Miras are seen to larger distances. We would anticipate that few, if any, of these stars are related to the short-period Miras which are found in metal-rich globular clusters and at considerable heights above the plane ($Z > 2.5$ kpc) (see Paper I). The progenitors of these short-period Miras will be largely K or early-M stars (see also Sections 7.1.1 and 7.8).

7.7 The circumstellar shells

Given the initial selection criteria for this survey (*IRAS* sources with $F_{25}/F_{12} > 0.5$), we would expect all of the stars selected to have dust shells. Olnon et al. (1984) showed that Miras and OH/IR sources occupied a rather well-defined part of the *IRAS* two-colour diagram. Since then, various people have used the *IRAS* colours, particularly the 25/12-μm flux ratio, to select sources as potential OH/IR candidates. All of the *IRAS* sources discussed here fall into the category of potential OH/IR emitters on the basis of their 25/12-μm flux ratio alone.

The two M stars from which 1612-MHz OH maser emission has been detected, 02404+2510 and 03287−1535 (see Section 7.9), are particularly interesting. While one of these stars, 03287−1535, obviously has a thick shell and a high mass-loss rate as deduced from its colour, $K-[12] = 3.9$, the other, 02404+2150, has only a moderate shell with $K-[12] = 1.9$. In general, 1612−MHz OH emission is detected from a few kinds of object, namely Mira variables (including their long-period counterparts the OH/IR sources), red supergiants with high mass-loss rates, and a few very peculiar objects thought to be young planetary nebulae (PNe) or transition objects between the AGB and PN phases. The two *IRAS* sources in question, which have only single-peak detections, are probably semiregular variables, and 1612-MHz emission from such stars is very rare. It is possible that they are in the faint phase of the helium-shell-flash cycle, so that they are temporarily out of the Mira phase due to reduced luminosity, but will return to being Miras on a time-scale of about 10^4 to 10^5 yr (e.g. Boothroyd & Sackmann 1988). They are therefore worth more detailed investigation, and it would be particularly interesting to know if the OH masers are single-peaked or if they have second, weaker peaks, i.e., to establish the OH expansion velocity.

It is clear from Fig. 3 that there is an isolated group of four stars with extreme *IRAS* colours, $[12]-[25] > 1.5$, namely 03430+0325, 04375−3216, 04523−1359 and 22229−6855. The only odd feature of these stars is the high value of their $[12]-[25]$ colour. In all other respects (as far as can be ascertained from the available information) these stars appear similar to the other M stars. Two of them, 04375−3216 and 04523−1359, have very weak *IRAS* fluxes, so it is possible that their peculiar colours are merely a consequence of large errors. However, 03430+0325 is relatively bright and there can be little doubt of its colour. It has been selected, on the basis of its *IRAS* colour, as a possible OH/IR source, but three searches for OH maser emission have been unsuccessful (Lewis, Eder & Terzian 1990; te Lintel Hekkert et al. 1991; Lewis 1992).

A number of the sources discussed here, with much less extreme colours than the four mentioned above, have been selected on the basis of their *IRAS* colours as potential OH masers. For example, Lewis (1992) lists second-epoch observations (non-detections) for 00025+0027, 00371+1355, 01217+2341, 01253+2816, 01438+1850, 01519+0427, 01527+1656, 01597+1601, 04191+0346, 22497+1733, 22553+1744, 23082+1903, 23196+1615 and 23492+0846, as well as 03430+0325. These stars, which have the same *IRAS* colours as OH/IR stars but do not exhibit masers, have been dubbed 'OH/IR star mimics' by Lewis (e.g. 1992), and a considerable amount has been written about them. The most obvious contribution we can make to the subject is to point out that, on the basis of near-infrared photometry, they are not Miras. Their circumstellar shells, although cool, are mostly very thin; their $K-[12]$ colours range from 1.3 to 2.1. Nevertheless, it is not obvious why 02404+2150, with $K-[12] = 1.9$ at a distance of over 4 kpc, should have an OH maser when none of these stars does.

Although the M stars have, on average, the thinnest shells of any of the *IRAS* sources studied in the course of this survey, those with thicker shells than the majority are potentially very interesting. The stars with the thickest shells, $K-[12] \geq 2.4$, and therefore the highest mass-loss rates, are listed in Table 7, where the mass-loss rates are derived from fig. 21 of Paper I. These stars may be representatives of the short-lived evolutionary phases discussed above, and as such are good candidates for radio molecular line searches [03287−1535 is a known 1612-MHz OH maser, as discussed above, and 20270−2858 has been examined but not detected (Paper I)]. Alternatively, they might be binaries in which the interaction of the two stars is responsible for the extra circumstellar material and/or its heating. It should, however, be borne in mind that the stars with $K-[12] \geq 2.4$ represent the extreme of a continuum with a range of values down to $K-[12] < 1$. This other extreme is more typical of bright M giants in the solar neighbourhood (see Fig. 9). If the calibration of $K-[12]$ against mass-loss rate derived in

Table 7. M(S)-stars with 'thick' shells.

IRAS name	K–[12] (mag)	K–L	D (kpc)	$\log(\dot{M})$ $M_\odot yr^{-1}$
03287 – 1535	3.93	0.41	1.1	-5.7
04258 – 0155	3.31	-	7.7	-6.1
19521 – 5131	3.89	0.51	8.1	-5.7
19575 – 4317	2.64	0.28	2.3	-6.4
20174 – 7853	3.39	0.29	4.6	-6.0
20240 – 2142	2.49	0.27	2.4	-6.6
20270 – 2858	2.68	0.51	4.0	-6.4
21060 – 0029	3.01	0.31	6.0	-6.2
22169 – 0955	2.40	0.43	2.7	-6.6
22296 + 2004	3.15	-	3.1	-6.2

Paper I (see Paper I, fig. 21) is also appropriate for these non-Miras, then most of them have mass-loss rates in excess of about $10^{-7}\,M_\odot\,yr^{-1}$.

Of the eight stars with L measurements in Table 7, four have $K-L \geq 0.4$. Only two stars (04120 – 6516 and 04238 – 6713) with $K-[12] \leq 2.4$ have such a large $K-L$. The high $K-L$ might indicate an atmospheric structure for these stars which is intermediate between that of the other M stars and that of the Miras. Alternatively, it could result from extra heating of circumstellar dust by a companion star. There is insufficient information to choose between these hypotheses.

These stars with 'thick' shells are rare. Of the 88 M stars within 1.8 kpc of the Sun, only one has $K-[12] \geq 2.4$. This compares with approximately 100 Miras, with pulsation periods greater than 300 d, in the same volume of space. The lifetime of a Mira is about 2×10^5 yr (Whitelock & Feast 1993, and references therein). Thus, if these M stars with high mass-loss rates are evolving through a normal phase of single-star evolution, it must be a short-lived one, of the order of 2000 yr. This is, however, considerably longer than the ~200 yr we would estimate it takes the dust shell to dissipate (in terms of its 12- and 25-μm flux) if the mass loss ceased abruptly (Whitelock et al. 1991a). It is likely that the mass loss does not cease abruptly, as the Mira instability strip is left during a helium-shell flash. It is also possible that an AGB star enters and leaves the Mira strip more than once due to successive helium flashes, and that the dust shell ejected by the Mira takes over 200 yr to dissipate each time the star stops pulsating. The figures given above are only rough estimates because of the uncertainty in the distances to the M stars. The general question of changing mass-loss rates on the AGB was considered by Zijlstra et al. (1992).

7.7.1 Possible members of the Magellanic clouds

Although three of the stars included in this work, 00221 – 7614, 00542 – 7334 and 04238 – 6713, could be supergiant members of the Magellanic Clouds, it seems highly unlikely that they are (see below), and they have therefore been treated in the same way as the rest of the sample. If they were members of the Clouds, then their bolometric magnitudes would exceed −9.3, making them among the most luminous M stars known. Note that Prévot et al. (1983) described 00221 – 7614 (their star 4) as a foreground star on the basis of its bright V magnitude, $V = 10.5$.

Table 8. Mean properties of M stars (see Fig. 16).

	Group 1	Group 2	Group 3
no. stars	27	101	26
Sp Type	5.2	5.9	7.0
J–K	1.30 ± 0.02	1.33 ± 0.01	1.30 ± 0.02
K–[12]	1.68 ± 0.13	1.47 ± 0.04	1.93 ± 0.13
V–K	6.33 ± 0.24	8.52 ± 0.88	7.31 ± 0.29
$\bar{z}$ (kpc)	1.33 ± 0.15	0.98 ± 0.07	1.50 ± 0.11
z_0 (pc)	> 500	> 330	> 560
$\Re$ (Y < 0/Y > 0)	0.8	1.9	4.2

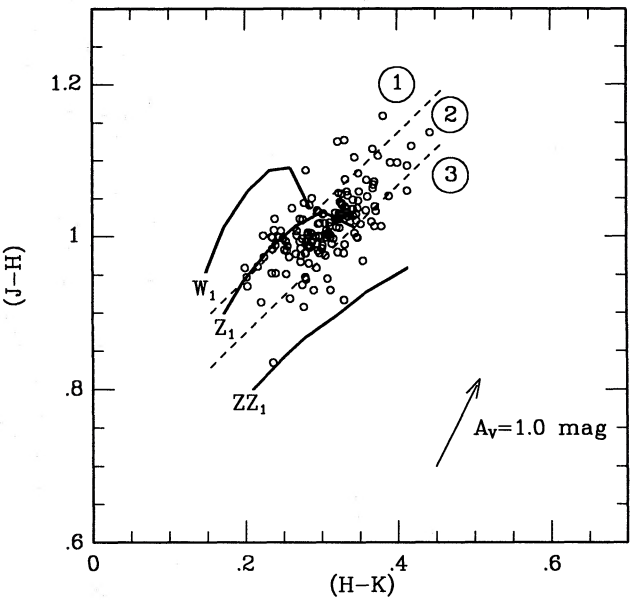

Figure 16. The stars from Fig. 6(a) compared to models with different metallicity, $\log(Z/Z_\odot)$. The solid lines are evolutionary tracks (Bessell et al. 1989) for the models, ZZ(+0.5), Z(0) and W(−0.5), after the transformation discussed by Feast et al. (1990) to force the Z model to coincide with nearby bright giants. The broken lines divide the colours into three groups as discussed in the text. A 1-mag reddening vector is also shown.

7.8 Metallicity effects

Following the finding that the *JHK* colours of stars in the inner Bulge differed from those in the outer Bulge (Frogel et al. 1990, Section 7.1.1 and Fig. 6), it is of interest to compare the properties of the Cap stars from different parts of the *JHK* two-colour diagram. Table 8 compares the properties of stars from the three regions in Fig. 16, divided by the dashed lines. Specifically, group 1 contains stars with $(J-H) > 0.965(H-K) + 0.75$, group 3 those with $(J-H) < 0.965(H-K) + 0.68$, and group 2 are those in between. The values tabulated are the means for the whole group or, in the case of spectral type, for those stars in the group which have the relevant measurement. The group to which each individual star belongs is indicated in the final column (class) of Table 3. Fig. 17 shows a plot of $V-K$ against $J-K$, with the members of the three groups distinguished.

Fig. 18 shows the BVI_C colours of those stars with optical photometry listed in Table 4, distinguished according to the

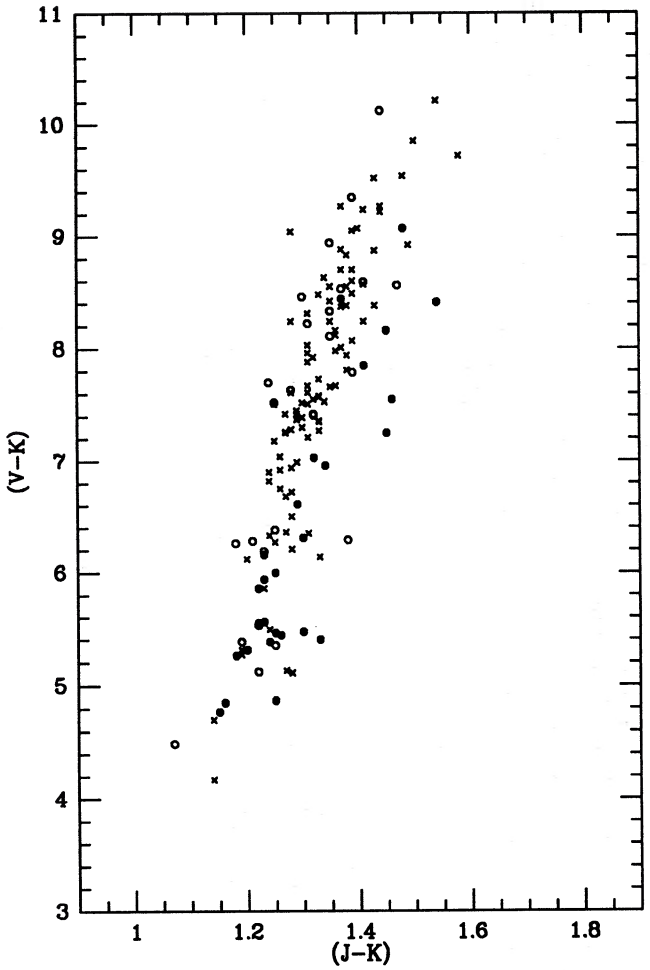

Figure 17. Combined optical near-infrared two-colour diagram. Open circles: group 1; crosses: group 2; closed circles: group 3. Note that the V and K measures were not made contemporaneously, so considerable scatter will be caused by variability as well as by uncertainties in the V mag.

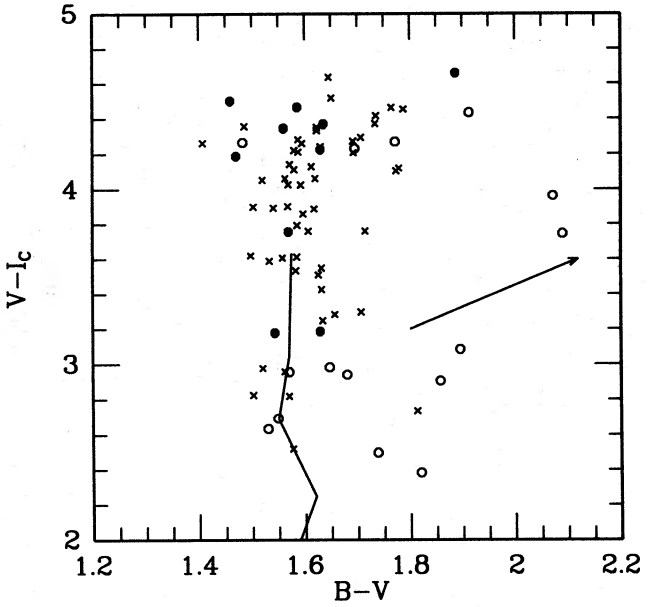

Figure 18. Optical colours from Table 4, open circles: group 1; crosses: group 2; closed circles: group 3. The solid line is the relation for field giants from Bessell (1990). The arrow is a reddening vector for $A_V = 1$ mag.

three groups defined above. There is no complete separation of the groups in this diagram, although there is a tendency for the group 1 stars to have larger values of $B-V$ and smaller values of $V-I_C$ than do the stars from group 3. It is possible that the largest values of $B-V$ are due to the effects of circumstellar reddening.

A detailed comparison of colours with models would be very helpful in understanding the characteristics of these stars. Unfortunately, there are as yet no models which are good enough at the low temperatures of these M stars to allow this to be done with confidence. In Fig. 16, three evolutionary tracks from Bessell et al. (1989) are compared to the observed colours. The early sections of the tracks run approximately parallel to the dashed lines which distinguish the three groups. Stars evolve from the lower left towards upper right; tracks for low-metallicity stars turn over at lower temperatures (where they become more uncertain) and a significant number of the points are outside the range covered by the tracks. It is possible that the colours are affected by circumstellar reddening as discussed below.

An examination of Fig. 18 suggests that $E(B-V) \sim 0.3$ mag is a plausible reddening for the redder stars if they have an intrinsic $(B-V) \sim 1.6$. Assuming that the wavelength dependence of the circumstellar reddening is similar to that of interstellar reddening, this $E(B-V)$ will result in $E(J-H) \sim 0.09$ and $E(H-K) \sim 0.05$. Thus the main effect of the reddening will be to push the colours to the upper right of Fig. 16. We expect objects near the ends of the evolutionary tracks to have higher mass-loss rates and therefore to experience greater reddening. Thus the observed sequence would be stretched with respect to the tracks and would appear more nearly parallel to the lines dividing our sample into three groups.

Despite the problems of disentangling circumstellar reddening effects, a qualitative comparison of the evolutionary tracks with the observations suggests various possible reasons for the differences between the three groups. It seems likely that metallicity, surface gravity and surface extension all play a role, but it is possible that metallicity is the dominant factor. A comparison with the models in Fig. 16 suggests that stars in group 3 have higher metallicity than those of group 1 and that the bulk of the stars have a metallicity close to solar or slightly higher, although the absolute calibration of metallicities is much less certain than the relative one. The distribution in Fig. 17 can also be understood in terms of metallicity effects. An increase in the metallicity of a star will increase $V-K$ and decrease $J-K$. None of the models discussed allows for abundance anomalies of the kind found in Bulge K stars by McWilliam & Rich (1994; see also Section 7.1.1), and it would clearly be important to investigate the effects on colours of altering the abundances of α-elements without changing those of the iron-peak elements.

Group 3 has the highest mean $K-[12]$ (Table 8) and therefore the highest mass-loss rate, which might be anticipated for the highest metallicity group. More curiously, group 1 has a higher $K-[12]$ than group 2. One might

expect that any group of low-metallicity M stars will contain a higher fraction of more evolved stars than will a higher metallicity group. This is because the molecular features characteristic of M stars will only become detectable in a low-metallicity atmosphere at low temperatures. The evolutionary tracks suggest that at low metallicity the most evolved stars, which will have the highest mass-loss rates, will be found amongst group 2 or 3 (unless the circumstellar reddening has the effect described above so that the observed tracks are stretched compared to the theoretical ones). Additionally, if observations of globular clusters such as 47 Tuc (Frogel, Persson & Kron 1981) are any guide, there will be significant numbers of small-amplitude variables, presumably with moderate mass-loss rates, on the earlier parts of the track, i.e., in the region of group 1. The scaleheight, z_0, was calculated assuming that $z_0 = 0.37 \times z_m$, where z_m is the median height above the plane. The inequality (see Table 8) derives from the incompleteness of the sample (see Section 7). The lower limit to the scaleheight of group 2 may simply be a consequence of incompleteness of the *IRAS* survey; the smaller mean $K-[12]$ for this group will render it incomplete at smaller distances than for the other groups.

Table 8 contains the ratio, $\mathscr{R}$, of the number of stars in the hemisphere towards the Galactic Centre to the number in the opposite hemisphere. There is a much stronger gradient, in the sense of more stars towards the Centre, in group 3 than in group 1. As noted previously, the section of sky not covered by the *IRAS* survey falls in the hemisphere towards the Centre, so that the actual gradient will be slightly steeper than listed. Thus these results suggest tentatively that the higher the metallicity the greater the concentration towards the Centre. It should also be borne in mind that 'metallicity' in this context will not necessarily mean [Fe/H] (see Section 7.1.1).

It is not entirely clear what the relation of this result is to the question of the Galactic distribution of the Mira variables. It has long been known (Oort & van Tulder 1942; Feast 1963) that the number of Miras increases strongly towards the Galactic Centre. This result refers to optically discovered Miras, the bulk of which have periods in the range 200 to 350 d. The more recent discussion of Jura & Kleinmann (1992a) and Jura, Yamamoto & Kleinmann (1993) suggests that the gradient is considerably more marked for the Miras with periods less than 300 d than it is for Miras in the period range 300 to 400 d or for those with thin dust shells and periods over 400 d (mostly in the range 400 to 500 d). A full quantitative discussion is difficult due both to the problems of completeness (Paper I) and to the fact that, for periods less than 300 d at least, the Miras cover a wide range of kinematic type (Feast 1963), so overall means can be misleading. These results suggest that the shorter period Miras, examples of which are found in disc globular clusters and which have thick disc or intermediate halo kinematics, are more concentrated to the Centre than are the longer period Miras which are more concentrated to the plane and which appear to be younger and/or more metal-rich. However, the galactic gradient for Miras with periods greater than 500 d is not known, as the classical OH/IR stars which probably represent the longest period end of the Mira sequence are again strongly concentrated to the Centre (Baud et al. 1981), although that trend may not continue right to the Centre. Further work should clarify some of these uncertainties and lead to a better understanding, both of late stages of stellar evolution and of Galactic structure. It may also be noted that this analysis, like most of these available, was carried out on stars well away from the plane and therefore cannot easily distinguish between the effects of a radial density gradient in the Galactic plane and a variation of the scaleheight, z_0, with radial distance. The latter could be important, e.g., for the shorter period Miras. There is also a possibility that some of the M stars in our survey may evolve into types of star other than oxygen-rich Miras, e.g., carbon-rich Miras.

7.9 Individual objects

Only stars with obvious pecularities, or for which there is some information about variability, are discussed below.

00127−6030, UY Tuc
This is a faint *IRAS* source whose catalogued colours changed significantly between versions 1 and 2 of the *IRAS* PSC. It would not have been included in this survey on the basis of the revised colours. Its spectral type is early (M3e) compared to that of most of the stars discussed here, and its infrared colours are rather blue. A Fourier analysis of the infrared photometry gives a 107-d period, in good agreement with the 105-d period listed in the GCVS, where it is described as a semiregular variable. The light curve (Fig. 5) shows a variable amplitude.

02404+2150
The near-infrared data show low-amplitude semiregular variability, but are inadequate for determining a period. The most likely periods are 184 or 370 d, which are one-year aliases of each other.

This source has been detected as a single-peak OH maser (Eder, Lewis & Terzian 1988, who assume that it is a double-peak source and that the second peak was below their detection threshold) and as an H_2O maser (Lewis & Engels 1991). 02404+2150 is definitely not a Mira variable now, but it may have been in the recent past. As discussed in Section 7.7, it may be a post-flash AGB star.

03287−1535
On the $(J-H)$ versus $(H-K)$ diagram this star falls among the normal M stars, while there is some indication of a weak L excess in the $(J-K)$ versus $(K-L)$ diagram. The $K-[12]$ and *IRAS* colours, together with the LRS spectrum which shows strong 10- and 20-μm silicate emission (type 29), suggest the presence of a relatively thick circumstellar shell of the variety more usually associated with O-rich Miras. It is included in Table 7. A Fourier analysis of the near-infrared photometry finds low-amplitude semiregular variability with a period of 108 d.

03287−1535 has been detected in CO (Nyman et al. 1992) and as a single-line 1612-MHz OH maser (Le Squeren et al. 1992). The stellar velocity deduced from these lines is -4.6 km s^{-1} (CO) and -4.5 km s^{-1} (OH). The fact that these velocities are essentially identical suggests that the source is not a double-peak OH emitter in which the second peak is below the detection threshold. This source is another candidate for the status of post-flash AGB star (see Section 7.7).

03318−8244
The *JHKL* data for this star show no clear periodicities, and the colours are those of a normal M star. The $K-[12]$ and $[12]-[25]$ colours are those of a moderately thick Mira-like shell. However, the *IRAS* flux is peak and the associated errors high, so better far-infrared data are required before the nature of the star is discussed further.

03324−4728
This star looks like a normal non-Mira on all of the two-colour diagrams. The 10 near-infrared observations show that it is variable, but provide no significant information about periodicity.

04120−6516
The *JHKL* and *IRAS* colours are those of a normal M star. The light curve is semiregular with a period of either 215 or 413 d. If 215 d is the correct period, then there is a tendency for shallow minima to follow deep ones in the manner of RV Tau stars. Such behaviour is seen in other M-type variables. The alternative *K* light curves are shown in Fig. 5.

04127+0110
There is nothing unusual about the colours of this star. It is a faint *IRAS* source whose catalogued colours changed significantly between versions 1 and 2 of the *IRAS* PSC. It would not have been included in this survey on the basis of the revised colours. The *JHKL* photometry shows very little variability. Surprisingly, the *IRAS* catalogue lists its variability index as Var = 9.

04238−6713
This has normal *JHK* colours, but perhaps a very weak $K-L$ excess. It is a semiregular variable with a period near 310 d (Fig. 5).

19521−5131
This star has normal *JHK* colours but shows a Mira-like excess at $K-L$ and $K-[12]$. It is listed in Table 7 as a 'thick' shell source. Its variations are semiregular and multiperiodic. It is, however, rather difficult to extract any definitive period information from the present data set, except that it may have two periods, of around 590 and 140 d, respectively. Fig. 5 shows the longer period which has the larger amplitude. The spectrum, which is illustrated in Fig. 19, shows an unusually strong Hα absorption line for the spectral type, M5, deduced from the strength of the TiO absorption. The radial velocity of 19521−5131 is the highest found among the M stars (see Table 5), and the star is presumably in the halo.

20120−4433, RZ Sgr
This is a well-studied lithium-rich S star (Catchpole & Feast 1976). Interestingly, it appears to be associated with visible nebulosity (Whitelock 1994), probably the result of an extended period of mass loss in the past. Its *JHKL* and *IRAS* colours place it among the normal M stars. Its LRS spectrum (type 16) does not show the signature of dust. Its variability, which is periodic with a large amplitude, together with its emission-line spectrum, are reminiscent of Mira-like behaviour. The data given here, which have been discussed by Whitelock & Catchpole (1985), indicate a period of 208 d (see Fig. 5). The photographic variability was studied by Gaposchkin (1947) using 515 observations; he describes it as well marked but peculiar, and suggests the star is multi-periodic. He derives a dominant period of 111.6 or 223.2 d, compared to Innes's (1903) earlier value of 212.4 d. On the basis of this the GCVS lists its variability class as SRb.

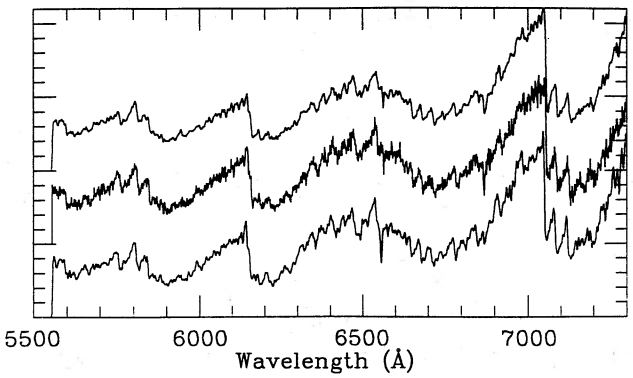

Figure 19. Spectra of two *IRAS* sources from the present investigation, 04257−3220 (middle) and 19521−5131 (bottom), compared with that of HD 210741, M5III (top). These stars all have the same spectral type, but note the great strength of Hα in the bottom spectrum.

Most solitary S stars are thought to be moderately massive. Reasons for suggesting that RZ Sgr does not fall into this category were given by Catchpole & Feast (1976) and by Whitelock (1994).

20240−2142
This star is listed in Table 7 as a 'thick' shell source, but aside from its $K-[12]$ it exhibits normal non-Mira colours. It is variable but not obviously periodic.

20270−2858
This exhibits normal non-Mira *JHK* colours, but shows a slight excess in $K-L$. This, together with the emission lines indicated in its M7e spectral type, suggests that it may be intermediate between Mira and non-Mira phases. It is variable and may be a multiperiodic, semiregular pulsator. It is listed in Table 7 as a 'thick' shell source.

20271−2340
This exhibits normal non-Mira colours. It is a semiregular variable with one period of 191 d (see Fig. 5) and another of possibly 218 or 499 d.

21270+0702
This exhibits normal non-Mira colours. It is a semiregular variable, but the data are not adequate to determine a period.

21377−0200 BD−2°5597
This exhibits normal non-Mira colours. It is variable, but the data are inadequate to determine the period. The star is in Stephenson's (1986a) survey for late-M stars, and its infrared colours have been discussed by Feast et al. (1990) and by Whitelock & Munari (1992). Optical variability was noted by Kaiser, Baldwin & Williams (1990), and optical photometry is given by Lahulla (1987). The magnitude, $V = 9.66$, is in agreement with the value determined from the GSC and measured by SWF.

22003−0010 AFGL 2835
Lahulla (1987) lists optical photometry for this star; the *V* magnitude is in agreement with the value derived from the GSC.

22169−0955, ZZ Aqr
This has non-Mira JHK colours but lies between the Miras and non-Miras in $K-L$. It is variable with a period of about 174 d (see Fig. 5) and seems similar to the Mira, SS Aqr, discussed in Paper I. It is listed in Table 7 as a 'thick' shell source.

22209−3508
This bright sources shows low-amplitude variability, but the data are inadequate to define the period. Its colours are normal for a non-Mira. It was examined for OH maser emission by Sivagnanam et al. (1990), but this was not detected.

23404+1713
The colours of this star are normal for a non-Mira and it shows only very low-amplitude variations.

23496−1607, Z Aqr, HD 223737
The *IRAS* and *JHKL* colours of this star are normal for a non-Mira, and it shows variability with a period which is consistent with the 135.5-d period (see Fig. 5) tabulated in the GCVS, where it is classified as SRa. Jura & Kleinmann (1992a) classify it as a Mira. Given its Me spectral type and the available information, it should probably be thought of as a border-line case between semiregular and Mira.

8 T TAURI STARS

This group comprises three *IRAS* sources: 02538+1953, 04451−0539, 23198−0230, which are described in more detail below. The three stars show very distinctive colours in all four two-colour diagrams. In Figs 1 and 2, their colours can be understood as the combination of a late-type star with a warm dust shell. Their $K-[12]$ colours (Fig. 3) indicate a moderately thick dust shell, while their positions in Fig. 4 suggest the presence of a cool component to the shell. Note also from Fig. 4 that these stars can be distinguished from the others on the basis of their *IRAS* colours alone. In summary, they all have very distinct and extensive dust shells.

These stars are probably closely related to the G and K stars with dust shells, also investigated as part of this survey and described in a previous paper (Whitelock et al. 1991b). In particular, the high lithium abundance (Pallavicini, Randich & Giampapa 1992) and moderate infrared variability of 23107−6833 (HD 219025) strongly suggest that it too is a pre-main-sequence star rather than an RS CVn object as previously proposed.

The *IRAS* variability index is zero for all three sources, but as 02538+1953 has only 3, and the other two stars only 2, hours-confirmed sightings (hereafter HCONS, see PSC-ES) this is not very informative. The near-infrared photometry indicates that all three are small-amplitude variables. Larger amplitude variability on a long time-scale is also indicated for 02538+1953.

8.1 Individual sources

02538+1953, WY Ari, LkHα 264
This is a well-known T Tau star, associated with the dark nebula, LD1454, whose infrared emission was discussed by Cohen (1974). The K magnitude listed by Cohen is somewhat fainter than the values given here. Our spectra show strong H, He, Ca II and Fe II emission, weak Na D emission, and an otherwise relatively featureless continuum. They are similar to those published by Cohen & Kuhi (1979), who classified the star as K3(C), indicating that at times the spectrum was fairly featureless, and by Downes & Keyes (1988), who classify it as of emission class 5 with a featureless continuum.

04451−0539
We identify this object with a pair of stars separated by 8.7 arcsec, the northern star being at a position angle of about 45° with respect to the southern one. The spectra of both stars (see Fig. 20) show H and Ca II emission, while the southern star also has weak He I and [O I] λ6300 lines. The northern star has a late-K or early-M continuum, while, although TiO bands are clearly present in the other star, the spectrum has a strongly veiled appearance. Both of the stars are probably T Tau objects and, following Cohen & Kuhi (1979), who deduced that all close pairs of T Tau stars are probably binaries, likely to be physically associated. Heliocentric velocities of -5 ± 7 and 10 ± 8 km s^{-1} were found for the northern and southern stars, respectively, from spectra in the blue region obtained at HJD 244 6467.3.

CCD photometry was obtained with a TEK512 chip on the 1.0-m telescope at Sutherland on a marginally photometric night. The northern star was found to have V, $(V-I)_C=15.0$, 2.3, while the values for the southern star were 15.6, 2.5 at HJD 244 7842.5. The red colour of the southern star is at odds with the rather flat spectrum shown in Fig. 20, but this indicates that the stellar continuum slope is strongly variable.

Only limited photometry was obtained of this object due to the difficulty in reliably separating the two components. Nevertheless, it is adequate to illustrate the variability but not to characterize it. The *JKL* colours of the two stars (Fig. 2) are quite different. Those of the northern component ($J-K=1.00$, $K-L=0.26$) are consistent with a normal M dwarf, while the southern component ($J-K=2.10$, $K-L=1.00$) shows the effects of emission from a warm dust shell. For the purpose of calculating $K-[12]$ for Fig. 3, it was assumed that the southern component was the *IRAS* source.

23198−0230, StHα 202
This star is variable, though not obviously periodic. It was brightening at K and becoming redder during the time

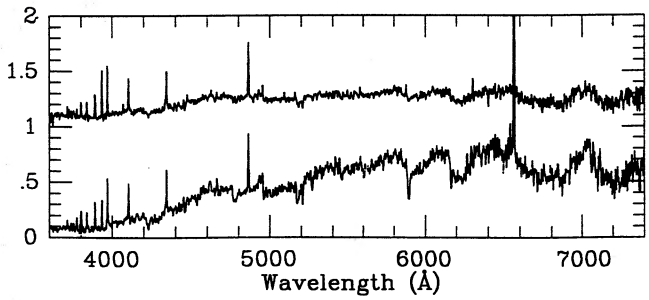

Figure 20. Spectra of the northern (lower) and southern (upper) components of 04451−0539, separated vertically for display. The zero level of the upper spectrum is halfway up the axis. The vertical axis shows relative flux, $F(\lambda)$. The Hα line is off scale for both spectra.

covered by these observations. Stephenson (1986b) detected Hα emission, while Downes & Keyes (1988) examined the spectrum in more detail and noted Hα as the only emission. They comment on the weak Mg b absorption and classify the star as F type, suggesting that it is probably a T Tau star. Our spectra support the assignment to the T Tau class, while showing more detail and suggesting a somewhat later spectral type. In particular, we find weak emission lines of Ca II, [O I] λ6300, [S II] $\lambda\lambda$4077, 6731 and [N II] λ6584. Although there is little evidence of Mg b absorption, the G band is prominent, there are CN bands at $\lambda\lambda$3885, 4215 and the Ca II H and K lines are present in absorption as well as in emission.

9 BINARY SYSTEMS

There are three sources falling into this category: 00016−3056, 02512−3758, 23198−0230. They are very different from each other and are therefore best discussed individually. The only common factor, beyond duplicity, is some level of interaction between the binary components which gives rise to the observed infrared excess. This excess (Fig. 3) is typically somewhat larger than that found for solitary M giants. There may be other binaries among the stars discussed in Section 7 (in particular, 20120−4433; see Section 7.9), although they are presumably not interacting to the extent that these three are. Perspective effects will probably be a significant factor in determining which binaries present clear pecularities.

The *IRAS* variability index is low for all three sources, but as 02512−3758 has only 3, and the other two stars only 2, HCONS this is not very informative. All three show near-infrared variability.

9.1 Individual sources

00016−3056

This is a 508-d eclipsing binary situated in the halo a few kpc above the Galactic plane. The *JHK* light curves show two eclipses as well as a pronounced reflection effect exceeding 0.5 mag at *J*. The primary is an early-M giant, possibly an AGB star; the nature of the secondary remains unclear. Whitelock et al. (1994b) describe the observations of this star in detail, and suggest that it may be a unique representative of a short-lived evolutionary phase. Note that if Unger et al. (1989) are correct in stating that the published *IRAS* fluxes are the result of 'a merger of a star and galaxy', then most of the 60-μm flux probably originates from the galaxy, and the colours on which its position in Fig. 3 is based will be erroneous. There is, however, no evidence for a galaxy close to the star and, in the absence of further information, we assume that all of the *IRAS* flux originates from the star.

02512−3758, SY For

This is a binary system comprising a semiregular variable and a hot subluminous companion (Feast 1975). Its position in the near-infrared two-colour diagrams has been discussed by Feast et al. (1984), who point out the similarity to *o* Ceti, a wide binary comprising a Mira variable and a white dwarf. Both SY For and *o* Ceti can be described as 'mildly symbiotic'. Their unusual colours probably arise from dust which is heated directly or indirectly by the white dwarf. The 230-d period found by Feast et al. in the early subset of these data does not persist in the later data, nor is there any sign of the 55-d period listed in the GCVS, supporting the classification of the star as a semiregular variable rather than as a Mira.

21392+0230

This object has peculiar *JHKL* and *IRAS* colours. It is a low-amplitude variable with a larger amplitude at *K* than at *J*, and a possible period of 900 d. It is conceivable that the period is orbital, but more observations are essential to confirm its reality. The existence of this object was pointed out to us by Tom Kinman (1983, private communication) who found it from an Hα survey with the Case Schmidt. It is listed in Stephenson's (1986) catalogue of Hα emission-line sources and its spectrum is described by Downes & Keyes (1988), who suggest it is a symbiotic star. Their spectrum contains strong emission lines of [O III], He I and the Balmer series superimposed on an absorption spectrum which includes the G band, Mg b, Na D and TiO absorption features. While our spectrum (Fig. 21), obtained in 1985 October, is quite similar to this, there are some differences in detail. We do not find any evidence of Mg b or TiO absorption, although Na D and the G band are clearly present. The [O III] λ4959 emission line is weaker than Hβ, and we see strong [Ne III] $\lambda\lambda$3869, 3968 which are blueward of the starting wavelength of the Downes & Keyes spectrum. The latter spectrum was obtained at least a year after ours, so there are evidently changes in the object on this kind of time-scale.

The infrared colours are similar to those of the D′ symbiotic stars (Allen 1982), which typically have G-type absorption features in their spectra. It seems likely that this object is in a similar evolutionary state, although it does not show the high-excitation lines (e.g., He II) usually associated with symbiotic stars. The *JHKL* flux arises from a combination of star and dust shell with the dust shell dominating at the longer wavelengths. It is therefore possible that the larger variation at *K* reflects variations of a hot star or disc which is heating the dust. The presence of TiO in the spectrum is surprising, as the *JHK* colours do not suggest an M-type star. Possibly the TiO is formed in the circumstellar shell in the same way as it is thought to be in certain RV Tau stars.

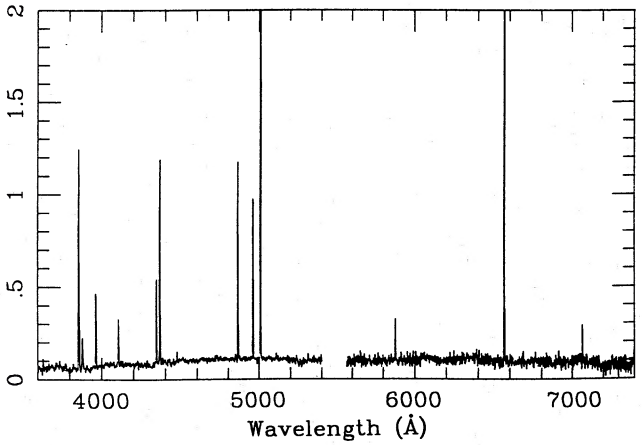

Figure 21. Spectrum of 21392+0230 on a relative flux, $F(\lambda)$, scale. Both Hα and [O III] λ5007 are off scale. Note the strong [Ne III] $\lambda\lambda$3869, 3968 lines, the great strength of [O III] λ4363, and that Hβ is clearly stronger than [O III] λ4959.

10 CARBON STARS

The two carbon stars are 01246 − 3248 and 04067 − 0922. They are very similar to each other and are found in the same part of each of the two-colour diagrams, clearly separated from the non-Mira M stars. Their colours are not very different from those of the O-rich Miras, presumably indicating similarities of temperature and infrared optical depth in their circumstellar shells. Only in Fig. 4 does the high value of [25]−[60] indicate a cool component to their dust shells which is absent from typical Mira shells. The *IRAS* colours of these two stars are very unusual for normal carbon stars. A comparison with fig. 2 from Hacking et al. (1985) indicates that, given our selection criterion in terms of *IRAS* flux ratio, we might expect to find only carbon stars with very thick circumstellar shells. Indeed, three such stars were among the Miras in this survey discussed in Paper I, but these two stars do not have very thick shells. An extensive study of *IRAS* colours was made by van der Veen & Habing (1988) who divided the *IRAS* two-colour diagram (similar to Fig. 4, but note that their definition of the *IRAS* colours is different from ours) into various regions, according to the type of star found in that region. The two carbon stars under discussion fall in their region VIb which, as van der Veen & Habing point out, suggests relatively hot dust close to the star and relatively cool dust at larger distances. On the 'Valinhos' classification scheme, described by Guglielmo et al. (1993), they fall in the region o2, again away from the bulk of the carbon stars.

01246 − 3248 (R Scl) is a well-studied carbon star which falls into the category of stars with detached circumstellar shells, i.e., stars which must have had much higher mass-loss rates in the not too distant past than they do currently (e.g. Olofsson et al. 1990; Le Bertre 1992; Young et al. 1993; Zuckerman 1993). These stars are most easily identified by their 60-μm excess, although there is a wealth of other evidence for the detached shell in the better studied examples, such as R Scl. 04067 − 0922 is probably a more distant example of the same phenomenon. Because they are carbon stars, and have therefore experienced dredge-up, we know that these stars must be on the thermally pulsing part of the AGB. The fact that they have detached shells suggests that they might have recently been Mira variables, but that they have left the Mira instability strip while undergoing a pulse minimum.

The near-infrared colours of these two stars are much more extreme than those of other non-Mira carbon stars (compare, for example, fig. 5 of Feast & Whitelock 1992). Their colours are quite similar to those of the relatively long-period carbon Miras (Glass et al. 1987).

Both carbon stars show clear variability in their infrared photometry, with some indication of multiperiodicity or chaotic behaviour. While not previously noted for R Scl (04067 − 0922 was unknown as a C star or as a variable prior to this study), double-period variations are quite common among SR variables (Houk 1963). Lloyd Evans (1987) has noted a tendency for such stars to have more extreme *IRAS* colours than those of variables with single periods. It seems likely that this behaviour is a manifestation of 'weak chaos' as described by Icke, Frank & Heske (1992) and predicted by them to be a characteristic of unstable mass-losing stars near the end of their AGB evolution. This might be the result of, or the cause of, higher mass-loss rates, and it is not clear whether these stars have undergone a recent reduction in their mass loss or whether the mass loss has a different character from that seen for Miras. Both stars have low *IRAS* variability indices, although R Scl has only 2 and 04067 − 0922 has only 3 HCONs.

It is interesting to note that the point representing RZ Sgr in Fig. 4 lies midway between the carbon stars and the rest of the O-rich stars. RZ Sgr is the only star in the sample known to be an S star, and it is therefore a candidate transition object between the M- and C-type stars. Its position in Fig. 4 could, however, be due entirely to the presence of a detached dust shell. RZ Sgr is also a moderately large-amplitude SR variable which is either multiperiodic or else has a changing period (see Section 7.9).

10.1 Individual sources

01246 − 3248, R Scl

This is a well-known bright carbon star and SRb variable, which has been given a spectral type C6,4 by Yamashita (1972) and C6,5 by Warner (1963). Le Bertre (1992) published 28 infrared observations for this star, from which he determined a period of 386 d; the GCVS lists 370 d. A Fourier analysis of the 65 *K* observations from Table 2 provides the periodogram shown in Fig. 22, on which four of the highest peaks are labelled. The tallest peak (P_1) corresponds to a period of 379 d. The second (P_2) is at 187.6 d and is a combination of the one-year alias of P_1, at 185.9 d, and the first harmonic at twice the frequency of P_1, at 189.5 d. The third peak (P_3) is at 2327 d, while the fourth is its one-year alias at 315.5 d. Fig. 23 illustrates the fit of curves, formed by summing second-order sinusoids with periods of 379.4 and 2315 d (these being the mean values of the periods found for the *JHKL* data), to the *J* and *K* data from Table 2. The data given here do not cover a sufficient time interval for us to draw definitive conclusions about the existence of the long period. It would be worth getting a long time-series to investigate the nature of the long-term trends. It is clear from Fig. 23 that observations covering only a short strength of light curve can be very deceptive for a multiperiodic variable.

04067 − 0922

The spectrum (Fig. 24) is weak, but the identification as a carbon star is unambiguous. The C_2 band at λ5635 is

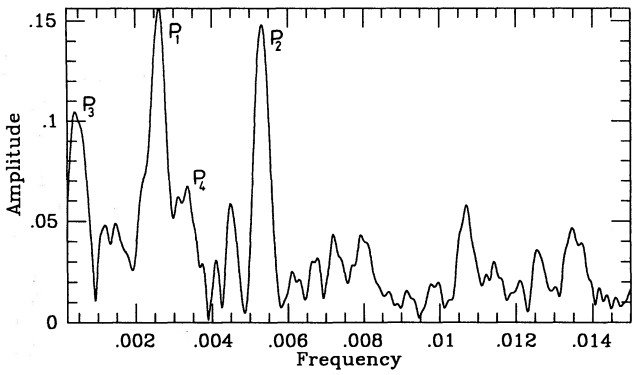

Figure 22. Periodogram of *K* mag for 01246 − 3248 (R Scl).

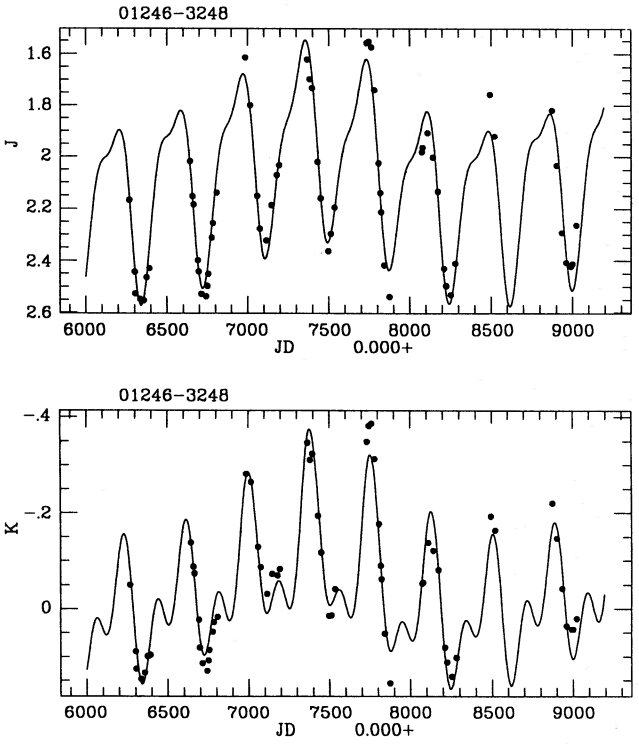

Figure 23. *J* and *K* light curves for 01246 − 3248 (R Scl). The fitted curve is the sum of two second-order sine waves with their interaction terms. The principal periods are 379.4 and 2315 d.

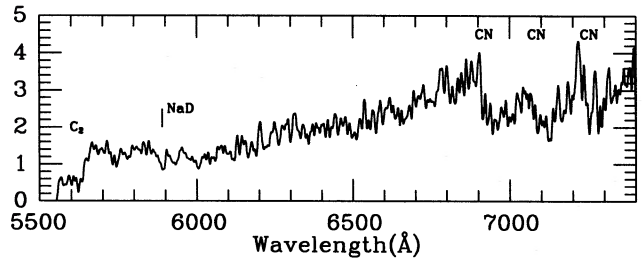

Figure 24. Relative flux spectrum, $F(\lambda)$, of the newly discovered carbon star, 04067 − 0922. Although the signal-to-noise ratio is low, it is clearly a carbon star. Various spectral features supporting this attribution are marked.

prominent, as are various CN bands at the red end of the spectrum. The Na D lines are weak, suggesting that the temperature is relatively high, and rather hotter than R Scl. Its *JHKL* colours are consistent with this spectral type. The *IRAS* colours are unusual but similar to those of R Scl (01246 − 3248). A Fourier analysis of the near-infrared data shows semiregular variations with a period of about 228 d. While this single period does not fit the observations particularly well, the data are not good enough to establish a second period with any degree of certainty. There are, however, indications that the variable is multiperiodic.

11 CONCLUSIONS

This paper concludes the SAAO survey of *IRAS* sources in the South Galactic Cap (references to earlier papers are given in Section 2). The study has provided basic data on a wide variety of dust shell sources. These include B stars with resolved shells, Be stars, Vega-like A stars, various peculiar C stars, active pre-main-sequence stars and a wide range of interacting binaries. However, the bulk of the stars examined are upper AGB sources undergoing heavy mass loss. The study of the most luminous examples, the Miras, demonstrates that our previous understanding of these stars has been severely biased owing to its reliance on optically selected samples. This work also confirms that Miras with different periods have different kinematics and scaleheights, strongly supporting the notion that they could not be evolutionarily related – an assumption still prevalent in much of the literature. One of the most interesting discoveries to come out of the present paper is that there are significant numbers of metal-rich AGB stars in the extended solar neighbourhood, of the variety previously thought to be unique to the Galactic Bulge. Furthermore, some fraction of these stars are found at moderate distances ($\gtrsim 1$ kpc) from the Galactic plane. What can be deduced about the non-Mira M stars is severely limited by, first, a high level of uncertainty in their distances, and secondly, the sensitivity constraints of the *IRAS* survey. This situation should be greatly improved in the near future by results from *HIPPARCOS* and the various near-infrared surveys of the South Galactic Cap which are either in progress or planned (Epchtein et al. 1994).

ACKNOWLEDGMENTS

We thank the following people who made some of the near-infrared observations: G. Roberts, J. Spencer Jones, C. D. Laney and H. Winkler. We are grateful to Tom Kinman for bringing the existence of 21392 + 0230 to our attention, and to the referee for helpful comments. This paper uses data retrieved from the HEASARC on-line service run by NASA and from SIMBAD, database of the Astronomical Data Centre, Strasbourg, France.

REFERENCES

Allen D. A., 1982, in Friedjung M., Viotti R., eds, Proc. IAU Colloq. 70, The Nature of Symbiotic Stars. Reidel, Dordrecht, p. 27
Balona L. A., Feast M. W., 1974, MNRAS, 167, 621
Baud B., Habing H. J., Matthews H. E., Winnberg A., 1981, A&A, 95, 156
Bessell M. S., 1990, PASP, 102, 1181
Bessell M. S., Brett J. M., Scholtz M., Wood P. R., 1989, A&AS, 77, 1
Bidelman W. P., 1980, Publ. Warner Swasey Obs., 2, 185
Boothroyd A. I., Sackmann I.-J., 1988, ApJ, 328, 632
Carter B. S., 1990, MNRAS, 242, 1
Catchpole R. M., Feast M. W., 1976, MNRAS, 175, 501
Catchpole R. M., Robertson B. S. C., Lloyd Evans T. H. H., Feast M. W., Glass I. S., Carter B. S., 1979, S. Afr. Astron. Obs., Circ., 1, 61
Cohen M., 1974, MNRAS, 169, 257
Cohen M., Kuhi L. V., 1979, ApJS, 41, 743
Cohen M., Wainscoat R. J., Walker H. J., Volk K., Schwartz D. E., 1989, AJ, 97, 1759
Deguchi S., Nakada Y., Forster J. R., 1989, MNRAS, 239, 825
Downes R. A., Keyes C. D., 1988, AJ, 96, 777
Eder J., Lewis B. M., Terzian Y., 1988, ApJS, 66, 183

Epchtein N., Omont A., Burton B., Persi P., 1994, Proc. Les Houches NATO Workshop on Science with Astronomical Near-Infrared Sky Surveys, Kluwer, Dordrecht

Feast M. W., 1963, MNRAS, 125, 367

Feast M. W., 1975, Observatory, 95, 19

Feast M. W., 1979, in Bateson F. M., Smak J., Urch I. H., eds, Proc. IAU Colloq. 46, Changing Trends in Variable Star Research. University of Waikato, Hamilton, NZ, p. 246

Feast M. W., Whitelock P. A., 1987, in Kwok S., Pottasch S. R., eds, Late Stages of Stellar Evolution. Reidel, Dordrecht, p. 33

Feast M. W., Whitelock P. A., 1992, MNRAS, 259, 6

Feast M. W., Woolley R., Yilmaz N., 1972, MNRAS, 158, 23

Feast M. W., Robertson B. S. C., Catchpole R. M., Lloyd Evans T., Glass I. S., Carter B. S., 1982, MNRAS, 201, 439

Feast M. W., Whitelock P. A., Catchpole R. M., Carter B. S., 1984, Observatory, 104, 217

Feast M. W., Whitelock P. A., Carter B. S., 1990, MNRAS, 247, 227

Feast M. W., Whitelock P. A., Sharples R., 1992, in Barbuy B., Renzini A., eds, Proc. IAU Symp. 149, The Stellar Population of Galaxies. Kluwer, Dordrecht, p. 77

Frogel J. A., Whitford A. E., 1987, ApJ, 320, 199

Frogel J. A., Persson S. E., Cohen J. G., 1981, ApJ, 246, 842

Frogel J. A., Terndrup D. M., Blanco V. M., Whitford A. E., 1990, ApJ, 353, 494

Gaposchkin S., 1947, Harvard Annals, 115, 129

Glass I. S., Feast M. W., 1982, MNRAS, 198, 199

Glass I. S., Catchpole R. M., Feast M. W., Whitelock P. A., Reid I. N., 1987, in Kwok S., Pottasch S. R., eds, Late Stages of Stellar Evolution. Reidel, Dordrecht, p. 51

Guglielmo F., Epchtein N., Le Bertre T., Fouqué P., Hron J., Kerschbaum F., Lépine J. R. D., 1993, A&AS, 99, 31

Hacking P. et al., 1985, PASP, 97, 616

Houk N., 1963, AJ, 68, 253

Houk N., Smith-Moore, M., 1988, Michigan Catalogue of Two-Dimensional Spectral Types for the HD stars, Vol. 4. Univ. Michigan, Michigan

Iben I., Renzini A., 1983, ARA&A, 21, 271

Icke V., Frank A., Heske A., 1992, A&A, 258, 341

Innes R. T. A., 1903, Cape Ann., 9, 143B

IRAS Science Team, 1986, *IRAS* Point Source Catalog, Version 1 (PSC)

IRAS Science Team, 1988, *IRAS* PSC-explanatory supplement, (PSC-ES)

Jones D. H. P., 1972, ApJ, 178, 467

Jones D. H. P., Fisher J. L., 1984, A&AS, 56, 449

Jura M., Kleinmann S. G., 1992a, ApJS, 79, 105

Jura M., Kleinmann S. G., 1992b, ApJS, 83, 329

Jura M., Yamamoto A., Kleinmann S. G., 1993, ApJ, 413, 298

Kaiser D. H., Baldwin M. E., Williams D. B., 1990, Inf. Bull. Variable Stars No. 3442

Kerschbaum F., Hron J., 1992, A&A, 263, 97

Kholopov P. N. et al., 1985, General Catalogue of Variable Stars, 4th edition. Nauka Publishing House, Moscow (GCVS)

Kleinmann S. G., 1989, in Johnson H. R., Zuckerman B., eds, Proc. IAU Colloq. 106, Evolution of Peculiar Red Giant Stars. Cambridge Univ. Press, Cambridge, p. 13

Kukarkin B. V. et al., 1982, New Catalogue of Suspected Variable Stars. Nauka Publishing House, Moscow (NSV)

Lahulla J. F., 1987, PASP, 99, 998

Le Bertre T., 1992, A&AS, 94, 377

Le Squeren A. M., Sivagnanam P., Dennefeld M., David P., 1992, A&A, 254, 133

Lewis B. M., 1992, ApJ, 396, 251

Lewis B. M., Engels D., 1991, MNRAS, 251, 391

Lewis B. M., Eder J., Terzian Y., 1990, ApJ, 362, 634

Lloyd Evans T., 1987, in Appenzeller I., Jordan C., eds, Proc. IAU Symp. 122, Circumstellar Matter. Reidel, Dordrecht, p. 541

McWilliam A., Rich R. M., 1994, ApJS, 91, 749

Majewski S. R., 1992, ApJS, 78, 87

Menzies J. W., Cousins A. W. J., Banfield R. M., Laing J. D., 1989, SAAO Circ. 13, 1

Mikami T., Heck A., 1982, PASJ, 34, 529

Neugebauer G., Leighton R. B., 1969, The Two-micron Sky Survey. NASA SP-3047, Washington

Norris J. E., 1993, in Smith G. H., Brodie J. P., eds, ASP Conf. Ser. Vol. 48, The Globular Cluster–Galaxy Connection. Astron. Soc. Pac., San Francisco, p. 259

Nyman L.-A. et al., 1992, A&AS, 93, 121

Olnon F. M., Raimond E., *IRAS* Science Team, 1986, A&AS, 65, 607

Olnon F. M., Baud B., Habing H. J., de Jong T., Harris S., Pottasch S. R., 1984, ApJ, 278, L41

Olofsson H., Carlström U., Eriksson K., Gustafsson B., Willson L. A., 1990, A&A, 230, L13

Oort J. H., van Tulder J. J. M., 1942, Bull. Astron. Inst. Neth., 9, 327

Pallavicini R., Randich S., Giampapa M. S., 1992, A&A, 253, 185

Prévot L., Martin N., Maurice E., Rebeirot E., Rousseau J., 1983, A&AS, 53, 255

Price S. P., Murdock T. L., 1983, The Revised AFGL Infrared Sky Survey Catalog. AFGL-TR-83-0161

Rich R. M., 1988, AJ, 95, 828

Russell J. L., Lasker B. M., McLean B. J., Sturch C. R., Jenkner H., 1990, AJ, 99, 2059

Sharples R. M., Whitelock P. A., Feast M. W., 1995, MNRAS, 272, 139 (SWF)

Sivagnanam P., Braz M. A., Le Squeren A. M., Tran Minh F., 1990, A&A, 233, 112

Stephenson C. B., 1986a, ApJ, 301, 927

Stephenson C. B., 1986b, ApJ, 300, 779

te Lintel Hekkert P., Caswell J. L., Habing H. J., Haynes R. F., Norris R. P., 1991, A&AS, 90, 327

Unger S. W., Wolstencroft R. D., Pedlar A., Savage A., Clowes R. G., Leggett S. K., Parker Q. A., 1989, MNRAS, 236, 425

van der Veen W. E. C. J., Habing H. J., 1988, A&A, 194, 125

Volk K., Cohen M., 1989, AJ, 98, 931

Volk K., Kwok S., Stencel R. E., Brugel E., 1991, ApJS, 77, 607

Wallerstein G., Dominy J. F., 1988, ApJ, 326, 292

Warner B., 1963, MNRAS, 126, 61

Whitelock P. A., 1986, MNRAS, 219, 525

Whitelock P. A., 1994, MNRAS, 270, L15

Whitelock P. A., Catchpole R. M., 1985, MNRAS, 212, 873

Whitelock P. A., Feast M. W., 1993, in Weinberger R., Acker A., eds, Proc. IAU Symp. 155, Planetary Nebulae. Kluwer, Dordrecht, p. 251

Whitelock P. A., Munari U., 1992, A&A, 255, 171

Whitelock P. A., Feast M. W., Catchpole R. M., 1989, MNRAS, 238, 7P

Whitelock P. A., Menzies J. W., Catchpole R. M., Feast M. W., Carter B. S., Marang F., Roberts G., Sekiguchi K., 1989b, MNRAS, 241, 393

Whitelock P. A., Feast M. W., Catchpole R. M., 1991a, MNRAS, 248, 276

Whitelock P. A., Menzies J. W., Catchpole R. M., Feast M. W., Roberts G., Marang F., 1991b, MNRAS, 250, 638

Whitelock P. A., Menzies J. W., Feast M. W., Marang F., Carter B. S., Roberts G., Catchpole R. M., Chapman J., 1994a, MNRAS, 267, 711 (Paper I)

Whitelock P. A., Menzies J. W., Catchpole R. M., Marang F., 1994b, MNRAS, 267, 881

Wood P. R., Bessell M. S., 1983, ApJ, 265, 748

Yamashita Y., 1972, Annals Tokyo Astron. Obs., 13, 169

Young K., Phillips T. G., Knapp G. R., 1993, ApJ, 409, 725

Zijlstra A. A., Loup C., Waters L. B. F. M., de Jong T., 1992, A&A, 265, L5

Zuckerman B., 1993, A&A, 276, 367

Zuckerman B., Dyck H. M., 1986, ApJ, 304, 394